The Pennsylvania State University
The Graduate School

A THEORETICAL AND EXPERIMENTAL STUDY OF ACOUSTIC PROPAGATION IN MULTISECTIONED CIRCULAR DUCTS

A Thesis in
Engineering Acoustics
by
Barry R. Wyerman

Submitted in Partial Fulfillment
of the Requirements
for the Degree of

Doctor of Philosophy

March 1976

The Pennsylvania State University

The Graduate School

A Theoretical and Experimental Study of Acoustic Propagation in Multisectioned Circular Ducts

A Thesis in

Engineering Acoustics

by

Barry R. Wyerman

Submitted in Partial Fulfillment
of the Requirement
for the Degree of

Doctor of Philosophy

March 1976

Date of Approval:

_____

_____
Gerhard Reethof
Professor of Mechanical Engineering
Chairman of Committee
Thesis Advisor

_____

_____
Jiri Tichy, Chairman of the
Committee on Acoustics
Professor of Architectural
Engineering

A Theoretical and Experimental Study of Acoustic Propagation in Multisectioned Circular Ducts

by

Barry R. Wyerman

An Abstract of a Thesis

in

Engineering Acoustics

Submitted in Partial Fulfillment
of the Requirements
for the Degree of

Doctor of Philosophy

March 1976

The Pennsylvania State University
The Graduate School

ABSTRACT

The propagation of plane waves and higher order acoustic modes in a circular multisectioned duct has been studied. A unique source array consisting of two concentric rings of sources, providing phase and amplitude control in the radial, as well as circumferential direction, was developed to generate plane waves and both spinning and non-spinning higher order modes. Measurements of attenuation and radial mode shapes were taken with finite length liners inserted between the hard wall sections of an anechoically terminated duct. Materials tested as liners included a glass fiber material and both sintered fiber metals and perforated sheet metals with a honeycomb backing. The fundamental acoustic properties of these materials were studied with emphasis on the attenuation of sound by the liners and the determination of local versus extended reaction behavior for the boundary condition. A search technique has been developed to find the complex eigenvalues for a liner under the assumption of a locally reacting boundary condition.

The experimental results were compared with a mathematical model for the multisectioned duct which includes the modal transmission and reflection effects at the interface between sections with different liner admittance. The good agreement between measurement and theory indicates that the multisectioned duct analysis can be used to predict the sound field in a complicated system of several different liner sections.

Furthermore, the local reaction boundary condition is valid for the sintered fiber metal and perforated panel liners but can only be used in cases of moderate sound attenuation for the glass fiber material. For each of the acoustic modes studied, the sound attenuation character-

istics of the fiber metal materials were significantly better than those for the perforated panels.

ACKNOWLEDGMENT

The author would like to express appreciation to the Chairman of his doctoral committee, Dr. Gerhard Reethof, for providing guidance, assistance and encouragement throughout this research, as well as his complete graduate program. The author's doctoral committee of Drs. Jiri Tichy, Sabih Hayek and Eugene Skudrzyk are also gratefully acknowledged for their instruction and guidance throughout his graduate program.

In addition, the author wishes to express his gratitude to Dr. O.H. McDaniel for invaluable suggestion and assistance throughout this investigation. Sincere appreciation is also extended to Mr. Robert Owens for assistance in the experimental and technical phases of this research.

This work was performed with support from the Langley Research Center of the National Aeronautics and Space Administration under Grant No. NG9-39-009-121.

TABLE OF CONTENTS

		Page
ACKNOWLEDGMENT		ii
LIST OF FIGURES		iv
LIST OF TABLES		ix
LIST OF SYMBOLS		x
CHAPTER I	INTRODUCTION	1
CHAPTER II	THEORY	6
2.1	Introduction	6
2.2	Infinite Hard-Walled Duct Theory	7
2.3	Acoustic Materials	17
2.4	Acoustic Propagation in a Lined Duct	22
2.5	Multisectioned Duct Theory	31
2.6	Eigenvalue Search Technique	44
CHAPTER III	EXPERIMENT	51
3.1	Introduction	51
3.2	Multisectioned Duct System	52
3.3	Source Array	57
3.4	Flow Resistance Measurements	74
3.5	Impedance Tube Measurements	76
3.6	Duct Liners	77
CHAPTER IV	DISCUSSION	80
4.1	Impedance Characteristics of Duct Liners	80
4.2	Eigenvalue Search Technique	86
4.3	Multisectioned Duct Model	92
4.4	Multisectioned Duct Measurements	95
4.5	Acoustic Performance of Duct Liners	146
CHAPTER V	SUMMARY, CONCLUSIONS AND RECOMMENDATIONS	154
REFERENCES		163
APPENDIX A		166

LIST OF FIGURES

Figure		Page
2.1	Properties of Bessel Functions of the First Kind of Integer Order $J_m(kr)$	11
2.2	Radial Mode Shapes for m = 0 Modes	13
2.3	Radial Mode Shapes for m = 1 Modes	13
2.4	Cut-off Frequencies for Higher Order Modes in a 12 Inch Diameter Duct	15
2.5	Fiber Metal Material with Air Cavity Backing	19
2.6	Perforated Panel with Resonant Cavities	19
2.7	Duct Lined with Porous Material	25
2.8	Complex Propagation Constants for Bulk Glass Fiber Material (h) and for the First Radial Mode (Ω) Propagating in a Duct Lined with One Inch Glass Fiber Material	28
2.9	Complex Propagation Constants for Bulk Glass Fiber Material (h) and for the Second Radial Mode (Ω) Propagating in a Duct Lined with One Inch Glass Fiber Material	29
2.10	Sound Field in Multisectioned Duct	33
2.11	Uniform Duct Section	33
2.12	Admittance Discontinuity Between Sections	33
2.13	Duct Termination Planes	35
2.14	Sound Power for Insertion Loss and Transmission Loss	36
2.15	Quadrants for Locating Ω and λ	47
2.16	Integration Contours	49
3.1	Experimental Duct System	53
3.2	Frequency Response of Undamped and Damped Probe Tubes	56
3.3	Amplitude Response of 2-1/4" Loudspeaker	59
3.4	Phase Response of 2-1/4" Loudspeaker	59

Figure		Page
3.5	Source Array with Thirteen Elements	60
3.6	Radial Mode Shape for the (0,1) Mode, 1400 Hz	63
3.7	Radial Mode Shape for the (0,2) Mode, 2535 Hz	65
3.8	Radial Mode Shape for the (1,1) Mode, 700 Hz	66
3.9	Radial Mode Shape for (1,2) Mode, 2000 Hz	67
3.10	Radial Mode Shape for (2,1) Mode, 1110 Hz	69
3.11	Radial Mode Shapes Generated for the (0,1) Mode at 1400 Hz Using Different Speakers in the Array. . .	70
3.12	Radial Mode Shapes Generated for the (1,1) Mode at 700 Hz Using Different Speakers in the Array . . .	71
3.13	Radial Mode Shapes Generated for the (0,2) Mode at 2535 Hz Using Different Speakers in the Array. . .	72
3.14	Flow Resistance for a Fiber Metal Material	75
4.1	Specific Normal Impedance for Fiber Metal, Flow Resistance 48 cgs rayls, Cavity Depth 7/8"	81
4.2	Specific Normal Impedance for Fiber Metal Flow Resistance 25 cgs rayls, Cavity Depth 7/8"	81
4.3	Specific Normal Impedance of 22% Open Area Perforate, Cavity Depth 7/8"	82
4.4	Specific Normal Impedance of 30% Open Area Perforate, Cavity Depth 7/8"	82
4.5	Specific Normal Impedance for One Inch Thick Glass Fiber Material	83
4.6	Ordering of Eigenvalues for FM 1 Liner, m=0	87
4.7	Attenuation for Successive Radial Modes for FM 1 Liner, m=0	88
4.8	Ordering of Eigenvalues for FM 1 Liner, m=1	90
4.9	Attenuation of Successive Radial Mode for FM 1 Liner, m=1	91
4.10	Multisectioned Duct Mode	92

Figure		Page
4.11	Radial Mode Shapes for (0,0) Mode, 500 Hz – FM 1 Liner	99
4.12	Radial Mode Shapes for (0,0) Mode, 800 Hz – FM 1 Liner	101
4.13	Radial Mode Shapes for (0,0) Mode, 1250 Hz – FM 1 Liner	102
4.14	Radial Mode Shapes for (0,1) Mode, 1390 Hz – FM 1 Liner	103
4.15	Radial Mode Shapes for (0,1) Mode, 1600 Hz – FM 1 Liner	105
4.16	Radial Mode Shapes for (0,1) Mode, 2000 Hz – FM 1 Liner	106
4.17	Radial Mode Shapes for (0,1) Mode, 2500 Hz – FM 1 Liner	107
4.18	Radial Mode Shapes for (1,1) Mode, 670 Hz – FM 1 Liner	108
4.19	Radial Mode Shapes for (1,1) Mode, 1000 Hz – FM 1 Liner	109
4.20	Radial Mode Shapes for (1,1) Mode, 1500 Hz – FM 1 Liner	110
4.21	Radial Mode Shapes for (2,1) Mode, 1250 Hz – FM 1 Liner	112
4.22	Radial Mode Shapes for (2,1) Mode, 1600 Hz – FM 1 Liner	114
4.23	Radial Mode Shapes for (0,1) Mode, 3000 Hz – FM 1 Liner	115
4.24	Radial Mode Shapes for (0,2) Mode, 2700 Hz – FM 1 Liner	116
4.25	Radial Mode Shapes for (0,2) Mode, 3100 Hz – FM 1 Liner	117
4.26	Radial Mode Shapes for (1,1) Mode, 2400 Hz – FM 1 Liner	119
4.27	Radial Mode Shapes for (1,2) Mode, 2300 Hz – FM 1 Liner	120

Figure		Page
4.28	Radial Mode Shapes for (0,0) Mode, 800 Hz - Perf 1 Liner	122
4.29	Radial Mode Shapes for (0,0) Mode, 800 Hz - FM 2 Liner	123
4.30	Radial Mode Shapes for (0,0) Mode, 800 Hz - One Foot Glass Fiber Liner	124
4.31	Radial Mode Shapes for (0,0) Mode, 800 Hz - Two Foot Glass Fiber Liner	125
4.32	Radial Mode Shapes for (0,0) Mode, 1250 Hz - One Foot Glass Fiber Liner	126
4.33	Radial Mode Shapes for (0,1) Mode, 1600 Hz - Perf 2 Liner	127
4.34	Radial Mode Shapes for (0,1) Mode, 1600 Hz - FM 2 Liner	128
4.35	Radial Mode Shape in Perf 2 Liner, 1600 Hz	129
4.36	Radial Mode Shapes for (0,1) Mode, 1600 Hz - One Foot Glass Fiber Liner	131
4.37	Radial Mode Shapes for (0,1) Mode, 2000 Hz - FM 2 Liner	132
4.38	Radial Mode Shapes for (0,1) Mode, 2000 Hz - Perf 1 Liner	133
4.39	Radial Mode Shapes for (0,1) Mode, 2500 Hz - Perf 2 Liner	134
4.40	Radial Mode Shape in Perf 2 Liner, 2500 Hz	135
4.41	Radial Mode Shapes for (1,1) Mode, 670 Hz - One Foot Glass Fiber	136
4.42	Radial Mode Shapes for (1,1) Mode at 1000 Hz - One Foot Glass Fiber Liner	138
4.43	Radial Mode Shapes for (1,1) Mode, 1000 Hz - Perf 2 Liner	139
4.44	Radial Mode Shapes for (1,1) Mode, 1500 Hz - FM 2 Liner	140
4.45	Radial Mode Shapes for (1,1) Mode, 1800 Hz - Perf 1 Liner	141

Figure		Page
4.46	Radial Mode Shapes for (2,1) Mode, 1250 Hz - One Foot Glass Fiber Liner	142
4.47	Radial Mode Shapes for (2,1) Mode, 1250 Hz - FM 2 Liner	143
4.48	Comparison Between Transmission Loss and Insertion Loss for FM 1 Liner	147
4.49	Insertion Loss for (0,0) Mode	148
4.50	Insertion Loss for (0,1) Mode	148
4.51	Insertion Loss for the (1,1) Mode	150
4.52	Insertion Loss for the (2,1) Mode	150
4.53	Insertion Loss for FM 1	151
4.54	Insertion Loss for Two Lengths of Glass Fiber Material, (0,1) Mode.	153
4.55	Insertion Loss for Two Lengths of Glass Fiber Materials, (1,1) Mode	153

LIST OF TABLES

Table		Page
2.1	Zeros of Derivatives of the Bessel Functions $J_m(x)$	12
A.1	The Generation of Spurious Modes Due to Phase Variations Between Elements of the Source Array . . .	168

LIST OF SYMBOLS

Letter Symbols	Description
a	Outer Radius of Lined Duct
b	Duct Radius
c	Speed of Sound
d	Thickness of Material, Cavity Depth
f	Frequency
g	Integer
h	Complex Propagation Constant for Bulk Material
k	Free Space Wavenumber
m	Circumferential Mode Number
p	Acoustic Pressure
r	Radial Coordinate of Cylindrical Coordinate System
t	Time
v	Velocity
z	Axial Coordinate of Cylindrical Coordinate System
A	Modal Amplitude of Acoustic Wave
D/Dt	Total Derivative
I	Eigenfunction Product Integral, Intensity
J	Bessel Function of the First Kind
K	Eigenvalue
M	Circumferential Order of Generated Mode
N	Number of Circumferentially Spaced Elements in an Array
P	Porosity of Bulk Material
Q	Source Strength

Letter Symbols	Description
R	Reflection Coefficient, Real Component of Acoustic Impedance
T	Transmission Coefficient
U	Velocity Potential
V	Velocity Potential
W	Duct Wave Coefficient
X	Imaginary Component of Acoustic Impedance
Y	Bessel Function of the Second Kind
Z	Acoustic Impedance

Greek Letters	Description
α	Absorption Coefficient
β	Acoustic Admittance
γ	Ratio of Specific Heats of Gas
δ	Dirac Delta Function
ε	Scaling Parameter for Nondimensional Quantities
Θ	Angular Coordinate of Cylindrical Coordinate System
λ	Wavelength
μ	Radial Mode Number
ν	Radial Mode Number
ρ	Density
σ	Real Component of Propagation Constant
τ	Imaginary Component of Propagation Constant
ϕ	Phase Characteristic of Source Element
ω	Circular Frequency
Ω	Propagation Constant
Γ	Propagation Constant

Superscripts	Description
+	Wave Traveling in Positive z Direction
-	Wave Traveling in Negative z Direction
j,k	Plane Number

Matrix Notation	Description
$\lfloor\ \rfloor$	Row Matrix
$\{\ \}$	Column Matrix
$[\ ]$	Square Matrix
$\lceil\ \rfloor$	Diagonal Matrix
$[I]$	Identity Matrix

CHAPTER I

INTRODUCTION

Although not a new topic, the subject of duct acoustics has become an area of renewed interest. This interest has been generated as a result of current jet engine noise reduction programs. A large portion of these programs have been oriented towards the application of acoustic treatment to jet engine inlet ducts. Additional interest in duct acoustics has been motivated by the need to suppress noise in air conditioning ducts and large air moving systems.

A typical solution to the reduction of noise from a duct system is to insert an acoustically absorbent liner material in the duct. This material attenuates the sound before it is radiated from the duct outlet. However, acoustic propagation in the duct and attenuation by the liner are complicated by several factors, including the modal content of the sound, the acoustic properties of the material, the finite length of the liner, the termination of the duct, and the presence of flow. The effect of each of these will be briefly discussed.

Much of the initial work in duct acoustics concentrated on the propagation and attenuation of plane waves. Studies to evaluate liner performance were concerned with assigning a single number rating to a material to describe its attenuation per unit length for the plane wave mode. However, this is not the only mode present within the duct. It has been shown that axial flow compressors and turbines generate higher order acoustic waves of a spiralling nature in a duct. Therefore, the importance of considering the attenuation of these higher order modes when evaluating liner performance must be emphasized.

Test methods for evaluating liner performance often do not yield significant information on attenuation by individual modes. As an example, a common test method measures the attenuation of sound through a lined duct section connected to a broad band noise at one end and to an anechoic or reverberant chamber at the other end. The insertion loss of the liner can be determined by measuring the sound attenuation as a function of frequency. However, the broad band noise source obscures the effects of higher order modes and this method can only yield comparative information on the sound attenuation characteristics of liners.

The acoustic properties of a duct lining material are specified by a normal impedance which determines the modal attenuation of sound through the duct. In certain cases, this impedance can be optimized to produce maximum attenuation but this result is difficult to achieve over a broad frequency range or for more than one mode.

When a finite length liner is inserted in a duct, the impedance discontinuity between the surface of the duct and the surface of the liner causes reflection of an incident wave. This introduces a standing wave in front of the liner. Furthermore, reflection from the termination plane of the duct must also be considered as it too will cause a standing wave.

The presence of uniform mean flow within a lined duct will modify the attenuation of the liner. In general terms, the attenuation of a lined duct increases for acoustic propagation against the direction of flow and decreases for propagation with the direction of flow.

The sound attenuation of individual liners can vary significantly with airflow velocity. As the airflow velocity is varied, the peak

attenuation varies in a manner which is dependent upon the change in acoustic properties of the liner. The effect of flow on locally reacting liners is to increase the acoustic resistance of the liners at low frequencies. Flow effects on reactance are less significant but tend to increase the reactance of the liner with increasing velocity. Thus for maximum benefits of sound attenuation, it is necessary to design lining treatment for the flow velocity region and acoustic environment in the duct in which it will be used.

Each of these factors will have an effect on the attenuation of sound in a lined duct. However, each effect must be understood separately before the combination of these effects may be studied. In a final analysis, the individual effects may be combined to simulate the environment of an actual jet engine for example.

Recently there has been an interest in acoustic propagation in circular ducts of several different sections. This work was motivated by the physical situation of sound radiating through the successive lined and unlined sections of an aircraft engine inlet duct. Due to the changes in liner impedance for each duct section, the boundary condition also changes and an acoustic wave is partially transmitted and partially reflected at the interface between different sections. Thus, it is possible to take advantage of the reflection effects between sections as well as the transmission effects of the liners to attenuate sound. Lansing and Zorumski (1) have performed a preliminary analysis of acoustic propagation in a multisectioned duct. Their results show that a combination of several different duct liners can perform significantly better than a uniform duct liner. Extensive parametric studies of optimum liner configurations have been performed by Beckemeyer and

Sawdy (2) to maximize sound attenuation for a two dimensional multi-sectioned duct.

Despite the promising analytic work in the area of multisectioned ducts, there is a lack of experimental data to substantiate these studies. Nonetheless, this analysis provides a unique approach, as well as a realistic model, for analyzing sound attenuation in lined duct systems.

The basic objective of this study is to investigate current multi-sectioned duct theory through both experimental and analytical techniques. The propagation of plane waves and higher order acoustic modes will be studied in an anechoically terminated circular duct with three sections. Measurements of attenuation and mode shapes will be made for a variety of liner materials over the full frequency range at which a mode can be generated. Sound fields necessary for excitation of various modes will be generated by a spinning mode synthesizer. This system is capable of generating the spinning modes characteristic of axial flow compressors and provides a means of experimentally studying the propagation and attenuation of higher order duct modes.

In addition, the fundamental properties of sound absorbing liners will be studied, with emphasis on the attenuation of sound by the liner and the determination of local versus extended reaction behavior.

This work will be conducted with no flow. Although high speed flow is present in an actual jet engine, the simple case of a lined duct without flow must be fully understood before progress can be made for the more complicated situation. It is hoped that the effects of flow will be the subject of a future research project.

Topics to be investigated in this study include:

1. The development of a source array capable of generating plane waves and higher order acoustic modes in a hollow circular duct
2. The experimental measurement of plane wave and higher order mode propagation in a multisectioned duct
3. The development of a mathematical model for acoustic propagation in a multisectioned duct
4. The analysis of boundary conditions and attenuation for duct liners of various acoustic materials

CHAPTER II

THEORY

2.1 Introduction

The basic theory of acoustic propagation in an infinite hollow circular duct will be investigated. Propagation in both an unlined and lined duct will be considered. This treatment will serve as an introduction to the more complex study of acoustic propagation in a multi-sectioned duct.

In addition, the acoustic characteristics of materials commonly used as duct liners will be described. A search technique was developed to locate the complex eigenvalues for a duct liner and will also be presented. The complex eigenvalues define the attenuation of individual acoustic modes through the lined duct.

Unless otherwise noted, the symbols used in this chapter and throughout the text will be defined in the list of symbols.

2.2 Infinite Hard-Walled Duct Theory

Throughout this study, the non-dimensional analysis presented by Zorumski (3) will be used. The wave equation will be derived and the solution to the wave equation in cylindrical coordinates will be studied for a hard-walled circular duct.

The continuity and momentum equations are

$$\frac{D\rho^*}{Dt^*} + \rho^* \bar{\nabla}^* \cdot \bar{v}^* = 0 \tag{2.1}$$

$$\rho^* \frac{D\bar{v}^*}{Dt^*} + \bar{\nabla}^* p^* = 0 \tag{2.2}$$

where the starred superscripts refer to dimensional quantities. The energy equation is given by

$$\frac{Dp^*}{Dt^*} = \frac{\gamma p^*}{\rho^*} \frac{D\rho^*}{Dt^*} \tag{2.3}$$

Throughout this analysis, it will be convenient to work with dimensionless quantities, but scales must first be established for each of the quantities. The length and times scales used will be $\frac{1}{k}$ and $\frac{1}{\omega}$ respectively. A dimensionless length can be formed by multiplying by the wavenumber k and a dimensionless time can be formed by multiplying by the angular frequency ω. Thus

$$\bar{R} = \bar{R}^* k \tag{2.4}$$

$$t = t^* \omega \tag{2.5}$$

In a similar manner, the scales chosen for velocity, density and pressure are c_a, the speed of sound, ρ_a the ambient density, and $\rho_a c_a^2$. A scaling parameter $\varepsilon << 1$ is introduced to account for the

small amplitude of variations in the nondimensional quantities. The resulting variables become

$$\rho^* = \rho_a \ (1 + \varepsilon \ \rho \ e^{-it}) \tag{2.6}$$

$$p^* = \rho_a c_a^2 \ (\frac{1}{\gamma} + \varepsilon \ p \ e^{-it}) \tag{2.7}$$

$$\overline{v}^* = c_a \varepsilon \ \overline{v} \ e^{-it} \tag{2.8}$$

Furthermore, the operators have the following form

$$\frac{D}{Dt^*} = \omega \ [\frac{D}{Dt} + \varepsilon \ \overline{v} \cdot \overline{\nabla}] \tag{2.9}$$

$$\overline{\nabla}^* = k \ \overline{\nabla} \tag{2.10}$$

$$\frac{D}{Dt} = -i \tag{2.11}$$

Using Equations 2.6, 2.7 and 2.8 and grouping similar powers of ε, the non-dimensional equations become.

$$\frac{Dp}{Dt} = \frac{D\rho}{Dt} \tag{2.12}$$

$$\frac{D\rho}{Dt} + \overline{\nabla} \cdot \overline{v} = 0 \tag{2.13}$$

$$\frac{D\overline{v}}{Dt} + \overline{\nabla} \ p = 0 \tag{2.14}$$

Operating on Equations 2.13 and 2.14 to eliminate the velocity results in the wave equation.

$$\nabla^2 p = \frac{D^2 p}{Dt^2} \tag{2.15}$$

In cylindrical coordinates, the non-dimensional wave equation becomes

$$\frac{\partial^2 p}{\partial r^2} + \frac{1}{r}\frac{\partial p}{\partial r} + \frac{1}{r^2}\frac{\partial^2 p}{\partial \Theta^2} + \frac{\partial^2 p}{\partial z^2} + p = 0 \tag{2.16}$$

Using the method of separation of variables, the solution to the wave equation for a single progressive wave is

$$p = \sum_{m=-\infty}^{\infty} J_m(\lambda r)\, e^{im\Theta}\, e^{-i(t-\Omega z)} \tag{2.17}$$

where

$$\Omega = \sqrt{1 - \lambda^2} \tag{2.18}$$

The radial dependence of the solution is given by the Bessel functions of the first-kind of order m and argument λr. Their behavior is shown in Figure 3.1. In addition, Neumann and Hankel functions are also solutions to the wave equation for the radial dependence. However, these functions are excluded for a hollow duct since they are infinite at the origin.

The boundary conditions for the duct must now be applied. The velocity is given in terms of the pressure by Equation 2.14

$$\overline{v} = -i \nabla p \tag{2.19}$$

For a hard-walled duct, the normal component of the velocity at the wall, r = b, must be zero. The boundary condition then becomes

$$v_r = -\frac{i}{\lambda} J_m'(\lambda b) = 0 \tag{2.20}$$

The values of λb which satisfy this equation are called eigenvalues. They will be located at positions where the Bessel functions in Figure 2.1 have zero slopes. These eigenvalues are well known (4) and are given in Table 2.1. Since there are an infinite number of these eigenvalues for a single value of m, a second index, μ, must be included in Equation 2.17. This index will specify which of the zero slope points is taken. Equation 2.17 now becomes

$$p = \sum_{m=-\infty}^{\infty} \sum_{\mu=0}^{\infty} J_m(\lambda_{m\mu} r)\, e^{im\theta}\, e^{-i(t-\Omega_{m\mu} z)} \tag{2.21}$$

and

$$\Omega_{m\mu} = \sqrt{1 - \lambda_{m^2\mu}} \tag{2.22}$$

Each acoustic mode is defined in terms of a particular value of m and μ as an (m, μ) mode. The value of m determines which of the Bessel functions J_m is specified and μ describes which of the eigenvalues is specified.

The first few radial mode shapes are shown in Figure 2.2 and 2.3 for circumferential modes of order m = 0 and m = 1 respectively. The eigenvalue at zero has meaning only for m = 0 modes where the mode shape has no radial dependence. For all other modes, the value of the Bessel function is zero at the origin and this represents a trivial solution. Therefore, all higher order modes will have a radial amplitude dependence. For the summation over μ, the first mode with radial dependence will be specified by $\mu = 1$. The value of μ will then be equal to the number of nodes between the center of the duct and the

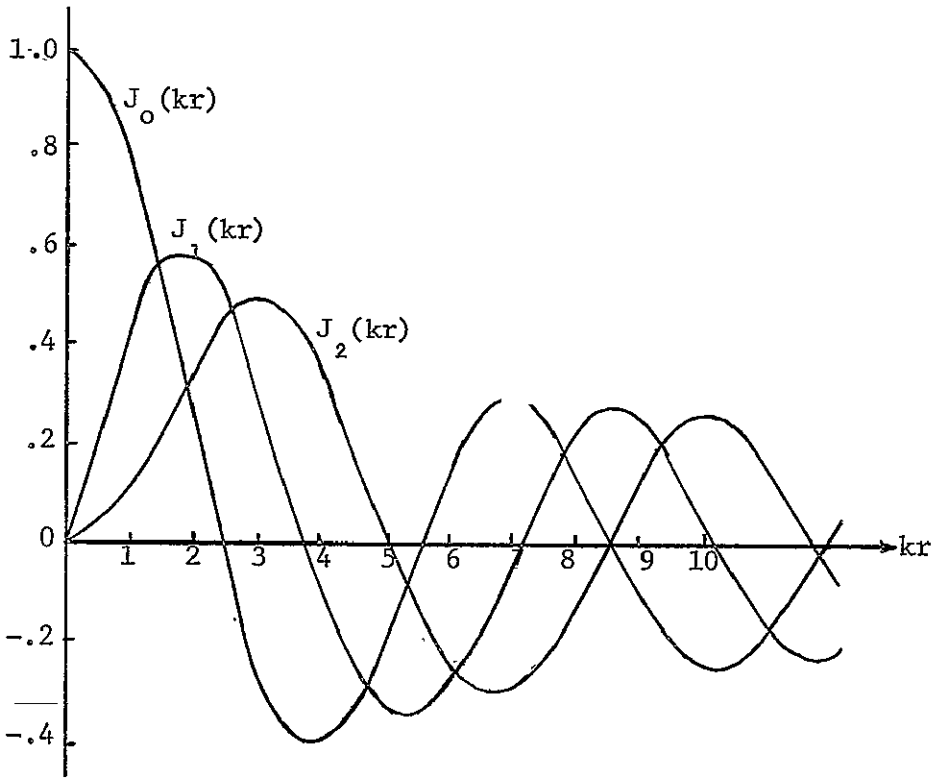

Figure 2.1 Properties of Bessel Functions of the First Kind of Integer Order $J_m(kr)$

TABLE 2.1

Zeros of Derivatives of the Bessel Functions $J_m(x)$

μ	m = 0	m = 1	m = 2	m = 3
1	0	1.8412	3.054	4.201
2	3.832	5.3314	6.706	8.015
3	7.016	8.5363	9.970	16.346
4	10.174	11.7060	13.170	14.586

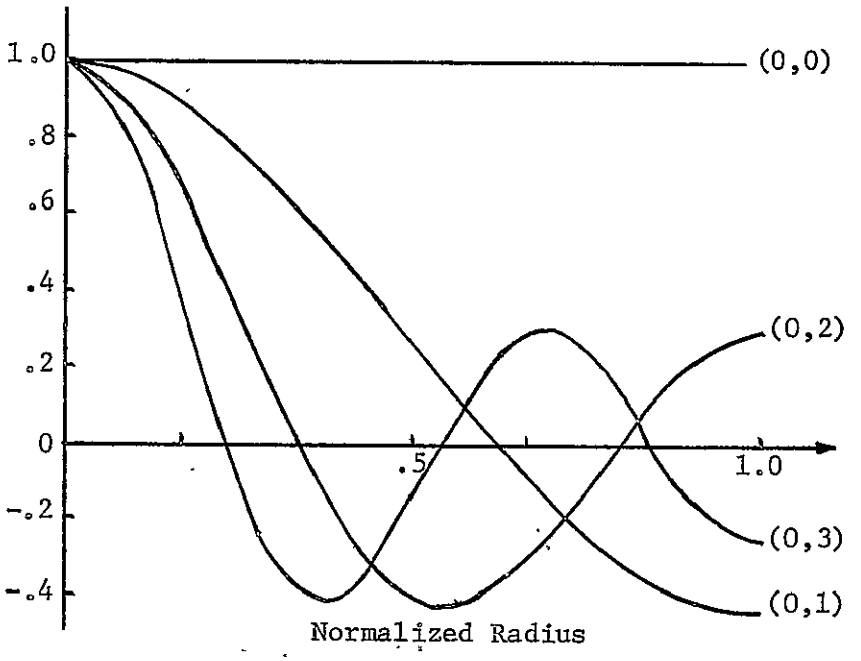

Figure 2.2 Radial Mode Shapes for m = 0 Modes

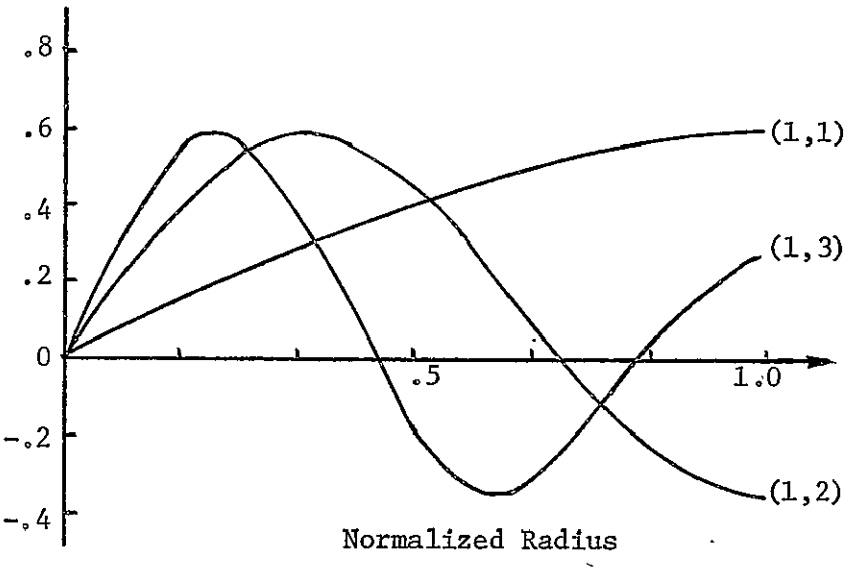

Figure 2.3 Radial Mode Shapes for m = 1 Modes

duct wall.

The analysis of radial mode shapes indicates that three distinct types of modes exist. First, there is a plane wave which has no radial or circumferential dependence. Second, there are higher order modes for m = 0 which have radial, but no circumferential, dependence. These modes have a maximum at the origin and one or more nodes between r = 0 and r = b, the duct wall. Third, there are modes for m = 1, 2, 3, . . . which have radial, as well as circumferential, dependence. These modes have a node at r = 0 and μ = 1 nodes in the region from the center to the duct wall. Due to the circumferential phase dependence, these waves are called spinning or spiral modes.

The wavenumber in the axial direction given by Equation 2.22 must be examined for three important cases. A dimensional wavenumber will be considered in order to determine the relationship of this parameter to the free space wavenumber and the frequency. Thus

$$k_z = k\Omega = \sqrt{k^2 - k^2_{m\mu}} \tag{2.23}$$

and

$$k_{m\mu} = \lambda_{m\mu} k \tag{2.24}$$

When $k^2 = k^2_{m\mu}$, the cut-off frequencies, f_c, for each of the higher order modes of the duct are determined by

$$f_c = \frac{c\, k_{m\mu}}{2\pi} \tag{2.25}$$

These cut-off frequencies are plotted as a function of frequency for a 12 inch diameter duct in Figure 2.4. When $k^2 > k^2_{m\mu}$, the driving frequency is above the cut-off frequency of a particular mode and the

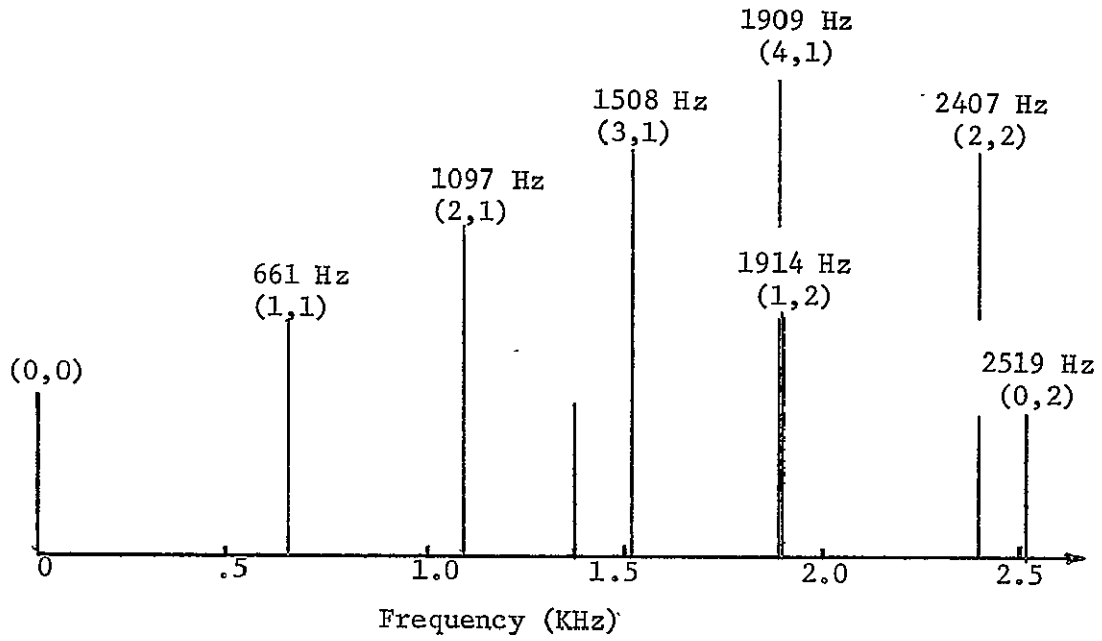

Figure 2.4 Cut-off Frequencies for Higher Order Modes in a 12 inch Diameter Duct

quantity under the radical is positive. Thus, k_z is real and there is undamped wave propagation. When $k^2 < k^2_{m\mu}$, the driving frequency is below the cut-off frequency and the expression under the radical is negative. Therefore, k_z is an imaginary quantity and represents exponentially damped wave propagation. Regions exist in Figure 2.4 where only a few modes can propagate and where several modes can propagate simultaneously. Therefore, the modal distribution in a duct will depend on frequency, duct diameter, and the phase and amplitude characteristics of the source exciting sound waves in the duct.

2.3 Acoustic Materials

There are several different sound absorbing materials available for applications as duct liners. These can be roughly grouped into three categories -- porous materials with or without facings, sintered fiber metals with an air cavity backing and Helmholtz resonators which include perforated panels with air cavity backings. Porous materials in general exhibit rather uniform absorption characteristics over a broad frequency range. Representative samples of this type of material include glass fiber materials and polyurethane foams. The use of these materials, however, is often restricted under adverse environmental conditions. In these cases, fiber metals and perforated panels are often used. For each of these sound absorbers, the material parameters or cavity depths may be modified so that maximum absorption can be tuned to a desired frequency range.

This section will describe how the acoustic characteristics of these three types of materials depend on the material properties. The materials considered included a sintered fiber metal material and a perforated sheet metal both with air cavity backings and a glass fiber material. A complete description of the physical properties of each material can be found in Section 3.6.

The acoustic properties of a material are commonly defined by the specific normal impedance Z which is the ratio of the pressure to the normal particle velocity at the surface. Unless otherwise noted, the term "impedance" as used in this study, will refer to the specific normal impedance defined above and have the dimensions of Nt-sec/m^3 or MKS rayls. If the pressure and velocity are out of phase, the impedance will be complex, having a real and imaginary component. The

impedance of a material can be predicted by theory and is a function of frequency, material properties and thickness, and mounting conditions. All of the materials considered in this study will have a rigid backing as a mounting condition.

An important physical property of a material is the specific flow resistance. This is defined as the pressure drop across the specimen divided by the particle velocity of air through and perpendicular to the face of the material. For bulk or porous materials, the specific flow resistance per unit thickness is commonly used. The flow resistance is essentially constant within a range of flow rates corresponding to moderate acoustic levels. Above this range, it increases rapidly with increasing values of velocity. Throughout this study, only moderate acoustic levels will be considered and the flow resistances will be considered constant.

The sintered fiber metal material with an air cavity backing is shown in Figure 2.5. Kilmer (5) has shown that the acoustical performance of a fiber metal can be determined from the flow resistance R_f and the cavity depth d. The normalized impedance for this combination is given by

$$\frac{Z}{\rho c} = R_f + i \cot(kd) \qquad (2.26)$$

Thus, the resistive component of the impedance is controlled solely by the flow resistance. The impedance and thus the absorption characteristics of this material can be tuned to a desired frequency range by changing the flow resistance and cavity depth.

Zwikker and Kosten (6) have shown that a perforated sheet metal with a cavity backing is a form of Helmholtz resonator. For the con-

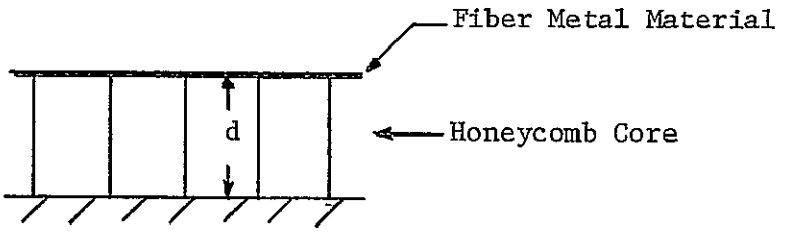

Figure 2.5 Fiber Metal Material with
Air Cavity Backing

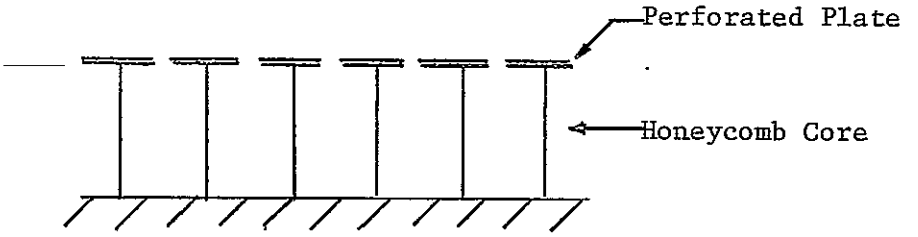

Figure 2.6 Perforated Panel with
Resonant Cavities

figuration of cavities and orifices shown in Figure 2.6, the normalized impedance is

$$\frac{Z}{\rho c} = \frac{1}{n_1} [R_t + i(\omega M_t - \frac{1}{\omega C_t})] \qquad (2.27)$$

where n_1 is the number of perforations per unit surface, M_t is the total mass of fluid vibrating in the perforation together with end corrections for the mass on each side, C_t is the compliance of the air in the cavity, and R_t is the acoustic resistance. The acoustic resistance is the sum of the radiation resistance of the perforation given by Kinsler and Frey (7) and the loss due to viscous flow through the perforation given by Morse and Ingard (8). The compliance is the major part of the reactance term at low frequencies.

Glass fiber materials and polyurethane foams can be modeled as a porous material with a flow resistance per unit thickness, R_f. For a material of thickness d and porosity P, the normalized impedance given by Beranek (9) is

$$\frac{Z}{\rho c} = \frac{G}{P} \coth[-i \frac{\omega}{c} Gd] \qquad (2.28)$$

where

$$G = (1 + \frac{i R_f}{\rho \omega}) P^{1/2}$$

The normal incidence absorption coefficient is a measure of the incident acoustic energy absorbed by a material. This can be determined from the impedance expressions given previously. The absorption coefficient α is related to the complex impedance by the following expression

$$\alpha = \frac{4R\rho c}{(R + \rho c)^2 + X^2} \tag{2.29}$$

where R and X are the real and imaginary components of the impedance. The absorption coefficient, however, has no direct relationship to the acoustic performance of a material as a duct liner. This behavior is related to the axial wavenumber and the eigenvalues given as solutions to the proper boundary conditions.

2.4 Acoustic Propagation in a Lined Duct

When a duct is lined with sound absorbing material, the boundary condition and the corresponding eigenvalues change from those given for a hard-walled duct. It will be assumed that the lining is locally reacting and the behavior of the material is completely determined by its normal impedance. The specific normal impedance is defined as the ratio of the pressure to the normal particle velocity at the surface of the material. If the pressure and velocity are out of phase, the impedance will be complex, having a real and imaginary part. Thus

$$Z = \frac{p}{v} = R - iX \tag{2.30}$$

In terms of an admittance $\beta = \frac{\rho c}{Z}$ the boundary condition becomes

$$\frac{1}{\beta} = \frac{p}{-i \nabla p} \tag{2.31}$$

Using Equation 2.21, the complete expression is

$$\beta bi \, J_m'(\lambda b) - m \, J_m(\lambda b) + \lambda b \, J_{m+1}(\lambda b) = 0 \tag{2.32}$$

For a complex admittance, the eigenvalues that are solutions to this equation will also be complex. Again, there are an infinite number of these eigenvalues for a particular m. Unlike the hard wall case, there is no cut-off frequency between successive modes.

In addition, if $\lambda_{m\mu}$ is complex, then the wavenumber in the axial direction $\Omega_{m\mu}$ given by Equation 2.22 will also be complex. Thus

$$\Omega_{m\mu} = \sigma + i \tau \tag{2.33}$$

For a lined duct, an individual mode will then have the following longitudinal pressure dependence

$$p_z = e^{i\Omega z} = e^{i\sigma z}\ e^{-\tau z} \qquad (2.34)$$

In this case, τ represents a damping term with the pressure decreasing exponentially with increasing z. Therefore, liner attenuation for an individual mode in an infinitely lined duct is given by

$$20 \log_{10} e^{-\tau z} = -8.69\ \tau z \qquad (2.35)$$

The location of the complex eigenvalues given by the local reaction boundary condition and Equation 2.32 will be discussed in a leter section.

It is often questioned whether the local reaction boundary condition adequately describes the acoustic interaction at the surface of a duct liner and whether it is appropriate for certain materials. This boundary condition assumes that the velocity at the surface depends only on the acoustic impedance and on the local pressure. It is generally considered valid for materials containing compartmented cavities which are isolated from each other. Examples of these types of duct liners include perforated panels with separated air cavity backings and materials backed by a closed cell honeycomb core cavity. The local reaction boundary condition is then a valid assumption when these materials are used as duct liners.

The local reaction boundary condition is not always valid for duct liners of porous materials. When an acoustic wave propagates through a duct containing this type of liner, part of the acoustic energy is transmitted through the liner itself. Therefore, the velocity at the surface depends on the combined actions of the propagating waves inside and outside the lining and cannot be merely expressed in terms of an

impedance and pressure at the surface. To determine the wavenumber and attenuation for a mode propagating in a duct with a porous material liner, the pressure and velocity must be matched at the interfaces between the air space and liner. This introduces the extended reaction boundary condition.

This boundary condition is reduced to the simultaneous solution of the wave equations within the air space and lining subject to proper continuity conditions. If the porous lining material is considered homogeneous and isotropic, acoustic propagation in the medium is assumed to satisfy the wave equation. This wave equation has a complex wavenumber h which defines attenuation of a wave propagating in the material in terms of real and imaginary components h_1 and h_2. The complex wavenumber h' and the complex density ρ' of the liner can be determined from bulk measurements of the material as explained by Scott (10). An alternative approach given by Pyett (11) compares standing wave tube measurements for samples of two different thicknesses to determine these parameters and is recommended for simplicity.

For the lined circular duct in Figure 2.7, the velocity potentials within the air space U and within the liner V must satisfy the following wave equations.

$$(\nabla^2 + k^2)\, U = 0 \tag{2.36}$$

$$(\nabla^2 + h^2)\, V = 0 \tag{2.37}$$

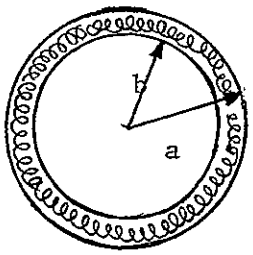

Figure 2.7 Duct Lined With Porous Material

In terms of a velocity potential $\overline{U}$, the pressure and velocity of a medium are given by

$$p = -i\,\omega\,\rho\,U$$

$$\overline{v} = -\,\overline{\nabla}\,U$$

where ρ is the density of the medium. The conditions to be satisfied specify that the pressure be finite at the origin, the velocity normal to the hard wall of the duct is zero, and the velocity and pressure must be continuous at the surface of the lining. These become

1) $p \rightarrow$ Finite at $r = 0$

2) $-\frac{\partial V}{\partial r} = 0$ at $r = a$

3) $-\frac{\partial U}{\partial r} = -\frac{\partial V}{\partial r}$ at $r = b$.

4) $-i\,\omega\,\rho_o U = -i\,\omega\,\rho'\,V$

For any mode of propagation along the duct, both U and V will have the same propagation constant Γ

$$U = U(r, \Theta)\; e^{i\Gamma z}\; e^{-i\omega t} \qquad (2.38)$$

$$V = V(r, \theta)\ e^{i\Gamma z}\ e^{-i\omega t} \tag{2.39}$$

Because of condition 1, the radial dependence of U within the air space will be defined only in terms of Bessel Function of the first kind, J_m. Within the liner, the radial dependence of V is given by Bessel Functions of the first and second kind, J_m and Y_m. All of the Bessel functions are of integer order due to the circumferential dependence of θ. Substituting Equations 2.38 and 2.39 in the wave Equations 2.36 and 2.37 and solving the wave equations subject to conditions 2, 3 and 4 yields

$$\begin{aligned}
&\rho_o J_m(\lambda b)\ [\{\tfrac{m}{b} J_m(\mu b) - \mu J_{m+1}(\mu b)\}\ \{\tfrac{m}{a} Y_m(\mu a) - \mu Y_{m+1}(\mu a)\} \\
&\quad - \{\tfrac{m}{b} Y_m(\mu b) - \mu Y_{m+1}(\mu b)\}\ \{\tfrac{m}{a} J_m(\mu a) - \mu J_{m+1}(\mu a)\}] \\
&\quad = \rho'\ \{\tfrac{m}{b} J_m(\lambda b) - \lambda J_{m+1}(\lambda b)\}\ [J_m(\mu b)\ \{\tfrac{m}{a} Y_m(\mu a) \\
&\quad - \mu Y_{m+1}(\mu a)\} - Y_m(\mu b)\ \{\tfrac{m}{a} J_m(\mu a) - \mu J_{m+1}(\mu b)\}]
\end{aligned} \tag{2.40}$$

where $\lambda^2 = k^2 - \Gamma^2$ and $\mu^2 = h^2 - \Gamma^2$. This equation gives the propagation constant of a mode in terms of the duct dimensions and material parameters. It is now necessary to determine whether this equation or the equation for the local reaction boundary condition predict proper attenuation for a duct liner of porous material.

Scott (12) developed a simplified equation corresponding to Equation (2.40) for a two-dimensional duct. When compared to the equation for the local reaction boundary condition, this equation will

yield the same values of propagation constant when $h^2 >> \Gamma^2$. This means that the attenuation constant and phase constant of the bulk lining material must be much greater than the attenuation constant and phase constant associated with the mode. When these conditions are satisfied, the results for the extended reaction boundary condition approximate the results given by the local reaction boundary condition.

Since the solution of Equation 2.40 is difficult, it is important to investigate conditions under which the local reaction boundary condition is valid for a porous liner material. The condition that $h^2 >> \Gamma^2$ stipulates that the attenuation in the duct must be substantially less than that in the bulk material and the velocity of propagation of a given mode in the duct must be much higher than that of the bulk material. For common glass fiber materials and mineral wools, the assumption is generally valid for wide air passages with diameters greater than 6 inches according to Scott.

Wyerman (13) has experimentally measured the attenuation constant and phase constant for several glass fiber materials of different densities using Pyett's two sample methods (11). Figure 2.8 shows a comparison between the attenuation and phase constants for a bulk glass fiber material and for the first radial mode of propagation of various circumferential orders in a 12 inch diameter duct lined with a one inch thick glass fiber material. For the propagating modes, these parameters were determined from the measured impedance and the local reaction boundary condition. Throughout the frequency range, the attenuation and phase constants are consistently less for the propagating modes than for the bulk material. These same parameters are shown in Figure 2.9 for the second radial mode of propagation. The phase constant for the

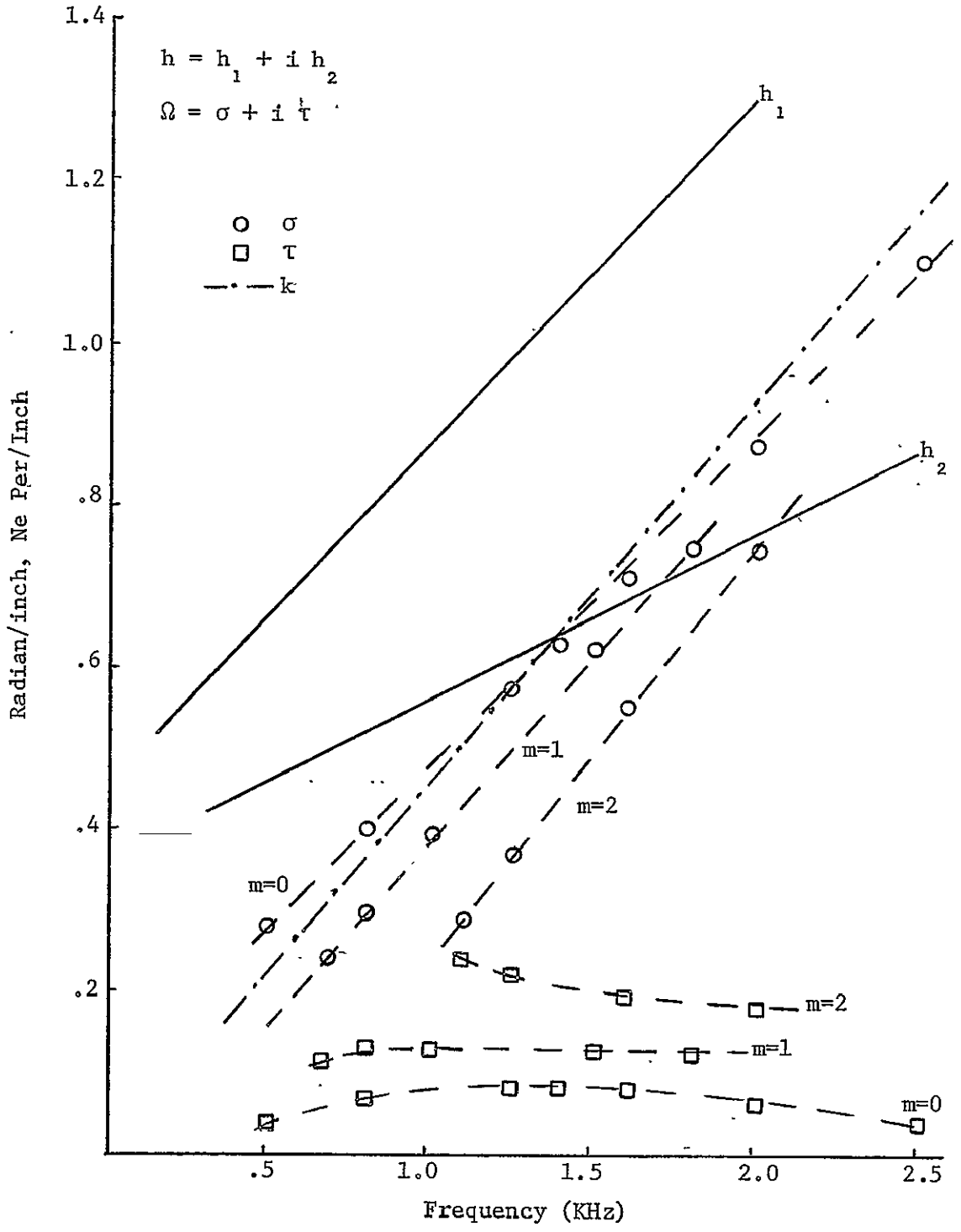

Figure 2.8 Complex Propagation Constants for Bulk Glass Fiber Material (h) and for the First Radial Mode (Ω) Propagating in a Duct Lined with One Inch Glass Fiber Material

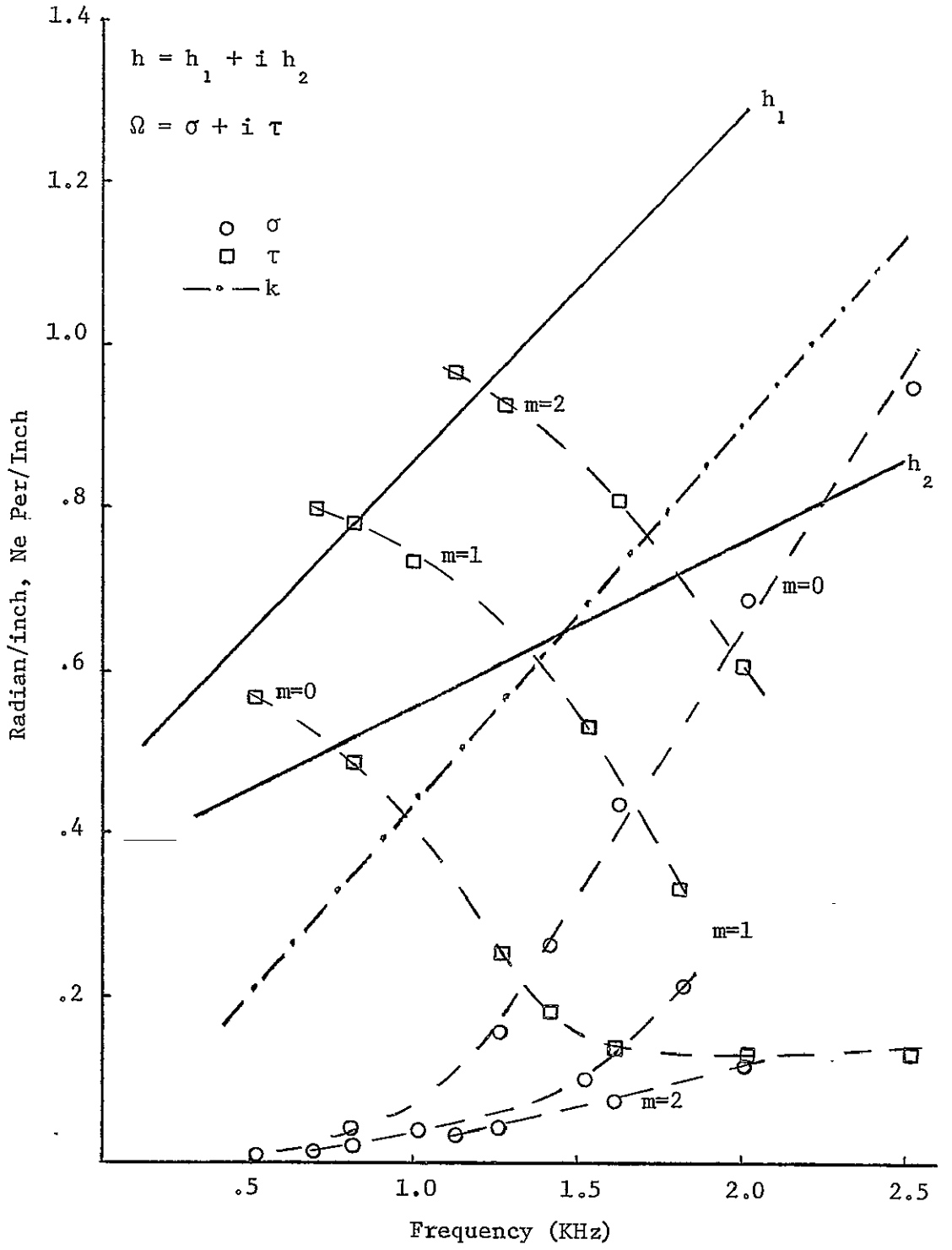

Figure 2.9 Complex Propagation Constants for Bulk Glass Fiber Material (h) and for the Second Radial Mode (Ω) Propagating in a Duct Lined with One Inch Glass Fiber Material

propagating mode is still less than that for the bulk material, but the value of the attenuation constant for each mode varies with respect to that for the material throughout the frequency range. The attenuation constant of the bulk material ranges from 40 to 75 dB/ft which is greater than the attenuation realized by the application of these materials as duct liners. Thus, for moderate attenuation, the assumption of a local reaction boundary condition seems valid for the glass fiber material duct liner.

Scott has outlined the proper boundary conditions for duct liners of glass fiber materials for two cases. For densely packed liner materials inserted in a duct with a diameter much greater than the free space wavelength, the application of the local reaction boundary condition is valid. When a duct lining contains a loosely packed material or when the air space in the duct is small compared with a wavelength, the extended reaction boundary condition must be considered.

2.5 Multisectioned Duct Theory

Duct liners are used as a means of attenuating sound along a path between a source and a receiver. For an infinite liner, the attenuation of an individual mode is given by Equation 2.35. However, in many situations, the duct is not infinitely lined but instead contains several finite sections of different liner materials. At the interface between two different duct sections, an impedance discontinuity exists and an incident acoustic wave will then be partially reflected and partially transmitted. Therefore, the infinite duct solution must be modified to account for these effects. Zorumski's multisectioned duct theory, presented in general form in Reference 3, will be applied to a hollow duct with no flow. Relationships will be developed to account for the acoustic coupling between sections. In this manner, the sound field may be defined everywhere throughout a complex duct system.

Characteristic functions $\Psi_{m\mu}(r)$ are chosen for the radial dependence of the sound field and are normalized so that

$$\int_0^b r\, \Psi_{m\mu}^2(r)\, dr = 1 \tag{2.41}$$

The characteristic functions for a hollow duct are defined in terms of the Bessel functions $J_m(\lambda_{m\mu} r)$ given by Equation 2.21. These are

$$\Psi_{m\mu}(r) = \frac{J_m(\lambda_{m\mu} r)}{N_{m\mu}} \tag{2.42}$$

where

$$N_{m\mu}^2 = \int_0^b r\, J_m^2(\lambda_{m\mu} r)\, dr$$

$$= \frac{b^2}{2} \qquad m = 0,\ \mu = 0 \tag{2.43}$$

$$= \frac{1}{2}\left[(b\lambda_{m\mu})^2 - m^2 - (\beta b)^2\right] \frac{J_m^2(\lambda_{m\mu} b)}{\lambda_{m\mu}^2} \qquad m \neq 0,\ \mu \neq 0$$

Furthermore, the characteristic functions are also orthogonal. Thus

$$\int_0^b r\, \Psi_{m\mu}(r)\, \Psi_{m\nu}(r)\, dr = 0 \quad \mu \neq \nu \tag{2.44}$$

For a uniform duct section containing the plane z^j shown in Figure 2.10, the acoustic field may be expressed as the sum of incident and reflected modes. Limiting consideration to circumferential harmonics, the subscript m will be eliminated after this point and the sound field can be expressed by

$$P_m(r, z) = \sum_{\mu=0}^{\infty} [A_\mu^{+j}\, \Psi_\mu^{+j}(r)\, e^{i\Omega_\mu^{+j}(z - z^j)}\, A_\mu^{-j}\, \Psi_\mu^{-j}(r)\, e^{i\Omega_\mu^{-j}(z-z^j)}] \tag{2.45}$$

This equation is known as the acoustic field equation. The coefficient A_μ^{+j} and A_μ^{-j} are the modal amplitudes of acoustic waves at z^j traveling in the positive and negative directions respectively. The negative sign in front of A_μ^{-j} has been introduced so that the reflection coefficient will have a positive real part. Although there are an infinite number of eigenvalues, the summation over μ in Equation 2.45 will be truncated to a finite number of terms. Written in matrix notation, this equation becomes

$$\begin{aligned} p_m(r,z) = {} & \left\lfloor \Psi_\mu^{+j}(r) \right\rfloor \left[\delta_{\mu\nu}\, e^{i\Omega_\mu^{+j}(z-z^j)} \right] \{A_\mu^{+j}\} \\ & - \left\lfloor \Psi_\mu^{-j}(r) \right\rfloor \left[\delta_{\mu\nu}\, e^{i\Omega_\mu^{+j}(z-z^j)} \right] \{A_\mu^{-j}\} \end{aligned} \tag{2.46}$$

Furthermore, it is obvious that

$$\lambda_\mu^{+j} = \lambda_\mu^{-j} \tag{2.47}$$

$$\Omega_\mu^{+j} = -\Omega_\mu^{-j} \tag{2.48}$$

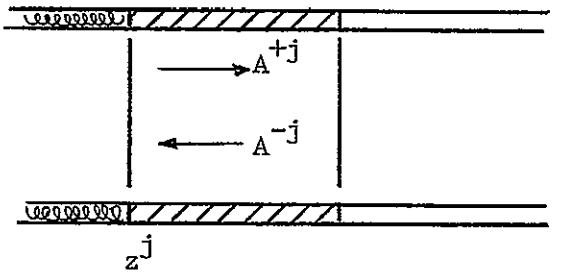

Figure 2.10 Sound Field in Multisectioned Duct

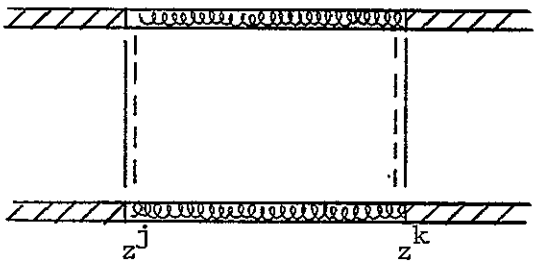

Figure 2.11 Uniform Duct Section

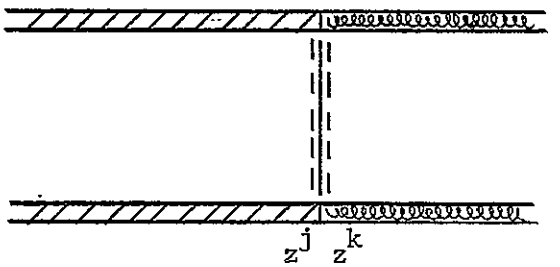

Figure 2.12 Admittance Discontinuity Between Sections

For a duct containing several different sections, planes are introduced at the interface between each section. The acoustic field can then be described everywhere in the duct in terms of the modal amplitude at each interface. If there are N planes, then there must be 2N sets of equations relating these amplitudes. These relationships are described by transmission and reflection matrices $T_{\mu\nu}^{+j+k}$ and $R_{\mu\nu}^{+j+k}$ which describe the coupling between amplitudes of an (m,μ) and an (m,ν) mode between the planes j and k.

As a simple example, the uniform duct section shown in Figure 2.11 will first be considered. Within this section, solutions to the wave equation are used to determine transmission and reflection relationships. Since there are no reflections in a uniform duct, the reflection matrix is the null matrix

$$[R_{\mu\nu}^{\pm j\pm k}] = [0] \tag{2.49}$$

The transmission characteristics within a uniform duct are given by the exponential dependence in Equation 2.45. Therefore, the transmission matrix is

$$[T_{\mu\nu}^{\pm j+k}] = [\delta_{\mu\nu}\, e^{i\Omega_{\mu}^{\pm j}\,(z_k - z_j)}] \tag{2.50}$$

The positive sign is used when $z^k > z^j$ and the negative sign is used for $z^k < z^j$.

The relfection and transmission matrices for an admittance discontinuity in the duct can be determined by matching the pressure and axial velocities at the interface. In Figure 2.12, planes z^j and z^k are chosen an infinitesimal distance apart. The axial velocity is related to the pressure throughout Equation 2.14 in the following manner

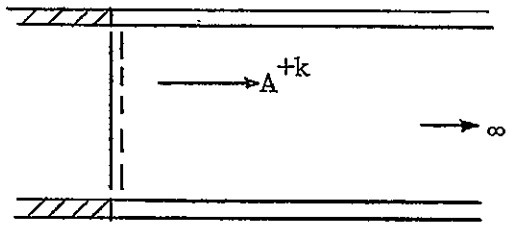

A) Anechoic Termination

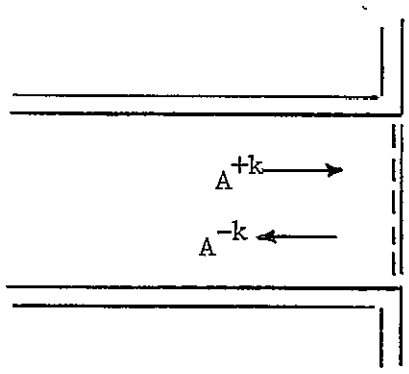

B) Flanged Termination

Figure 2.13 Duct Termination Planes

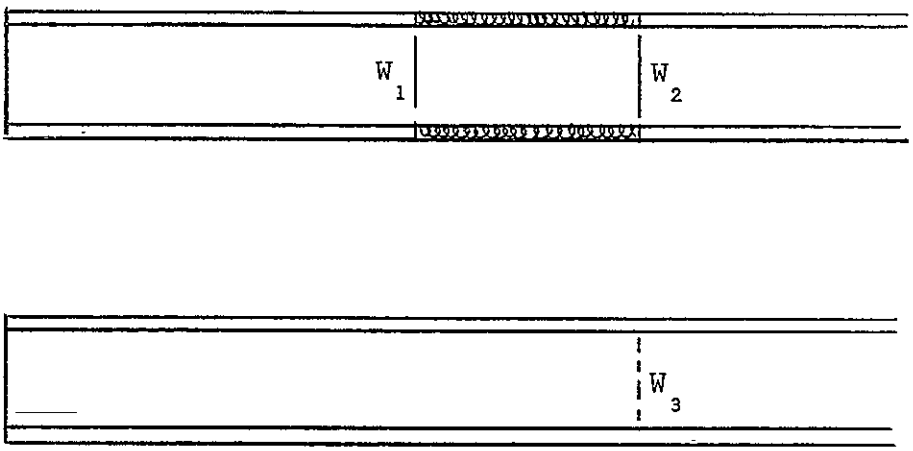

Figure 2.14 Sound Power for Insertion Loss and Transmission Loss

$$v_z = -i\frac{\partial p}{\partial z} \tag{2.51}$$

This dependence can be expressed in terms of an axial modal admittance matrix $[\beta_\mu]$ which has the form

$$[\beta_\mu] = [\Omega_\mu] \tag{2.52}$$

Continuity of pressure and velocity on each side of the interface in Figure 2.12 yields the following equations

$$\lfloor \Psi_\nu^{-j}(r) \rfloor \, [\beta_\nu^{-j}] \cdot \{A_\nu^{-j}\} + \lfloor \Psi_\nu^{+j}(r) \rfloor \, [\beta_\nu^{+k}] \cdot \{A_\nu^{+k}\}$$

$$= \lfloor \Psi_\nu^{+j}(r) \rfloor \, [\beta_\nu^{+j}] \, \{A_\nu^{+j}\} + \lfloor \Psi_\nu^{-k}(r) \rfloor \, [\beta_\nu^{-k}] \, \{A_\nu^{-k}\} \tag{2.53}$$

$$\lfloor \Psi_\nu^{-j}(r) \rfloor \, \{A_\nu^{-j}\} + \lfloor \Psi_\nu^{+k}(r) \rfloor \, \{A_\nu^{+k}\}$$

$$= \lfloor \Psi_\nu^{+j}(r) \rfloor \, \{A_\nu^{+j}\} + \lfloor \Psi_\nu^{-k}(r) \rfloor \, \{A_\nu^{-k}\} \tag{2.54}$$

The terms in these equations have been arranged so that the left hand side contains waves traveling out of the region between the two planes and the right hand side contains waves traveling into this region. The $\Psi_\mu^{+j}(r)$ term can be eliminated by utilizing the orthogonality properties of the modes. Multiplying Equation 2.53 by $r\{\Psi_\mu^{-j}(r)\}dr$ and Equation 2.54 by $r[\beta_\mu^{-j}] \, \{\Psi_\mu^{-j}(r)\}dr$ and integrating each equation from $r = 0$ to $r - b$ results in

$$[I_{\mu\nu}^{-j-j}]\ [\beta_{\nu}^{-j}]\ \{A_{\nu}^{-j}\} + [I_{\mu\nu}^{-j+k}]\ [\beta_{\nu}^{+k}]\ \{A_{\nu}^{+k}\}$$

$$= [I_{\mu\nu}^{-j+j}]\ [\beta_{\nu}^{+j}]\ \{A_{\nu}^{+j}\} + [I_{\nu}^{-j-k}]\ [\beta_{\nu}^{-k}]\ \{A_{\nu}^{-k}\} \tag{2.55}$$

$$[I_{\mu\nu}^{-j-j}]\ \{A_{\nu}^{-j}\} + [I_{\mu\nu}^{-j+k}]\ \{A_{\nu}^{+k}\}$$

$$= [I_{\mu\nu}^{-j+j}]\ \{A_{\nu}^{+j}\} + [I_{\mu\nu}^{-j-k}]\ \{A_{\nu}^{-k}\} \tag{2.56}$$

The term

$$[I_{\mu\nu}^{jk}] = {}_{o}\int^{b} r\ [\{\Psi_{\mu}^{j}(r)\}\ [\Psi_{\nu}^{k}(r)]]dr \tag{2.57}$$

is called the integral matrix and the elements are given by

$$I_{\mu\nu}^{jk} = \frac{i\ b\Psi_{\mu}^{j}(b)\ \Psi^{k}{}_{\nu}(b)}{\Omega^{j^2} - \Omega^{k^2}}\ [\beta^{j} - \beta^{k}] \tag{2.58}$$

and

$$\begin{aligned} I_{\mu\nu}^{jj} &= 1 \quad \mu = \nu \\ I_{\mu\nu} &= 0 \quad \mu \neq \nu \end{aligned} \tag{2.59}$$

Thus, $[I_{\mu\nu}^{jj}]$ is an identity matrix and can be excluded in the following notation.

The amplitudes $\{A_{\nu}^{-j}\}$ can be eliminated from Equations 2.55 and 2.56 by operating on these equations with the proper matrices. These operations are expressed by matrices of the form $[W_{\mu\nu}^{jk}]$ amd the resulting equation is

$$[W_{\mu\nu}^{-j+k}]\ \{A_{\nu}^{+k}\} = [W_{\mu\nu}^{-j+j}]\ \{A_{\nu}^{-j}\} + [W_{\mu\nu}^{-j-k}]\ \{A_{\nu}^{-k}\} \tag{2.60}$$

The matrix $[W_{\mu\nu}^{k}]$ has the following form

$$[W_{\mu\nu}^{jk}] = [I_{\mu\nu}^{jk}]\ [\beta_{\nu}^{k}] - [\beta_{\mu}^{j}]\ [I_{\mu\nu}^{jk}] \tag{2.61}$$

where

$$W_{\mu\nu}^{jk} = \frac{i\, b\, \psi_{\mu}^{j}(b)\ \psi_{\nu}^{k}(b)}{\Omega_{\mu}^{j} + \Omega_{\nu}^{+k}}\ [\beta^{k} - \beta^{j}] \tag{2.62}$$

Furthermore, the matrix $[W_{\mu\nu}^{+j-j}]$ is a diagonal matrix with elements given by

$$W_{\mu\nu}^{+j-j} = 2\ \delta_{\mu\nu}\Omega_{\nu}^{-j} \tag{2.63}$$

Multiplying Equation 2.60 by $[W^{-j+k}]^{-1}$ gives

$$\{A_{\nu}^{+k}\} = [R_{\mu\nu}^{+k-k}]\ \{A_{\nu}^{-k}\} + [T_{\mu\nu}^{+k+j}]\ \{A_{\nu}^{+j}\} \tag{2.64}$$

where the reflection and transmission matrices are

$$[R_{\mu\nu}^{+k-k}] = [W_{\mu\nu}^{-j+k}]^{-1}\ [W_{\mu\nu}^{-j-k}] \tag{2.65}$$

$$[T_{\mu\nu}^{+k+j}] = [W_{\mu\nu}^{-j+k}]^{-1}\ [W_{\mu\nu}^{-j+j}] \tag{2.66}$$

Thus, the amplitudes $\{A_{\nu}^{+k}\}$ are related to the amplitudes $\{A_{\nu}^{-k}\}$ by a reflection matrix and to the amplitudes $\{A_{\nu}^{+j}\}$ by a transmission matrix.

In a similar manner, $\{A_{\nu}^{+k}\}$ may be eliminated from Equations 2.53 and 2.54 so that

$$\{A_{\nu}^{-j}\} = [R_{\mu\nu}^{-j+j}]\ \{A_{\nu}^{+j}\} + [T_{\mu\nu}^{-j-k}]\ \{A_{\nu}^{-k}\} \tag{2.67}$$

In this case, the reflection and transmission matrices are given by

$$[R_{\mu\nu}^{-j+j}] = [W_{\mu\nu}^{+k-j}]^{-1}\ [W_{\mu\nu}^{+k+j}] \tag{2.68}$$

$$[T_{\mu\nu}^{-j-k}] = [W_{\mu\nu}^{+k-j}]^{-1} [W_{\mu\nu}^{+k-k}] \tag{2.69}$$

It is interesting to note the form of the reflection matrices given by Equations 2.65 and 2.68. Since $W_{\mu\nu}^{jk}$ in Equation 2.62 is proportional to the admittance changes in the duct, the reflection matrix is also proportional to the admittance changes.

Equations of the form of 2.64 and 2.67 can be written for each of the planes within a complex duct system of N sections. This will yield 2N-2 sets of equations. However, since there are 2N sets of unknown modal amplitudes, the number of unknowns will always exceed the number of equations. To complete the set of equations, radiation conditions must be specified at the duct termination planes.

Acoustic reflection and radiation from the end of the duct is dependent upon how the duct is terminated. For the infinite duct in Figure 2.13, there is no reflection from the end and

$$\{A_{\nu}^{-k}\} = \{0\} \tag{2.70}$$

If the duct is terminated with an open end as in Figure 2.13, the reflected component of the modal amplitude is given by

$$\{A_{\nu}^{-k}\} = [R_{\mu\nu}^{-k+k}] \{A_{\nu}^{+k}\} \tag{2.71}$$

For the cases of a flanged or unflanged open end, the radiation reflection matrices are known and given by Zorumski (14) and Lansing (15) respectively. These can also be used to compute far field radiation and directivity patterns.

At the duct inlet, the source distribution at a point (r_0, θ_0) can be represented as the product of a Dirac delta function and the source

strength Θ

$$V(r) = \frac{2\pi\ \Theta\ \delta(r-r_0)\ \partial(\Theta-\Theta_0)}{r} \tag{2.72}$$

Using the momentum equation, the acoustic field equation and the modal orthogonal relations, the radiation equation is defined by the following expression

$$\{A_\mu^{+j}\} = -\{A_\mu^{-j}\} + Q\{\frac{\psi_\mu^{+j}(r_0)\ e^{-im\Theta_0}}{\Omega_\mu^{+j}}\} \tag{2.73}$$

The source distribution and Equation 2.72 can be modified to account for an array containing several sources. The extension of this analysis to a complex source array will be described in a later section.

The previously described radiation and source matrices are combined with the transmission and reflection matrices for each duct section to yield a complete set of matrix equations for the wave amplitudes. A typical set of equations for a duct containing N sections is given by Equation 2.74. Solving this equation for the modal amplitudes at each interface, the pressure can be described everywhere in the duct by the acoustic field equation.

As a result of this analysis, the modal amplitudes for each section can be used to calculate the sound power level at positions throughout the duct. The intensity I at any point in the duct is given by

$$I = \frac{1}{2}\,Re\,(pv'') \tag{2.75}$$

where v'' is the complex conjugate of the velocity in the axial direction. The total sound power W can be determined by integrating the intensity over the cross-sectional area of the duct, and the sound power level is calculated with respect to a reference acoustic power level W_o of 10^{-12}

$$
\begin{bmatrix}
[I] & & & & [I] \\
-[T^{+2+1}] & [I] & & & \\
 & \ddots & & & \\
 & & -[T^{(N-1)(N-2)}] & [I] & -[R^{(N-1)(N-1)}] \\
 & & & -[T^{(N-1)(N-1)}] & [I] \\
 & & & [I] & -[T^{-1-2}] \\
 & -[R^{-2+2}] & & [I] & -[T^{-2-3}] \\
 & & & & \ddots \\
 & & & & [I] \quad -[T^{-(N-1)-N}] \\
 & & -[R^{-N+N}] & & [I]
\end{bmatrix}
\begin{Bmatrix}
\{A^{+1}\} \\
\{A^{+2}\} \\
\\
\\
\{A^{+N-1}\} \\
\{A^{+N}\} \\
\{A^{-1}\} \\
\{A^{-2}\} \\
\\
\\
\{A^{-(N-1)}\} \\
\{A^{-N}\}
\end{Bmatrix}
=
\begin{Bmatrix}
\{ Q \}
\end{Bmatrix}
\tag{2.74}
$$

Watts/m^2.

$$L_w = 10 \log_{10} \frac{W}{W_0} \tag{2.76}$$

The effectiveness of a duct liner can be measured by the transmission loss and the insertion loss. The transmission loss is the difference between the sound power level in front of and at the end of the liner. The insertion loss is the difference between the sound power level at the same point with and without the liner inserted in the duct. If the sound power levels are calculated at the positions in Figure 2.14, the transmission loss and insertion loss for a finite length liner are given respectively by

$$TL = 10 \log_{10} W_1 - 10 \log_{10} W_2 \tag{2.77}$$

$$IL = 10 \log_{10} W_3 - 10 \log_{10} W_2 \tag{2.78}$$

The insertion loss is helpful to describe the effectiveness of a liner in a particular application while the transmission loss defines attenuation properties of sound transmitted through the liner.

2.6 Eigenvalue Search Technique

Acoustic propagation through a duct in the axial direction is determined by the axial wavenumber. This parameter is related to eigenvalues which are solutions to the local reaction boundary condition given by Equation 2.32

$$\beta \, b i \, J_m(\lambda b) - m \, J_m(\lambda b) - \lambda . b \, J_{m+1}(\lambda b) = 0 \qquad (2.32)$$

Several methods have been developed for locating the eigenvalues for a circular duct.

For a hard-walled duct, the admittance is zero and the local reaction boundary condition reduces to Equation 2.20. In these cases, the eigenvalues are real and well ordered and can be found in tabulated form (4). Even if these values were not known, they could easily be determined using iteration techniques. This is because the eigenvalues are real and there is a one to one correspondence between the argument and the value of the Bessel function.

For a lined duct with a complex admittance β, the eigenvalues given by Equation 2.32 are complex. In this case it becomes difficult to observe the dependence between complex arguments and complex values of the Bessel functions. Therefore, iteration methods become more difficult and uncertain for values of complex admittance. Several alternate schemes have thus been devised. Fisher (16) has developed a series solution to the eigenvalue equation which converges for small admittance. Rice (17) has extended this technique for finding eigenvalues to include both large and small admittances. Similar approximations for very large or very small admittances are given by Morse and Ingard (8). Although this method yields reasonable estimates for

eigenvalues, these approximations on the admittances cannot be made for all materials.

Graphical techniques and nomograms are available for determining these eigenvalues (18, 8), but there are restrictions with these techniques. First, the accuracy is limited in choosing eigenvalues from graphical techniques and second, eigenvalues for only the first one or two radial modes are given by these methods. Thus, alternate methods must be examined for locating exact eigenvalues.

Benzakein (19) has transformed the boundary condition equation into a first-order nonlinear differential equation and then integrated it numerically to locate eigenvalues. Zorumski (20) has also used this differential equation method to solve for complex eigenvalues for a circular duct. This method maintains a one to one correspondence between eigenvalues on the real axis for $\beta = 0$ and the complex eigenvalues. The integration is started at the point $\beta = 0$ and the end points are related to the desired specific admittance.

As an alternative to these methods, a search technique using both contour integrations and an iteration technique was developed. This method locates eigenvalues in the complex plane for all values of admittance. This technique was based on the Principle of the Argument which is described in detail by Copson (21). This principle is stated by the following expression

$$\frac{1}{2\pi i} \int_C \frac{f'(z)}{f(z)}\, dz = p - q \qquad (2.79)$$

The left hand side of Equation 2.79 indicates an integration around a closed contour C in the complex plane. On the right hand side, p is the sum of the orders of zeroes within this contour and q is the sum of

the orders of poles. Since we are performing an integration around a closed contour, Equation 2.79 can be further simplified to

$$\frac{1}{2\pi} \left[\text{Arg } F(z)\right]_c = p - q \tag{2.80}$$

Now the number and order of zoeroes and poles can be determined by observing the change in the argument of the function around a closed contour and examining how many times the argument crosses the branch cut formed by the negative real axis.

This contour integration is effective in finding the boundaries of the roots of a function in the complex plane with no previous knowledge of the location or behavior of the roots. Once these boundaries have been defined, a first approximation can be chosen and an iteration technique used to locate the exact value of the root.

This same technique can be used in locating eigenvalue in the complex plane for a duct wall with an arbitrary complex admittance. Successive eigenvalues can be obtained by performing contour integrations around regions throughout the complex plane. The eigenvalue equation and the behavior of its roots must first be investigated.

Letting $K = \lambda b_{pil}$ the eigenvalue equation for the local reaction boundary condition becomes

$$F(K) = \beta bi\, J_m(K) - m\, J_m(K) + K\, J_{m+1}(K) \tag{2.81}$$

The eigenvalues are the zeroes of this function and are defined at values of K such that $F(K) = 0$. The location of these eigenvalues in the complex plane is determined by the properties and location of the wavenumber in the axial direction Ω. From Equation 2.18 we see that

for a progressive wave, Ω must be located in quadrant I of Figure 2.15, with $\sigma > 0$ and $\tau > 0$ in order that the wave be attenuated and not amplified as it propagates. Therefore, from Equation 2.22, λ is located in quadrant IV of Figure 2.15.

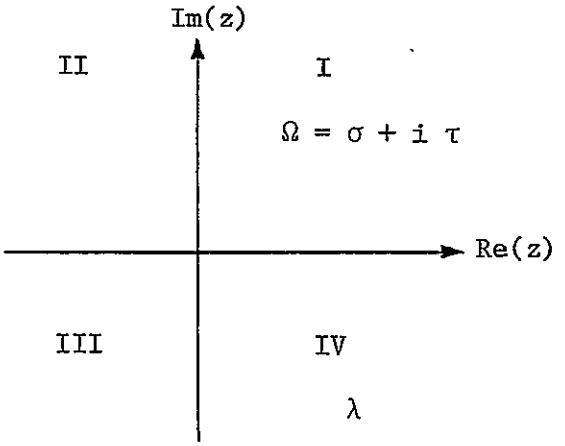

Figure 2.15 Quadrants for Locating Ω and λ

There is an additional eigenvalue $-\lambda$ located in quadrant II which also satisfies Equation 2.80. However, it is the morror image of the eigenvalue in quadrant IV and need not be considered by the search technique.

Now that the quadrant containing the successive eigenvalues has been located, integration contours can be defined. The integration contours chosen are shown in Figure 2.16 and are expanded outward from the origin in successive radial increments. The maximum radial increment between successive eigenvalues would be expected to be of the same order or less than the increments between successive eigenvalues for a hard-walled duct. However, since the increments between complex eigenvalues are not always clearly defined, these contours were expanded outward from the origin in radial increments of 1.0. Integrations are performed in the clockwise direction according to Equation 2.80. Each contour of integration was divided into 10 steps along the path in the radial

direction and into 23 steps along paths in the angular direction. When integration paths were near an eigenvalue that was located either within or exterior to the contour, additional subdivisions in step size were made.

Since there are no poles associated with Equation 2.32, the integration yields either zero or a positive number indicating the number of eigenvalues within the integration contour. When the results of the integration were zero, the contour was expanded radially from the origin and a further integration was performed with the new contour. When regions containing two eigenvalues were located, the contours were divided into smaller radial increments until a region containing only one root was obtained. Situations where two successive eigenvalues are located in proximity to each other are discussed by Zorumski (20). For certain specialized cases of admittance, the lowest eigenvalue coalesces with a higher eigenvalue to form a double eigenvalue. In this case, the double eigenvalue is a solution to Equation 2.32 and its derivative. The resulting eigenfunctions are orthogonal to themselves and are linearly amplified in addition to being attenuated at the expected rate. Admittance values producing double eigenvalues were neglected in this study.

Once the boundaries of a radial contour containing a single root are defined, additional divisions shown in Figure 2.16 were made in the angular direction. Integrations around these contours are performed to further define the boundaries of the region containing the eigenvalue. A first approximation to the eigenvalue was chosen at the center of the contour and the Newton Raphson Iteration Technique (22) was used to lcoate the eigenvalue to the required degree of accuracy.

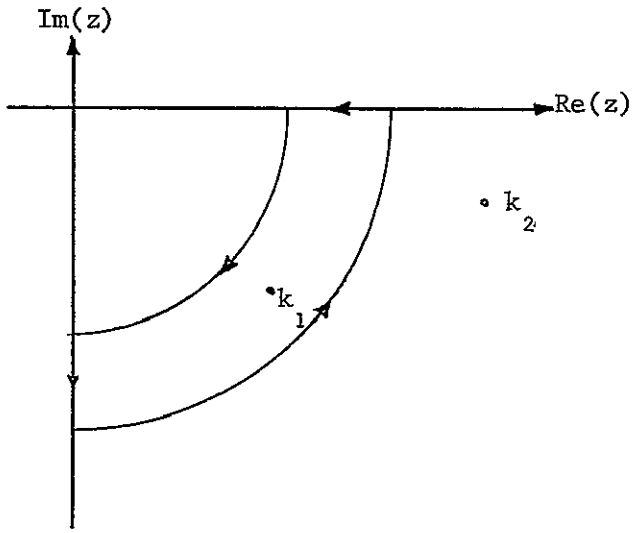

A) Increments in Radial Direction

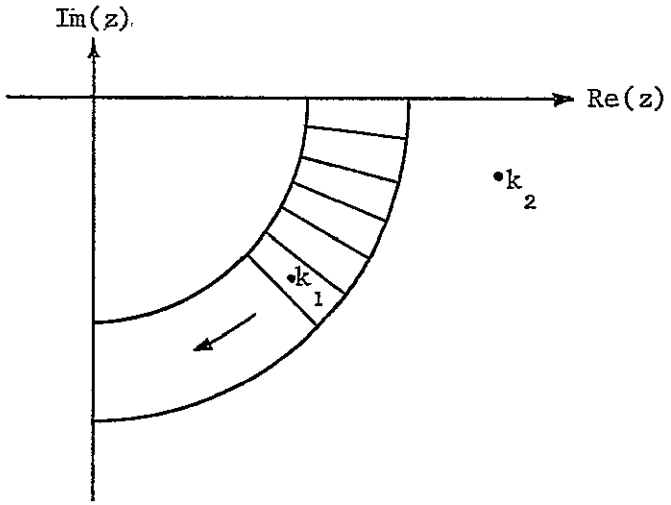

B) Increments in Angular Direction

Figure 2.16 Integration Contours

This method locates eigenvalues in successive radial increments outward from the origin. The correct order of these eigenvalues can be determined from examination since their real component is interlaced between the real zeroes of the Bessel Function and their derivatives the extreme cases for soft and hard walls respectively.

The complex eigenvalues describe both the attenuation of an individual mode through the liner and the radial mode shape. In addition, these parameters are needed to calculate coupling coefficients between modes at each interface of the multisectioned duct system.

CHAPTER III

EXPERIMENT

3.1 Introduction

To perform an experimental investigation of multisectioned duct theory, a simple configuration consisting of an anechoically terminated duct with three sections was chosen. Furthermore, since the eigenvalues and corresponding mode shapes for a hard-walled duct are well known, the beginning and end sections of the duct system had rigid walls. Between these two sections, liners of various materials were inserted and radial mode shapes were measured at various positions thsoughout the duct. Despite the fact that no flow was considered, the section in front of the liner will be called the upstream section and the section behind the liner will be called the downstream section. This terminology does not strictly define the direction of acoustic propagation in cases where flow exists. Flow can occur in a direction either with or against the direction of acoustic propagation. However, the effect of flow will not be considered in this study.

The remainder of this chapter will describe the duct system, the source array developed to generate higher order acoustic modes, the liner materials, and the measurement techniques used in this study.

3.2 Multisectioned Duct System

The complete duct system used in this experiment is shown in Figure 3.1. The hard-walled sections were made of commercially available cement pipe with a 12 inch inner diameter and a 5/8 inch wall thickness. The cement pipe was chosen to eliminate coupling between vibrations of the duct wall and the acoustic field. Although the diameter of the duct is 12 inches, there are deviations of up to ± 1/2 inch in the diameter at positions throughout its length. The effect of these variations on the radial mode shapes will be discussed in Section 3.3 The test section was also made of cement pipe with a 14 inch inside diameter. This section will accommodate one inch thick liners of different acoustic materials with no change in cross sectional area throughout the duct. Both the upstream section and test section were placed on moveable carriages. This arrangement facilitated the removal and replacement of liners and the alignment of the complete system for testing.

To eliminate acoustic reflection from the end of the duct, an anechoic termination was coupled to the downstream section. This arrangement simulates a semi-infinite duct. A flanged or unflanged open ended duct could have also been used in this experiment. However, since the open end causes reflection of an incident wave, the anechoic termination was chosen to reduce these reflections. The termination was made of hardened liquid fiberlass in the shape of a hollow cone. The cone was filled with glass fiber material with a density of 1.5 pounds per cubic foot. The construction of this termination was based on results provided by Carrier Corporation (23) for design of a termination for plane wave propagation within a duct. Before this termination was

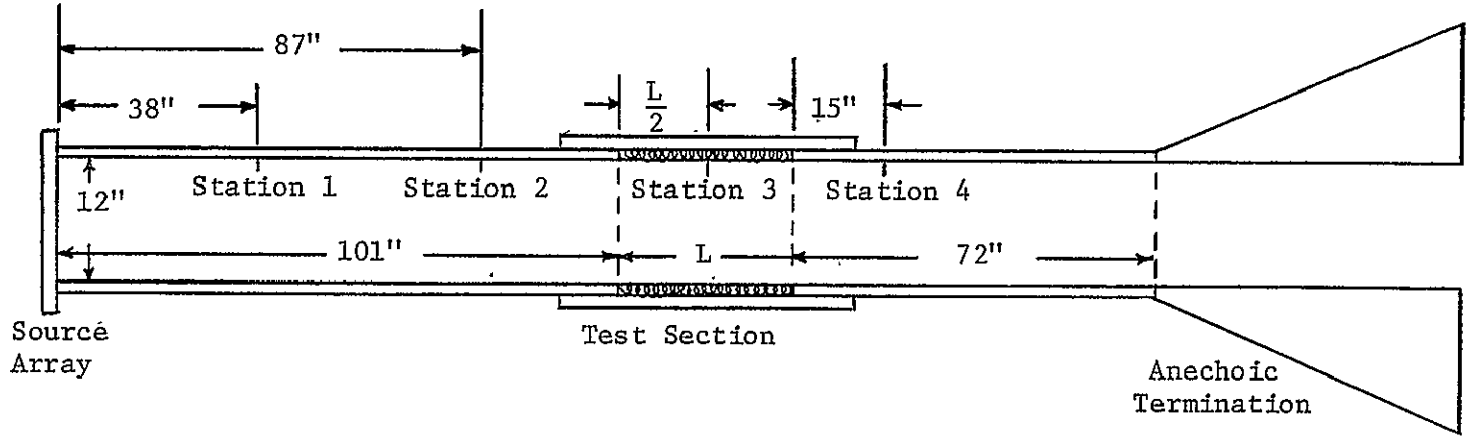

Figure 3.1 Experimental Duct System

chosen, the performance of several additional configurations to reduce acoustic reflection from the end of the duct were investigated. These included a glass fiber cone which was inserted in the end of the duct, wedges of glass fiber material also inserted in the duct, a sample of glass fiber material sealing the end of the duct, and the previously described anechoic termination with glass fiber wedges inserted in the end. The best performance was obtained with the termination and when the glass fiber wedges were inserted in the duct. However, as there was no significant difference between the results for these two configurations, the cone shaped termination was chosen for use. This termination was also used in the experimental studies of Harrington (24) and McDaniel (25). Preliminary tests for a plane wave revealed a standing wave ratio of less than 2 dB at 500 Hz in a hard-walled duct with this termination. However, for higher order modes, there is a standing wave ratio of over 6 dB near the cut-off frequency which decreases with frequency. This performance is partially explained by the work of Vajnshtejn (26) who calculated the reflection coefficients at the open end of a duct for higher order modes. This study was an extension of Levine and Schwinger's (27) work for plane waves. The results showed that maximum reflection for individual modes occurred at their cut-off frequencies and decreased as the frequency was increased. Although the open ended duct is not exactly similar to the anechoic termination described here, it does provide an indication of the difficulty in designing a termintion to eliminate acoustic reflection near the cut-off frequencies. In subsequent measurements with plane waves and higher order modes, the uniformity of amplitudes and mode shapes at several locations throughout the duct were indications of a reasonably good

anechoic termination.

Traversing microphone probes were designed to measure the radial mode shapes at stations thorughout the duct. A linear motion potentiometer accurately measured the radial displacement of the probes. Within the upstream and downstream hard walled sections, one probe was moved to the different stations shown in Figure 3.1. Within the test section, modes shapes were measured with an additional probe located at the center of the liner.

The microphone probe tubes were 4 mm in diameter and coupled to one half inch condenser microphones. (28). Although smaller diameter probes were available for use, the larger probes were chosen for their increased sensitivity. The presence of the probe should not obscure the acoustic field since even at 8000 Hz, well above the upper limit for measurements, the diameter of the probe is less than one-tenth of a wavelength.

Resonances of the probe tube will appear when the length of the probe is equal to odd multiples of a quarter of a wavelength. To obtain a uniform frequency response, steel wool was inserted in the probes to damp these resonances in the manner recommended by Brüel and Kjaer (28). The response of one of the probes is shown in Figure 3.2 with and without damping. This adjustment was necessary because the two probes were of different lengths and the corresponding resonances for each probe would occur at different frequencies. With each of the probe tubes damped, a more uniform frequency response can be obtained and used in comparing relative amplitudes between the levels measured within the liner section and within the hard-walled sections.

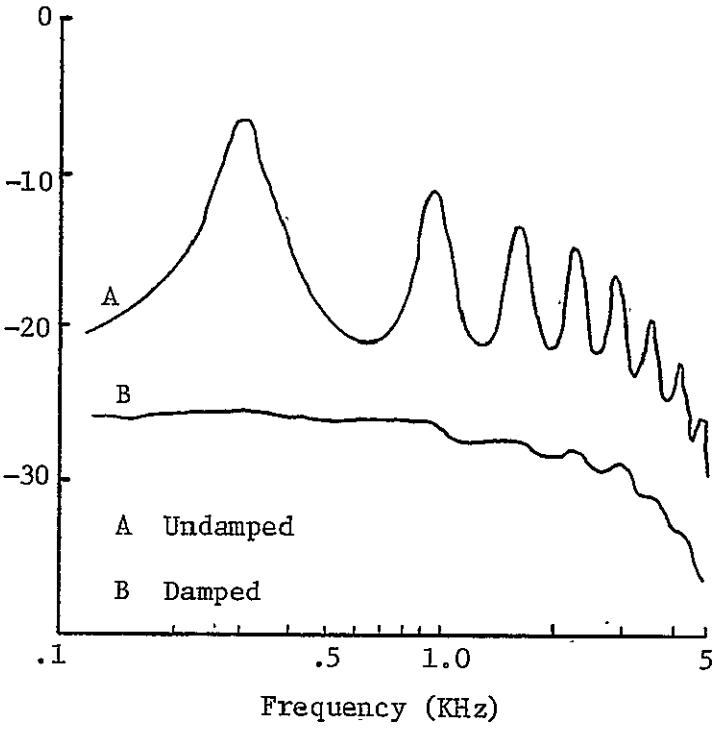

Figure 3.2 Frequency Response of Undamped and Damped Probe Tubes

3.3 Source Array

A complex source array was developed to generate plane waves and higher order acoustic modes within the duct. Seiner (29) provided the initial groundwork for development of a spinning mode synthesizer. Eight loudspeakers were located in an equally spaced circular array and phased so that the system could generate a spinning mode. Tests in an anechoic chamber confirmed the use of this system to generate higher order spinning modes. Oslac (30) has extended this concept and designed an array consisting of 16 speakers, circumferentially spaced in a baffle which was coupled to the end of a duct. With the increased number of elements in this configuration, improved results were obtained in generating mode shapes of a high spin number. Oslac has shown that the upper limit m_{max} for generation of a circumferential mode by such an array is given by

$$m_{max} = \left(\frac{N}{2} - 1\right) \tag{3.1}$$

where N is the number of speakers in one ring. This characteristic becomes important when considering the limitations of a source array.

McDaniel (25) has developed an improved source array which included a speaker at the center of the array in addition to the speakers placed in an outer ring. This provides radial as well as circumferential shading in the array. Obviously, the additional speaker at the center could only be used in generating a non-spinning, m = 0, mode. However, the encouraging results from this design prompted the use of additional elements in the radial direction. Such a design would provide additional radial shaping for both spinning and non-spinning modes and would provide a better match to desired mode shapes. The optimum configuration would

provide for continuous phasing and shading in amplitude in the circumferential and radial directions. The limiting factor in such a design would be the size of the transducers.

Based on these previous concepts, an improved array was designed with two concentric rings of 2-1/4 inch loudspeakers placed in a 3/8 inch aluminum baffle. The baffle was then coupled to the end of the duct. This speaker was small enough so that several elements could be included in the array. It also had reasonably good frequency response over the frequency range of interest for generation of the desired acoustic modes. Typical amplitude and phase response with respect to a one volt driving voltage for the speaker as a function of frequency are shown in Figures 3.3 and 3.4.

To insure that the desired duct modes would be generated with maximum efficiency by the array, speakers should be located near positions where the radial pressure distribution is a maximum. Referring to the mode shapes in Figures 2.2 and 2.3, the concentric rings of speakers were placed around a speaker at the center. Eight speakers were placed in an outer ring at a radius of 5 inches and 4 speakers were placed in an inner ring at a radius of 2.5 inches. The frequency response of several speakers was measured in order to choose elements for the array with near uniform phase and amplitude characteristics. The source array is shown in Figure 3.5.

To generate a single higher order duct mode, elements of the source array must be individually adjusted in phase and amplitude to correspond to the radial and circumferential pressure distribution of that mode. The radial pressure distribution for individual modes is given by the

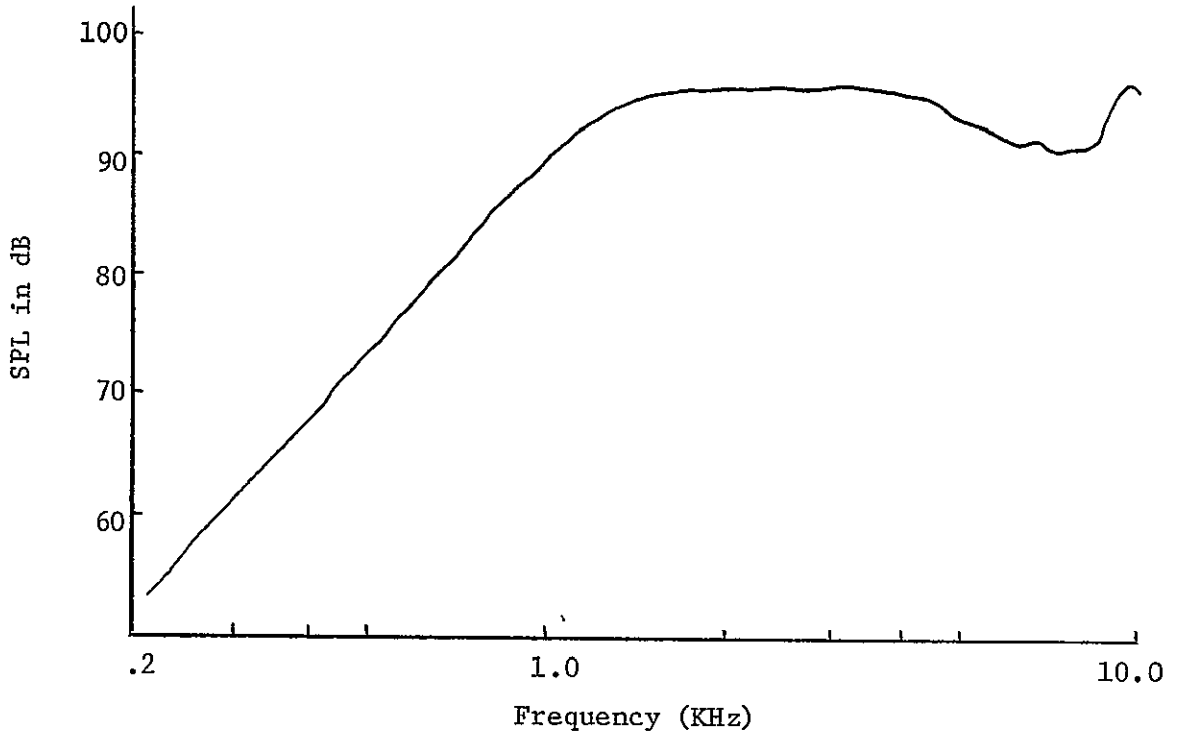

Figure 3.3 Amplitude Response of 2-1/4" Loudspeaker

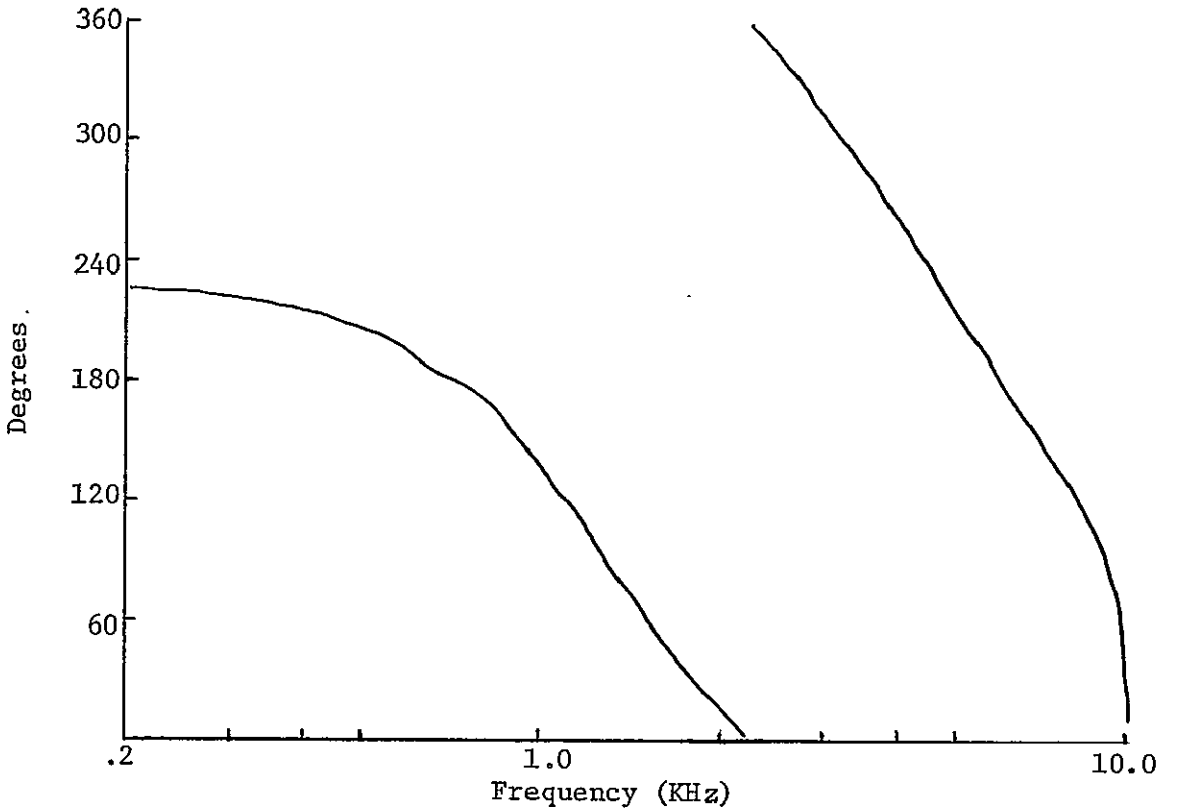

Figure 3.4 Phase Response of 2-1/4" Loudspeaker

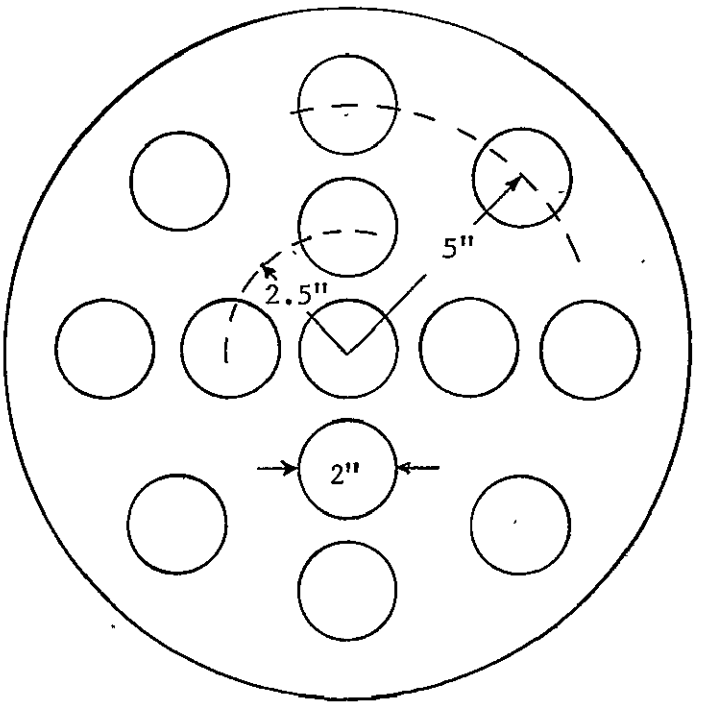

Figure 3.5 Source Array with Thirteen Elements

Bessel functions and the mode shapes in Figure 2.2 and 2.3. The circumferential distribution is given by the exponential term $e^{jm\Theta}$ in the solution to the wave equation. All of the elements within a ring at one radial position are adjusted to the same amplitude. These elements are further adjusted in phase to correspond to the circumferential order m of the desired mode. For a ring of N elements, there will be a progressive phase difference of $\frac{2\pi m}{N}$ radians between elements. The change in phase in the circumferential direction must then complete $2\pi m$ radians. The relative amplitudes for elements at different radial positions are chosen from the radial mode shapes in Figure 2.2 and 2.3. Whenever the pressure distribution crosses the r axis, a complete reversal in phase must also be accounted for between elements on each side of the null point.

A complete description of the electronics necessary to provide phase and amplitude control for each element in the array is given by Oslac (30). Although Oslac has shown that it is possible to combine several modes with such an array, the propagation of only individual modes will be studied here. For the remainder of this study, the generation of a mode will refer to the generation of known mode shapes for a hard-walled duct.

The source strength of a typical element of the array was determined by placing the speaker in a baffle and measuring far field pressure response. The far field radiated pressure from a piston in an infinite baffle at a position r_1 on-axis is given by Kinsler and Frey (7) as

$$p = \frac{-i\, k\, \rho\, c\, \Theta\, e^{ikr_1}}{2\, \pi\, r_1} \qquad (3.2)$$

The frequency response of an individual speaker was recorded at several

on-axis positions in an anechoic chamber and analyzed in order to determine the source strength as a function of frequency.

Preliminary attempts to generate higher order acoustic modes were made with the source array coupled to the end of a hard-walled duct with an anechoic termination. Both spinning and non-spinning modes could be generated within the duct at and above their cut-off frequencies and the corresponding mode shapes were well defined at positions throughout the duct. In addition, measurements of pressure and phase were made at circumferential positions to insure that the mode contained the required spinning or non-spinning characteristics. The generation of individual higher order modes will be studied to determine the modal purity obtainable with the source array.

An indication of the degree of modal purity can be determined from the measured level of the null in the radial pressure distribution. Any contamination from other modes will raise the level of the null.

A difference often exists between the radial location of the null as measured and predicted by theory. This could easily be due to the slight variations in duct diameter and the uniformity of the circular cross section. These variations would tend to redistribute the acoustic energy in the radial direction. In fact, a shift of the measured null to positions on either side of the predicted null is experienced for both spinning and non-spinning modes at positions along the length of the duct.

The mode shape for the first non-spinning (m = 0) radial mode is shown in Figure 3.6. This was generated at 1400 Hz and measured at a position several duct diameters from the source array. The comparison between measurement and theory is also shown. The agreement in this case

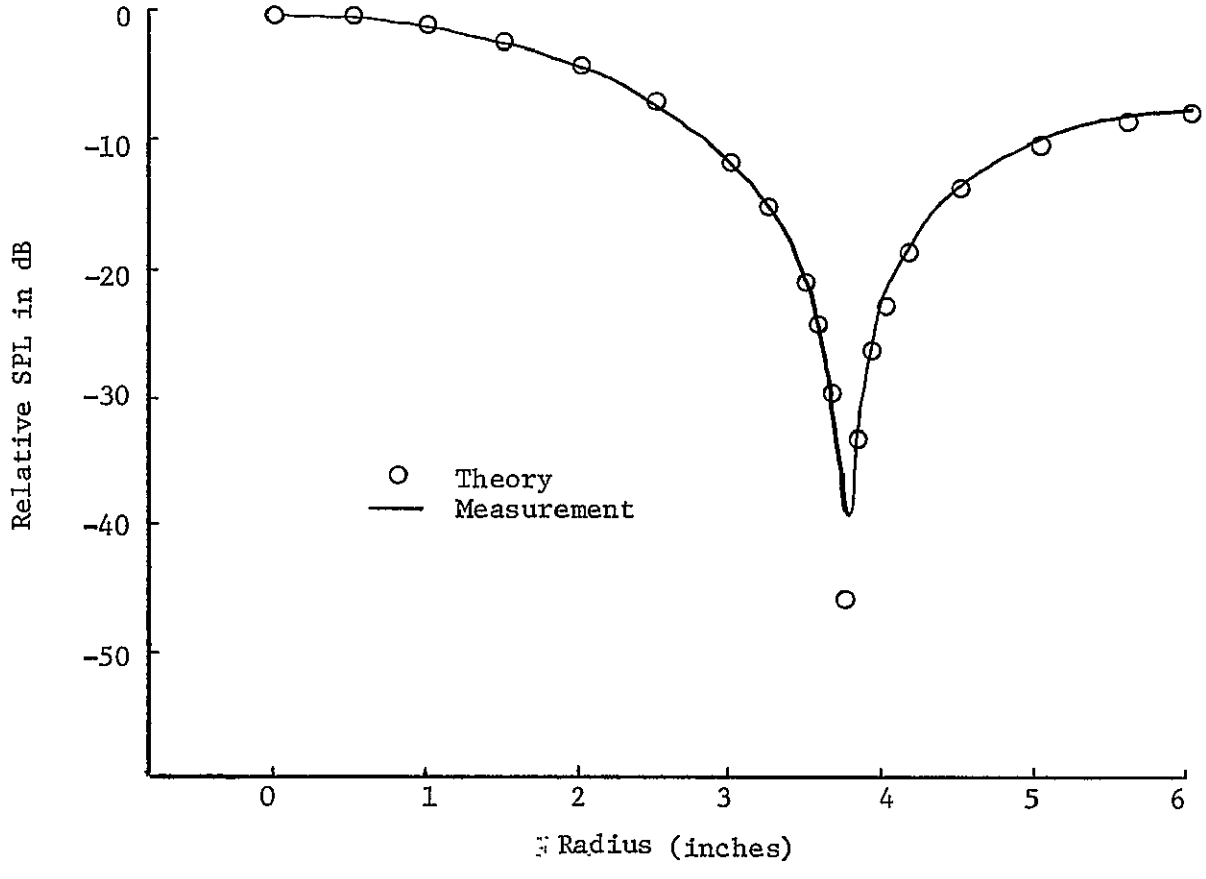

Figure 3.6 Radial Mode Shape for the (0,1) Mode, 1400 Hz

is very good with modal purity deteriorating slightly at higher frequencies. This mode could be generated with reasonable purity at frequencies up to the cut-off frequency for the second radial mode. The second radial mode is shown in Figure 3.7 at 2535 Hz. Although there is a difference in the location of the nulls, the general shape of the mode is fairly well established.

Spinning modes were investigated next in the anechoically terminated duct. Radial mode shapes for the first spinning mode at 700 Hz are shown in Figure 3.8. It was possible to generate this mode in a frequency range up to the cut-off frequency for the next radial mode. The second radial mode, the (1, 2) mode is shown in Figure 3.9 at 1925 Hz. There is good agreement between measured and predicted mode shapes in both cases. For a spinning mode, the absence of a clearly defined null at the center is not a positive indication that a poor mode shape exists. When measuring radial mode patterns near the center of the duct, probe alignment becomes a critical factor. For example, the first spinning mode has a maximum level at the wall and a null at the center where the dB level should drop to $-\infty$. If the probe is aligned off center, it will never reach this null. For an error of only one degree in alignment, the greatest difference between the level at the wall and the "measured center" becomes only 32 dB. Although a proper mode shape could exist in the duct, measurements would reveal a poor indication of this mode if the probe is misaligned. In all cases, precautions were made to ensure that the probe was aligned and traveled to the center of the duct.

Equation 3.1 restricts the use of the complete source array for generating spinning modes above the order m = 1. These higher modes can only be generated with the eight outer elements of the array. A

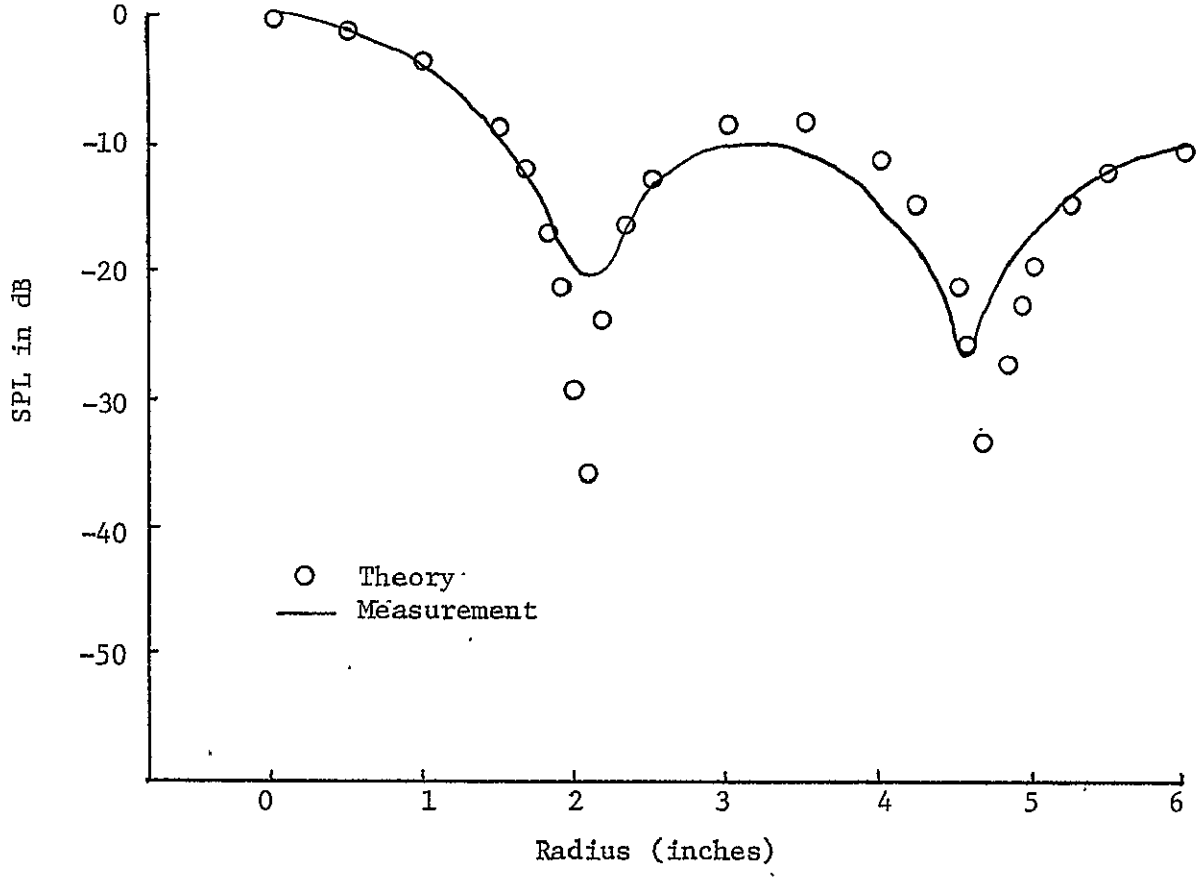

Figure 3.7 Radial Mode Shape for the (0,2) Mode, 2535 Hz

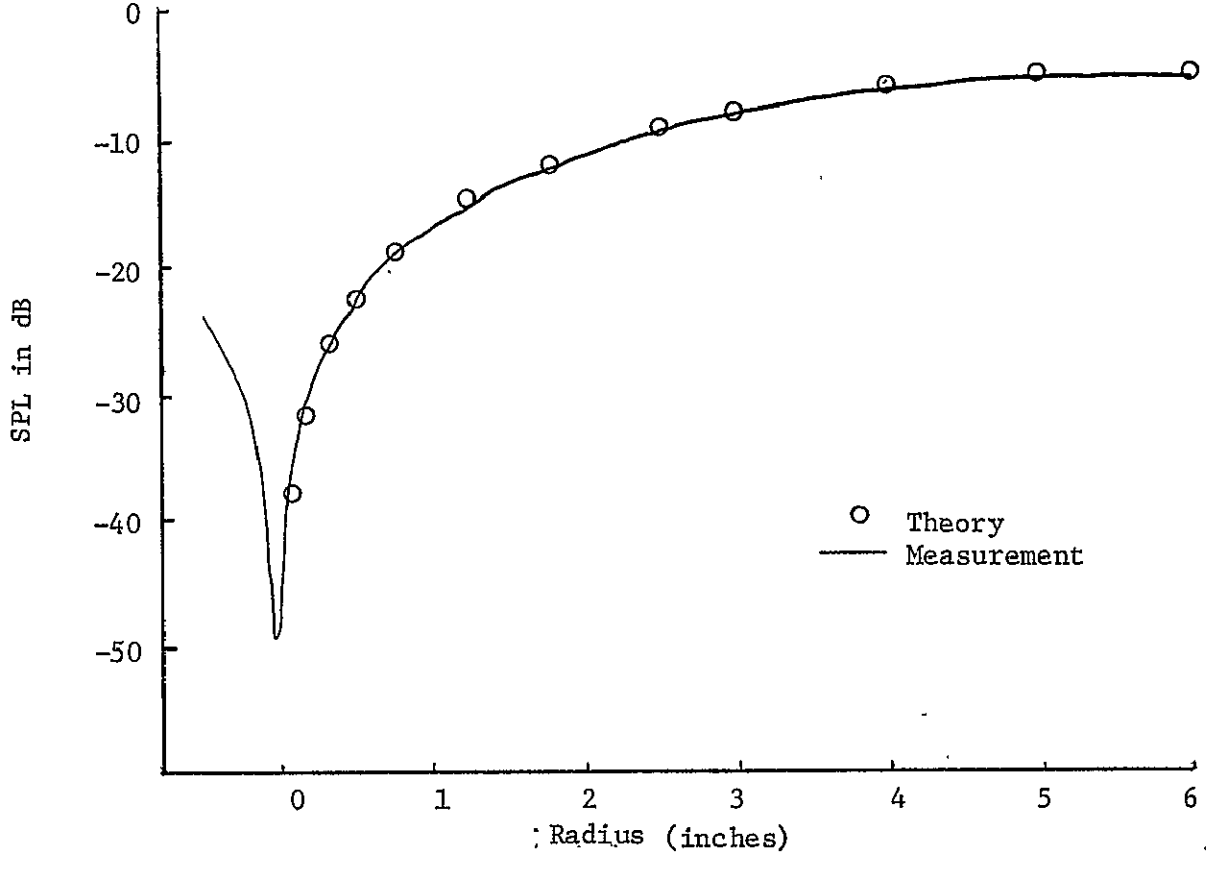

Figure 3.8 Radial Mode Shape for the (1,1) Mode, 700 Hz

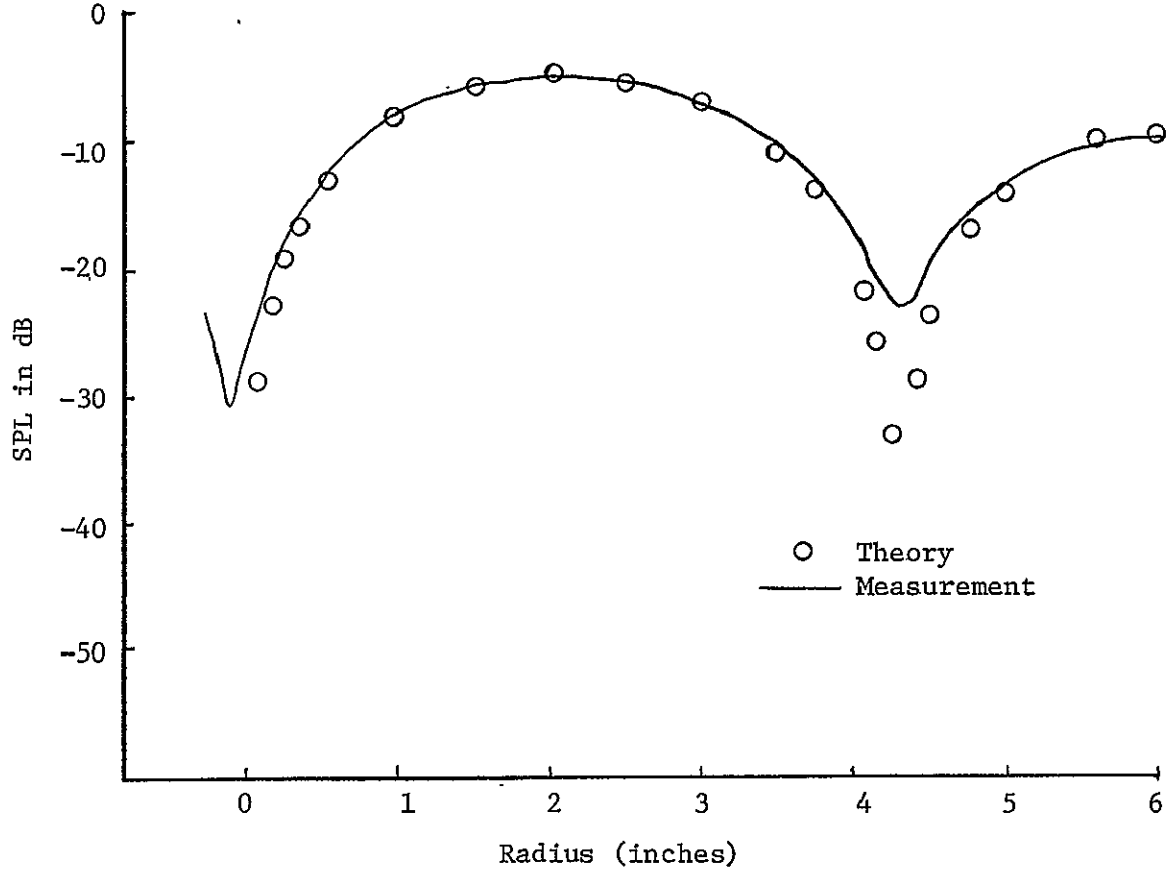

Figure 3.9 Radial Mode Shape for (1,2) Mode, 2000 Hz.

spinning mode of order m = 2 generated at 1110 Hz is shown in Figure 3.10. The agreement between measurement and theory is good except near the center of the duct. This is partially because only the outer ring of elements in the source array is used to match the sound field. In addition, this mode is being generated in a frequency range where spurious modes, created by phase variations between individual elements of the array, can also propagate. The absence of a clearly defined null at the center is an indication of contamination from suprious plane waves generated at a reduced level by the array. An analysis of these spurious modes is given in Appendix A. Nontheless, the mode does contain the general radial pattern and proper spin characteristics.

Mode shapes generated with only the outer ring of speakers were compared with mode shapes generated using the entire array. For a (0, 1) mode, the mode shapes generated with the entire array properly adjusted and with combinations of speakers operating are shown in Figure 3.11. Similar results for the (1, 1) mode are shown in Figure 3.12. Thus, the mode shapes are enhanced considerably by providing radial shading as well as circumferential phasing with this unique array. The advantage of providing radial shading becomes especially important when generating modes at frequencies where several lower order modes with the same circumferential dependence can also propagate. Evidence of this is shown in Figure 3.13 when a (0, 2) mode is being generated with the entire array and then with only the outer ring of speakers. From the difference between radial mode shapes, the radial pressure distribution is greatly enhanced by the radial shaping provided by the array.

Mode shapes generated in the semi-infinite duct system included the

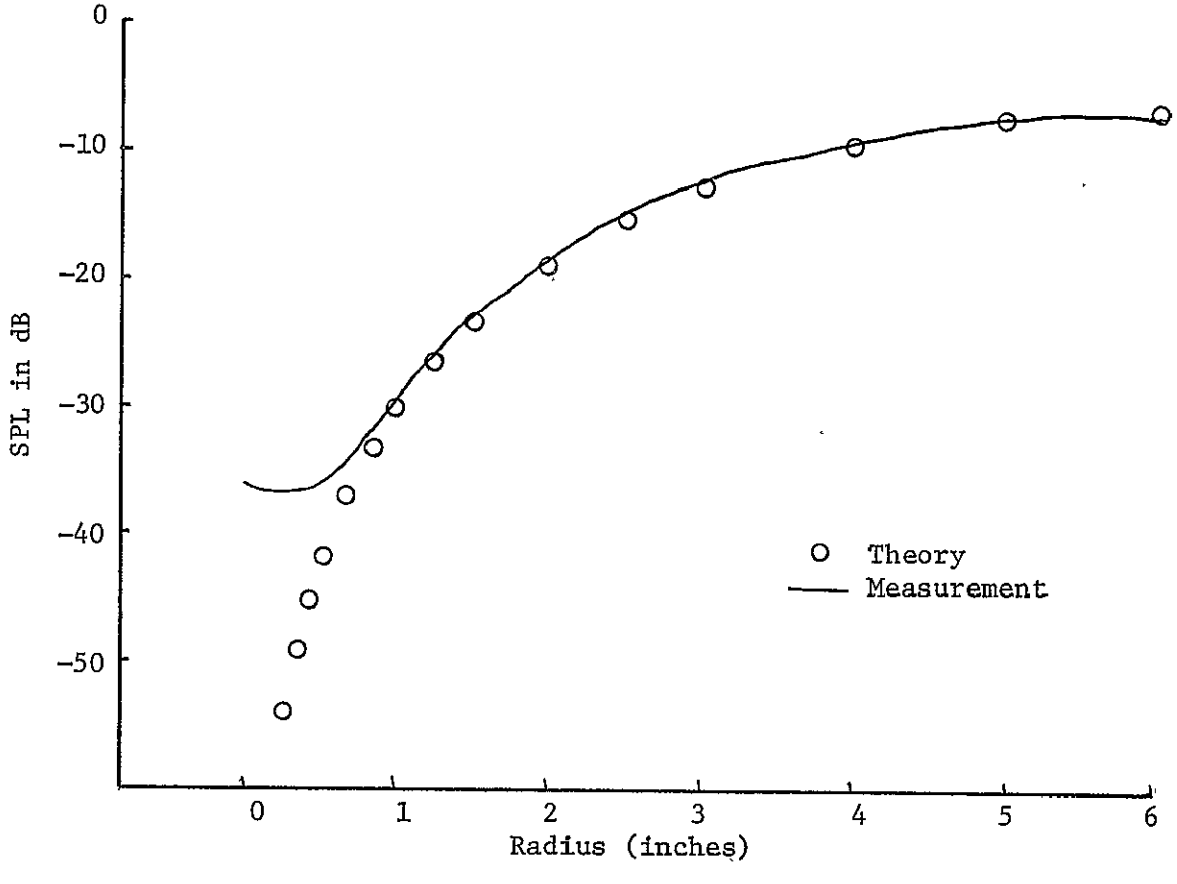

Figure 3.10 Radial Mode Shape for (2,1) Mode, 1110 Hz

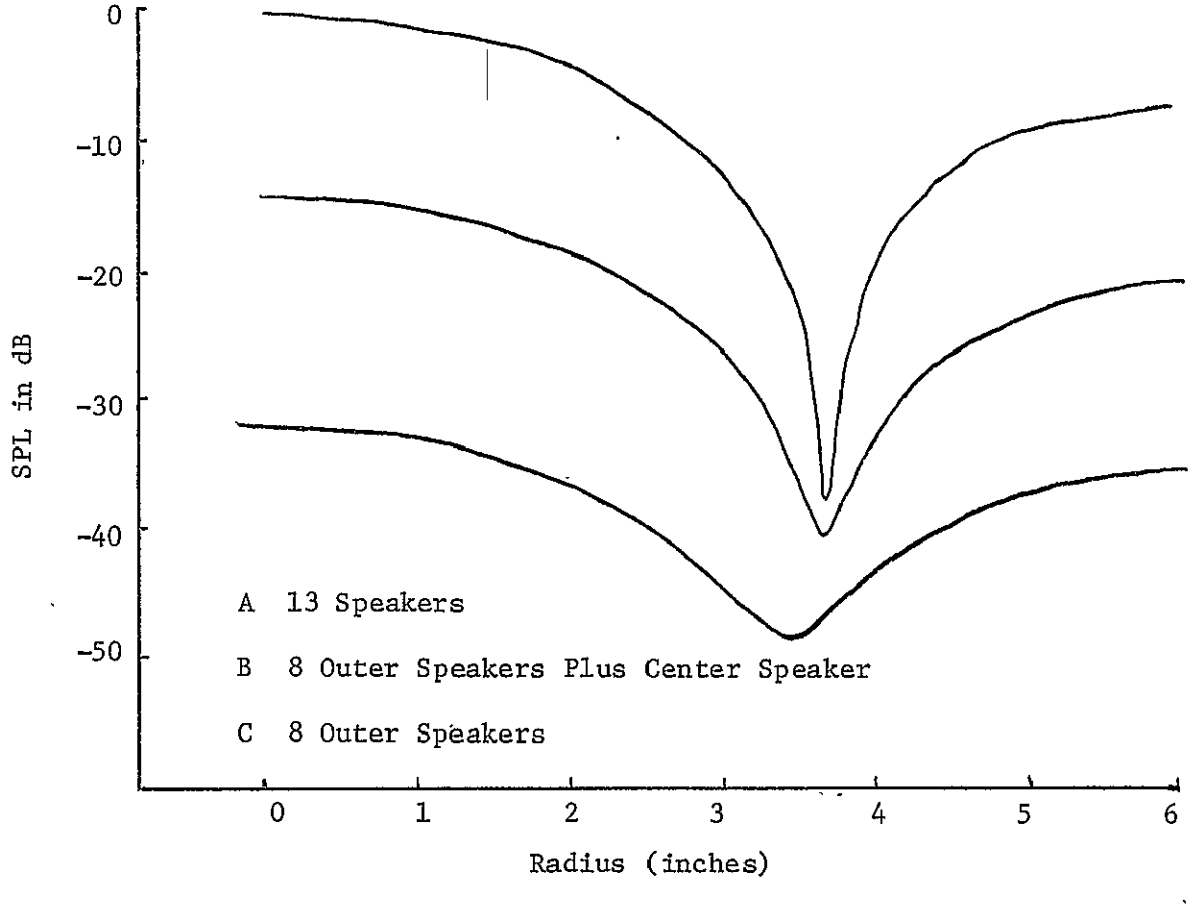

Figure 3.11 Radial Mode Shapes Generated for the (0,1) Mode at 1400 Hz Using Different Speakers in the Array

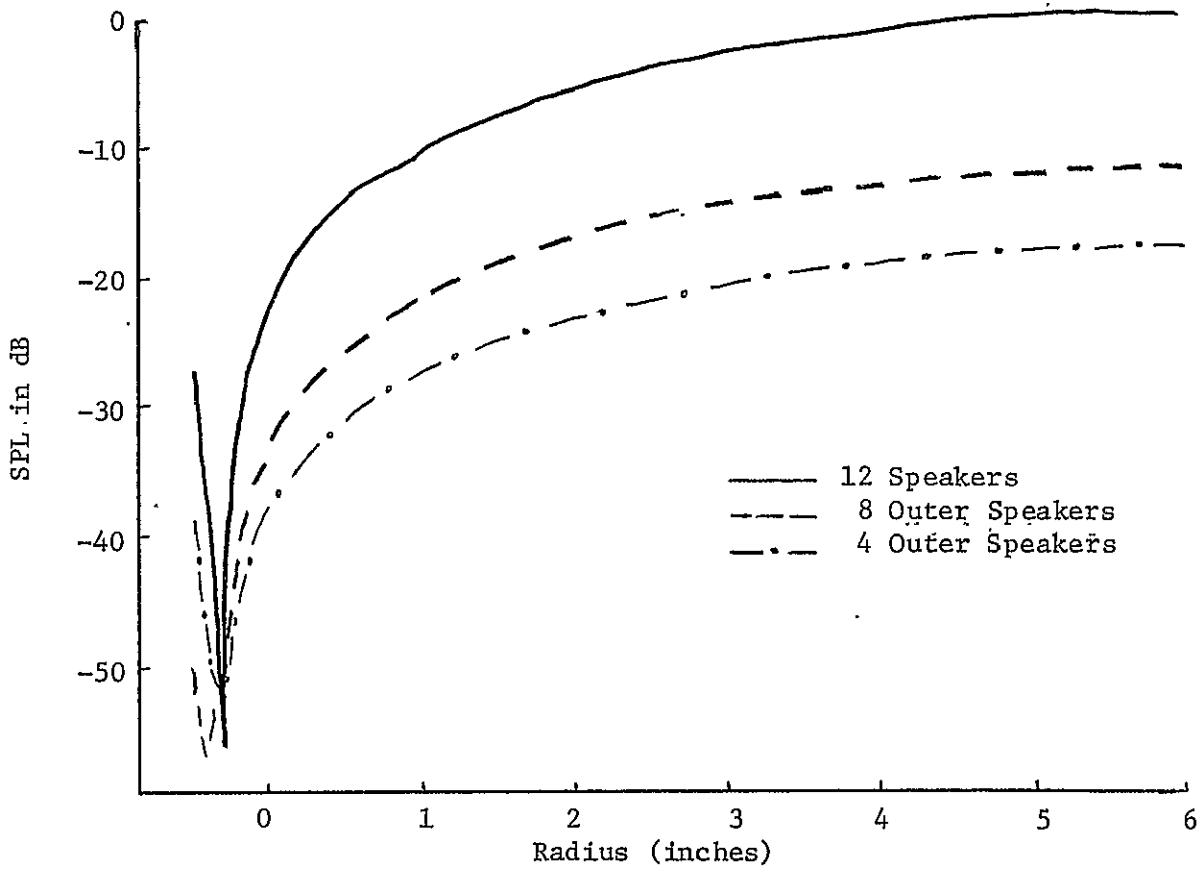

Figure 3.12 Radial Mode Shapes Generated for the (1,1) Mode at 700 Hz Using Different Speakers in the Array

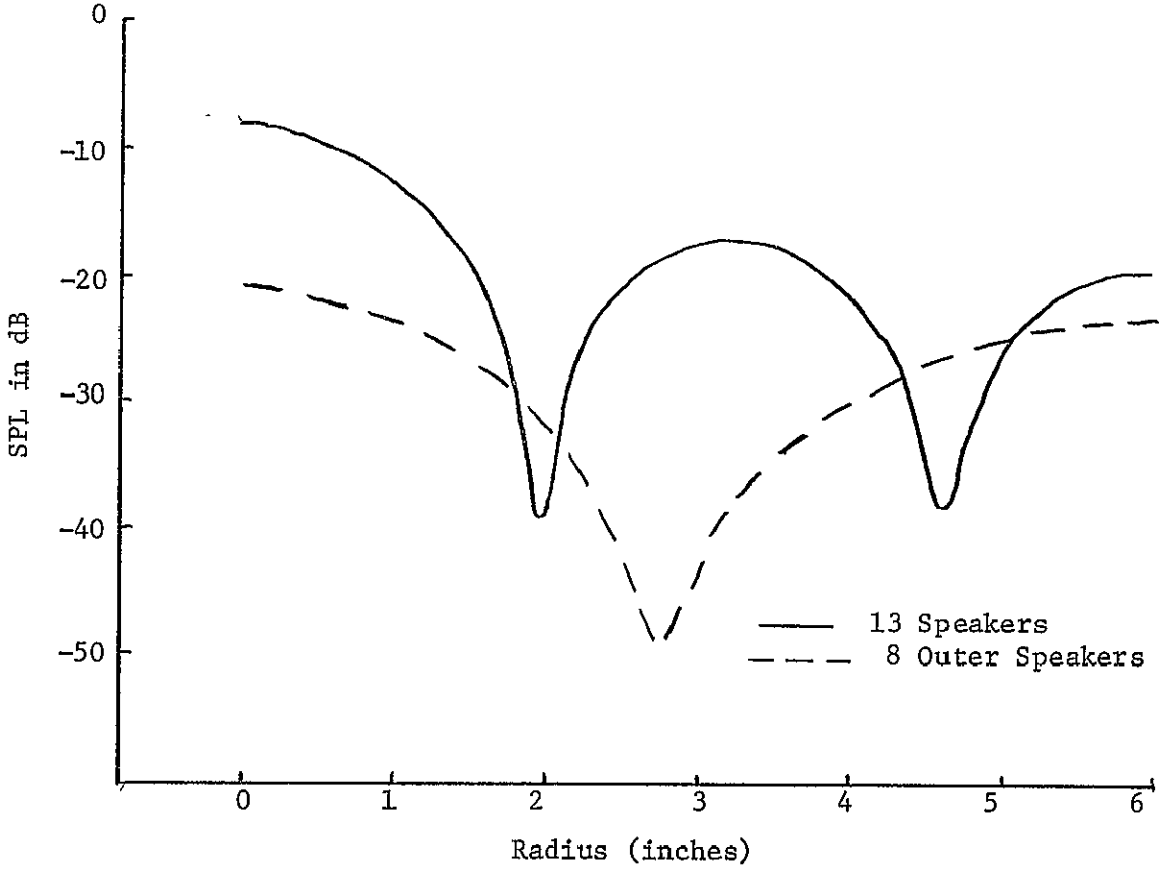

Figure 3.13 Radial Mode Shapes Generated for the (0,2) Mode at 2535 Hz Using Different Speakers in the Array

plane wave, (0, 0) mode, the (0, 1) and (0, 2) non-spinning higher order modes and the (1, 1), (1, 2) and (2, 1) spinning modes. Reasonable modal purity was obtained for all cases except the (2, 1) mode.

3.4 Flow Resistance Measurements . . .

One of the fundamental parameters used in predicting the acoustic performance of a sound absorbing material is the flow resistance. The flow resistance of each material was measured with an apparatus designed according to specifications outlined in ASTM Standard C522-64 (31). The apparatus permits control of the flow rate through a sample so that flow resistance can be measured over a range of velocities. A complete description of the apparatus and testing method can be found in References 5 and 13.

Measurements were made at flow rates within a range of particle velocities corresponding to moderate acoustic levels. For the flow rates considered, the pressure drop associated with the flow resistance is on the order of a few thousandths of an inch of water and was measured with a pressure transducer as opposed to a micromanometer. In all cases, the sample size was 8.73 cm^2 in area.

Three samples of each material were chosen from random locations and tested in order to determine an average flow resistance representative of the entire liner. Typical results for flow resistance measurements on three samples of fiber metal material are shown in Figure 3.14. The differences between samples are the result of variations in material properties. More important, however, is the fact that the flow resistance is essentially constant throughout the range of flow rates considered. The average values for each material are given in Section 3.6 where the materials chosen as duct liners are fully described.

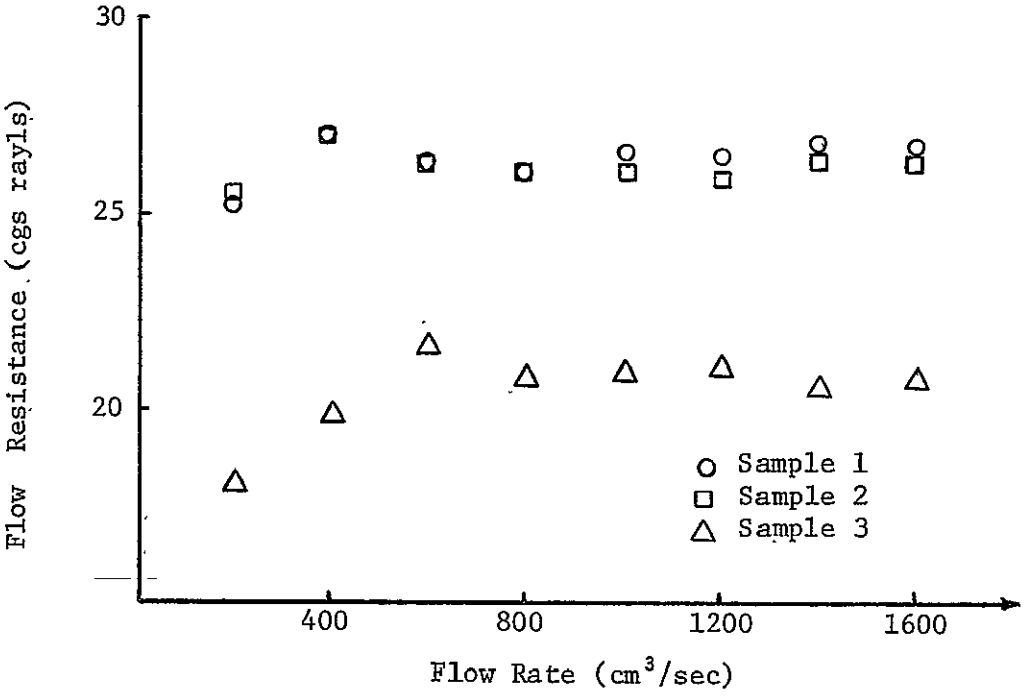

Figure 3.14 Flow Resistance for a Fiber Metal Material

3.5 Impedance Tube Measurements

Measurements of the normal impedance and absorption coefficient of a material as a function of frequency can be made using a standing wave tube. A Brüel and Kjaer Type 4002 Standing Wave Apparatus, which meets the specifications of ASTM Standard C384-58 (32), was used for these measurements. A moveable probe microphone is used to measure the standing wave ratio and the distance to the first node of the standing wave pattern. These parameters are used to calculate the impedance and absorption coefficient.

The frequency range over which plane waves may propagate within the standing wave tube has an upper limit determined by its diameter and the corresponding cut-off frequencies for the first higher order mode. The propagation of higher order modes is restricted below this cut-off frequency and only plane waves can exist. To extend measurements with plane waves over a broader frequency range, two tubes with diameters of 3 cm and 10 cm were used. This also provides a comparison of measured values in an overlapping frequency range. Measurements were possible from 250 Hz up to 4000 Hz with an overlapping frequency range existing between 800 Hz and 2000 Hz for the two tubes. A complete description of the testing method and apparatus is given in References 5 and 13.

3.6 Duct Liners

Duct liners of three different materials were chosen in order to study their attenuation properties and the local reaction boundary condition. No attempt was made to optimize the impedance parameters of our liners by altering material thickness, material properties, or cavity depth. Instead, it was decided to choose materials that could be inserted within the one inch depth provided by the test section.

Two types of sintered fiber metals with differing acoustic properties were used as duct liners. These materials were provided by Brunswick Corporation and are commercially known as Brunscoustic Plate (Fuzzy Hole Perforate, 27% open area) and FM 134. The flow resistance of each material, tested by the technique described in Section 3.4, was 48 cgs rayls and 25 cgs rayls respectively. The fiber metals were tested with a 7/8 inch thick closed cell honeycomb core backing. The honeycomb core, produced by Hexcel Corporation under the trade name of Acousti Core, contained 3/16 inch cavities. The special core geometry of this material allowed it to be formed into a circular configuration without the saddling problems inherent when ordinary honeycomb is rolled or deformed along an axis. To seal the cavities, a layer of sheet metal was tightly wrapped around the honeycomb material before inserting the liner in the test section. This configuration is then a close representation of the materials used by the aircraft industries in acoustically treating aircraft engine inlet duct and fan exhaust systems.

A perforated sheet metal with a closed cell honeycomb core backing was also used as a duct liner. The use of perforated panels as acoustic treatment is of considerable interest because of the reduced cost of this material as compared to the fiber metals. Two samples of per-

forated sheet metal were chosen with specifications on hole alignment, hole spacing and size, and open area that resembled current perforated materials used in acoustic applications. The materials chosen each had 1/16 inch diameter holes on staggered centers - one of 20 gauge aluminum with 1/8 inch centers and 22.5% open area, and the other of 24 gauge steel with 7/64 inch centers and 30% open area. A cavity depth behind the material was provided by the 7/8 inch thick flexible honeycomb core described previously. The configuration was inserted in the one inch depth of the duct test section for evaluation.

Both the fiber metal and perforated sheet metal materials were fabricated into 28-1/2 inch long acoustic liners with a 12 inch inner diameter. Any further mention of the fiber metal or perforated liners will refer to these lengths.

A rigid round glass fiber material of one inch thickness was the third type of material chosen for use as a liner. This material is a commercially available product distributed by Johns Manville and used for pipe insulation. Although fiberglass materials are generally designed for insulation purposes, they also possess remarkably good sound absorbing properties. Furthermore, since their tolerances and specifications are chosen for their primary purpose, there is often a considerable variation in the resulting acoustic properties of the materials. This variation is most noticeable in the flow resistance where it is not uncommon to have variations in the flow resistance within 25% of a nominal value. The average flow resistance for this material was 78 cgs rayles/inch. Duct liners of glass fiber material in lengths of 12 inches and 24 inches were inserted within the test section for evaluation.

Throughout the remainder of this study, the following abbreviations for each material will be used.

1. FM 1 - Fibermetal, 48 cgs rayls, 7/8 inch cavity
2. FM 2 - Fibermetal, 25 cgs rayls, 7/8 inch cavity
3. Perf 1 - Perforated panel, 22.5% open area, 7/8 inch cavity
4. Perf 2 - Perforated panel, 30% open area, 7/8 inch cavity
5. Fiberglass - One inch thick fiberglass liner

CHAPTER IV

DISCUSSION

4.1 Impedance Characteristics of Duct Liners

In order to determine the average impedance characteristics for each liner material, three samples were taken from random locations and tested in a standing wave tube. This involved tests fo three separate samples within both the large and small impedance tubes. In most cases, there was a negligible variation between the resulting impedance characteristics for individual samples and for large and small samples.

The impedance for the two fiber metals and two perforated panels, with 7/8 inch honeycomb backing, are presented in Figures 4.1 through 4.4. Throughout the overlapping frequency range, there is no significant difference between the real and imaginary components of the impedance for both materials. The measured values of impedance are also compared with values calculated from the expressions in Section 2.3 Throughout the entire frequency range, there is good agreement between these values.

The impedance characteristics for the one thick glass fiber material, as measured by the impedance tube are shown in Figure 4.5. Since there is a marked difference between the real and imaginary components of impedance within the overlapping frequency range, measurements with the small and large tube are separated. This phenomenon is characteristic for each of the three samples and not just peculiar to one sample.

To eliminate the possibility that gross material variations between individual samples was the cause of this discrepancy, further tests were conducted on one sample. The sample was first tested within

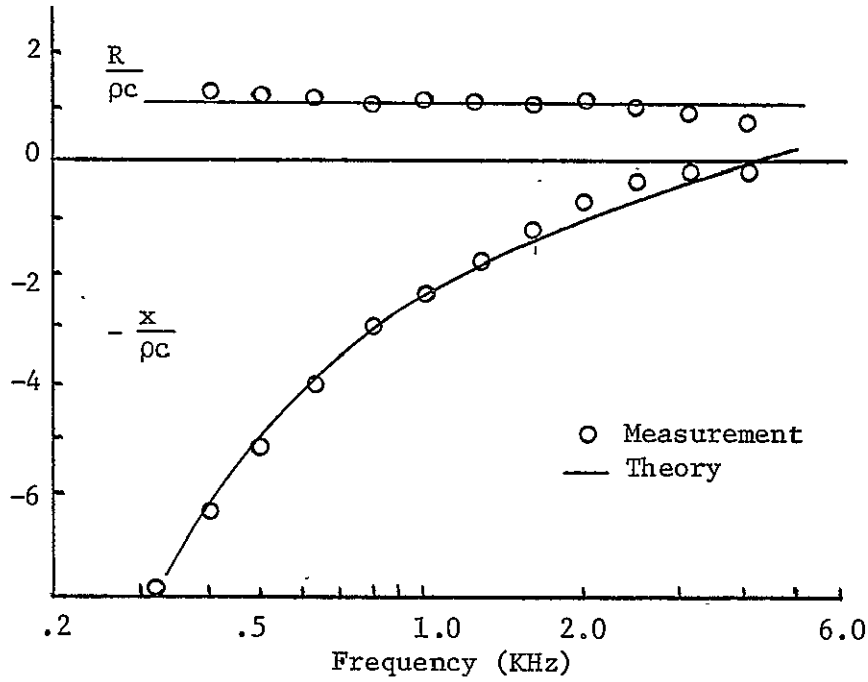

Figure 4.1 Specific Normal Impedance for Fiber Metal, Flow Resistance 48 cgs rayls, Cavity Depth 7/8"

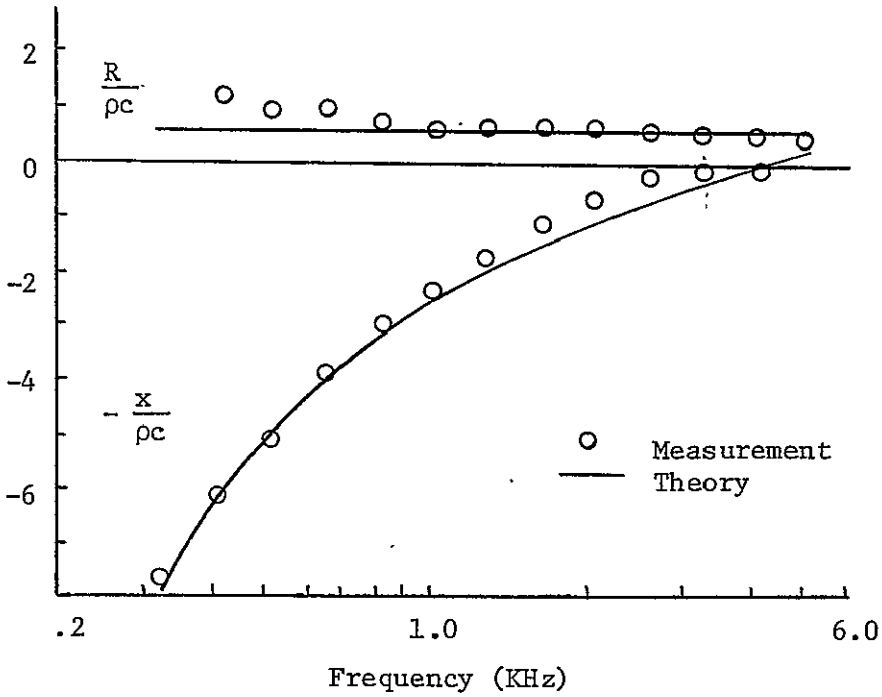

Figure 4.2 Specific Normal Impedance for Fiber Metal Flow Resistance 25 cgs rayls, Cavity Depth 7/8"

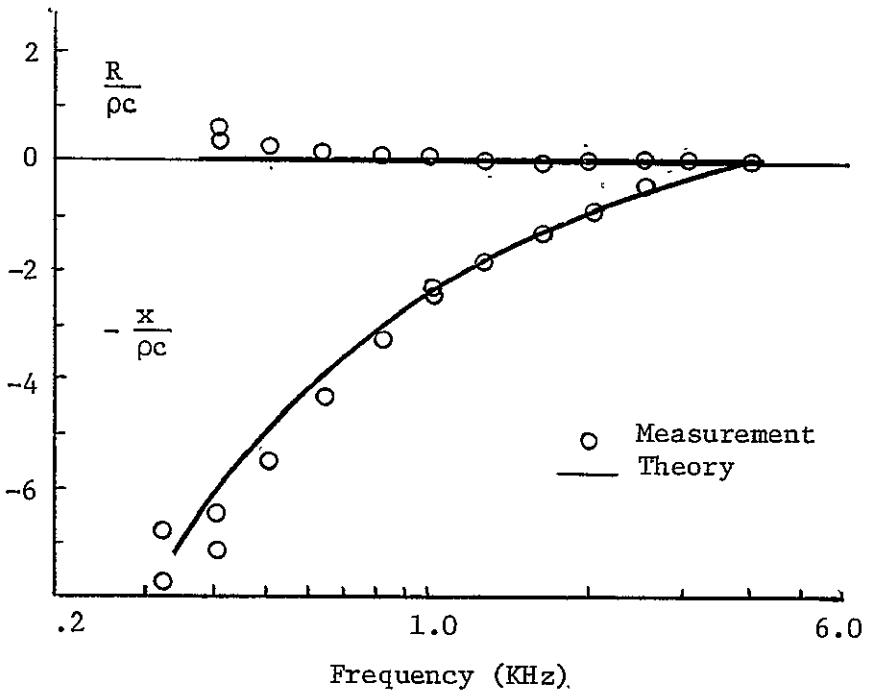

Figure 4.3 Specific Normal Impedance of 22% Open Area Perforate, Cavity Depth 7/8"

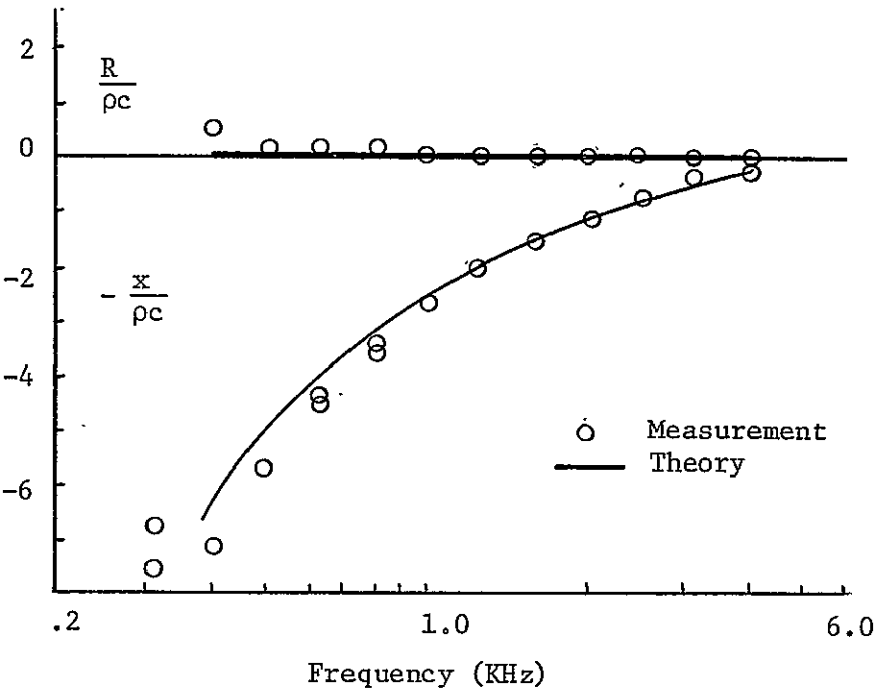

Figure 4.4 Specific Normal Impedance of 30% Open Area Perforate, Cavity Depth 7/8"

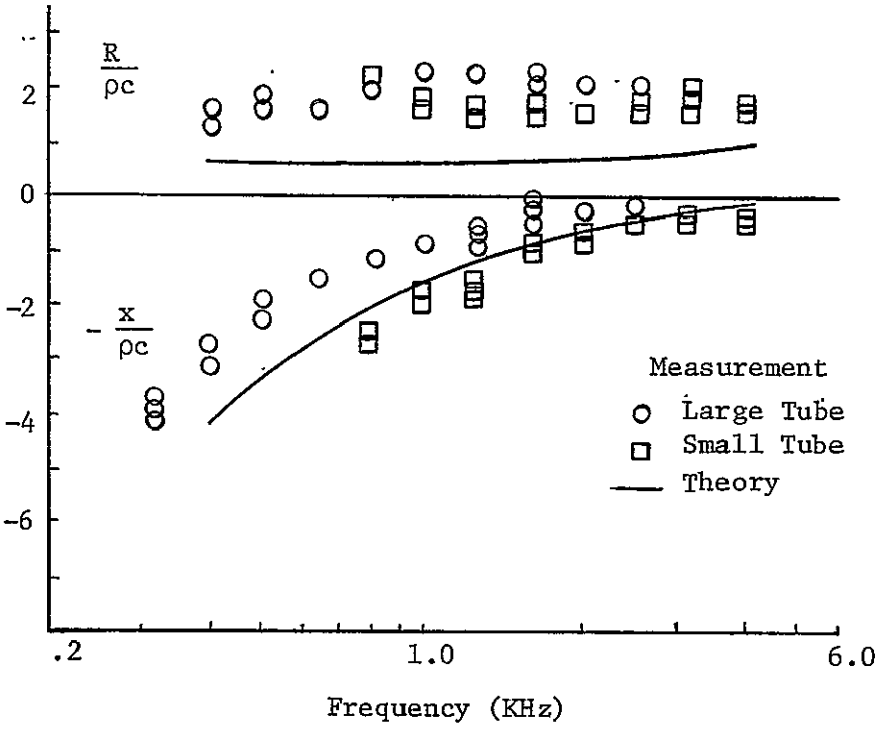

Figure 4.5 Specific Normal Impedance for One Inch Thick Glass Fiber Material

the large impedance tube. Next, three separate smaller samples were cut from this piece and individually tested within the smaller tube. Again; this same discrepancy was evident in the overlapping frequency range. This characteristic, however, is not representative of all glass fiber materials. Previous impedance tube testing with glass fiber materials of different densities and thicknesses showed no variations in measured acoustic properties within the overlapping frequency range (13).

The discrepancy for this particular material is unable to be explained. In cases where these variations exist, greater emphasis will be given to measurements with the larger sample of material.

The calculated impedance values for the glass fiber material are also presented in this figure. For the flow resistance value of 78 cgs rayls, the theory underpredicts the real component of the impedance. It has been shown by Wyerman (13) that the value of flow resistance affects only the real component of the impedance and leaves the imaginary component relatively changed for frequencies below 2000 Hz. Furthermore, a flow resistance of over 140 cgs rayls would be necessary to predict impadance values corresponding to those measured with the standing wave tube. This same result was found for measurements on several different glass fiber materials, indicating that the flow resistance, as used in Beranek's theory (9), does not account for the total dissipation within the material and other dissipation mechanisms must be present. Beranek has remedied this problem by introducing a dynamic flow resistance to compensate for this factor. This parameter is determined from standing wave tube measurements by fitting the experimental results to curves for the impedance calculated at different flow

resistances values. However, this new parameter has no relationship to the static flow resistance and has values both above and below the measured static values for different materials. This indicates that other dissipation mechanisms are involved within the material that are not included in the flow resistance term.

Although the impedance of a material can be reasonably predicted by theory for all cases except the glass fiber material, the measured values of impedance will be used with the eigenvalue equation and the eigenvalue search technique. For the glass fiber material, the measured impedance for the larger sample will be used to locate the eigenvalues.

It is obvious from the characteristics of materials considered in this study that an optimum impedance exists where sound attenuation through a liner is maximized. Within this study, however, no attempt was made to model duct liners for optimum impedance characteristics. Instead, liners of different acoustic materials were chosen for evaluation that could be readily inserted in the test section of the duct system.

4.2 Eigenvalue Search Technique

The eigenvalues for a lined duct section are determined by solutions to the local reaction boundary conditions. These solutions were located by the eigenvalue search technique described in Section 2.6. To establish the validity of this method, preliminary tests were performed and compared with the results given by Molloy and Hanegman (18) and by Zorumski and Mason (20). In all cases, the contour integration located the region containing the eigenvalue and the first approximation converged to the exact value using the iteration technique. This method thus provided an efficient and reliable method for locating the complex eigenvalues for a liner material.

The behavior of eigenvalues for the fiber metal liner FM 1 will be described for individual circumferential modes.

The eigenvalues at several frequencies for a non-spinning mode, $m = 0$, are shown in Figure 4.6. The real components of the eigenvalues are interlaced between the real zeroes of the Bessel function J_o and its derivative J'_o. These values are the extreme cases for soft and hard duct walls respectively. The general trend of the frequency dependence of these modes can be seen in each figure. A graphical representation of the coalescence of eigenvalues can be seen from the Morse Charts (8) and from Zorumski's (20) treatment of the behavior of eigenvalues and double eigenvalues for different values of impedance.

The attenuation for individual radial modes within a lined duct is related to the eigenvalues by the wavenumber in the axial direction and Equations 2.22 and 2.35. This attenuation is plotted for non-spinning modes for the fibermetal material in Figure 4.7. There are definite delineations between attenuation for each mode both above and

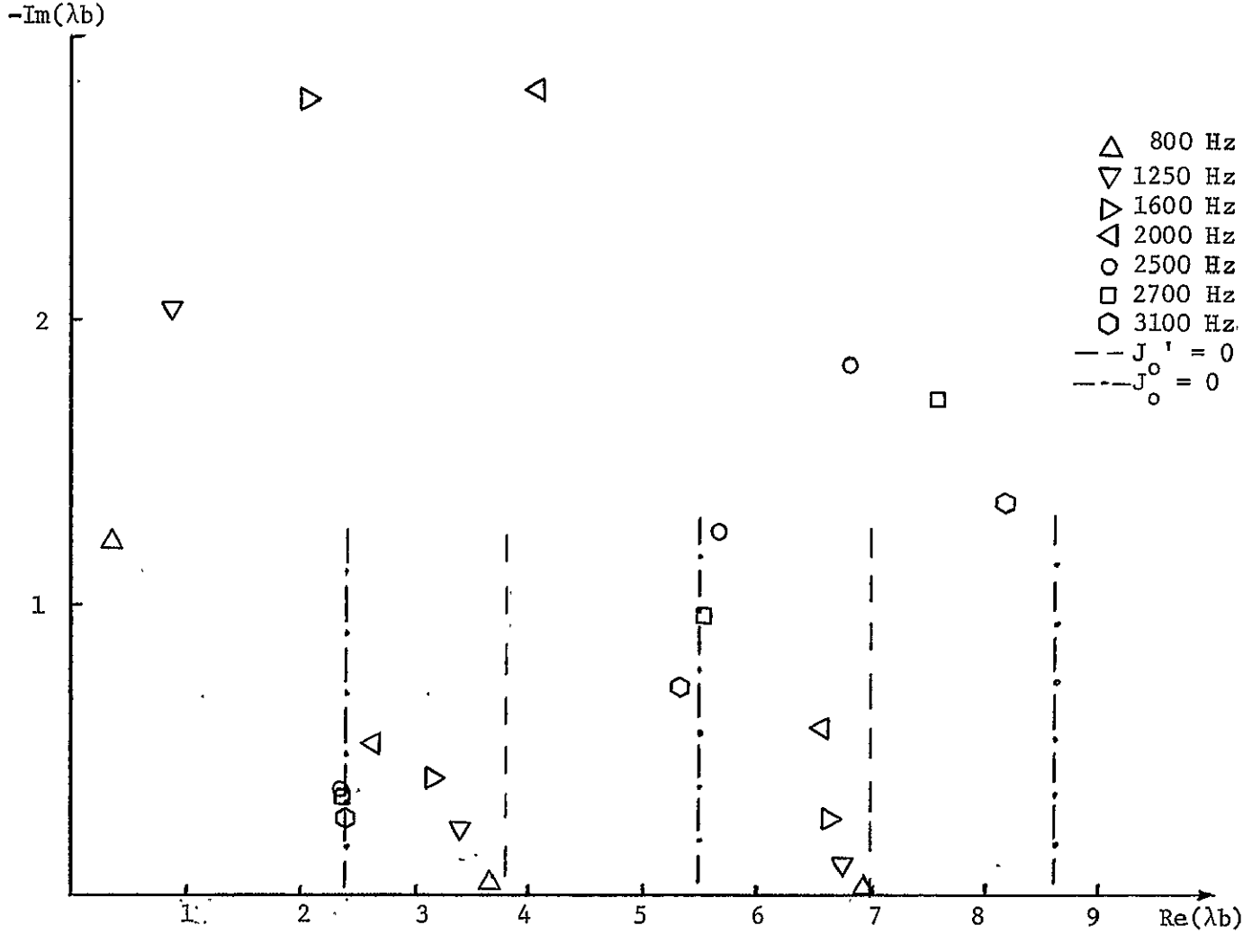

Figure 4.6 Ordering of Eigenvalues for FM 1 Liner, m = 0

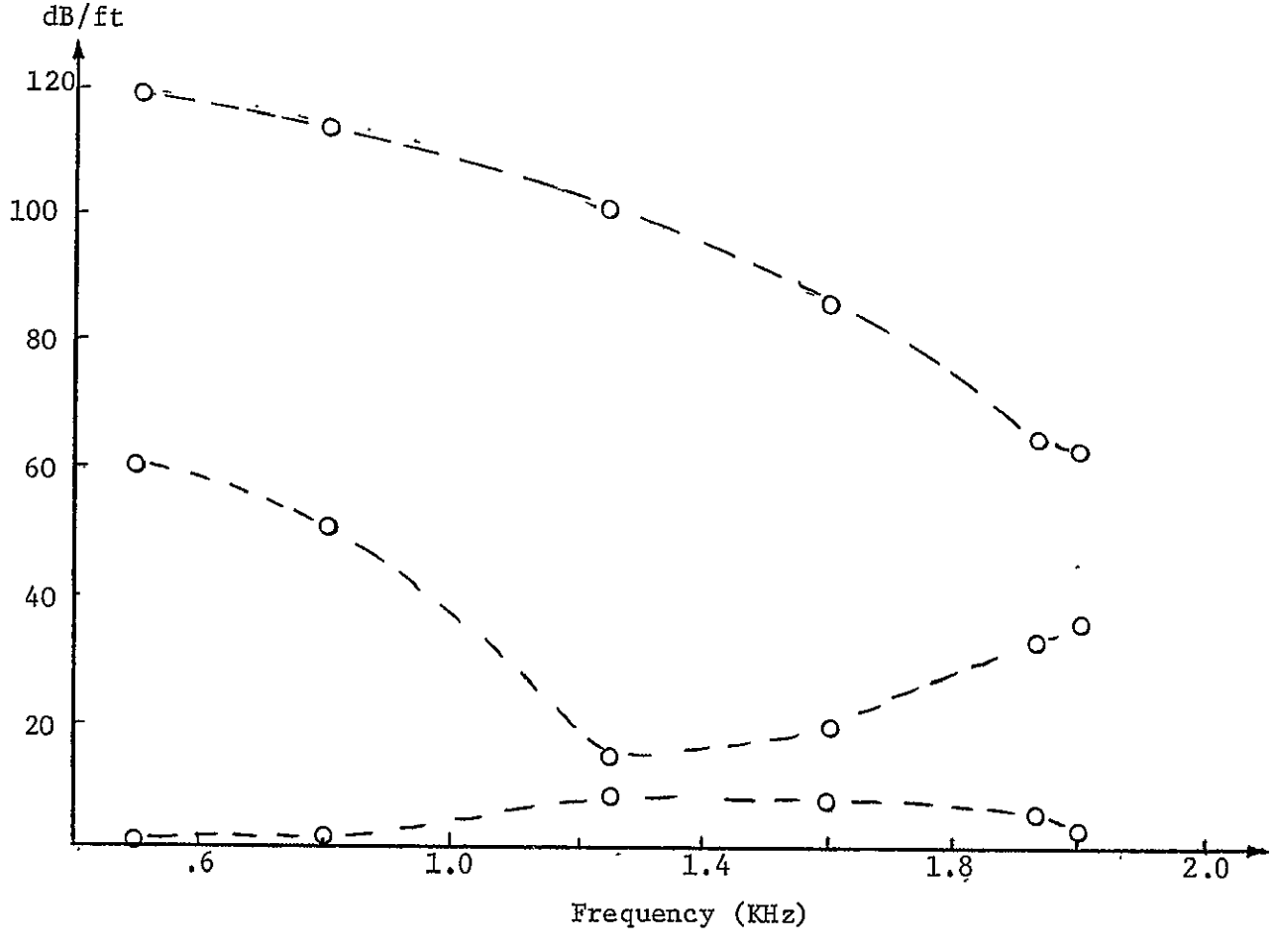

Figure 4.7 Attenuation for Successive Radial Modes for FM 1 Liner, m = 0

below the hard wall cut-off frequencies. Near these frequencies, the attenuation of individual modes is on the same order. Therefore, there is a little distinction between the attenuation characteristics of two successive radial modes in this frequency domain.

Similar results for eigenvalues are given in Figure 4.8 for an $m = 1$ spinning mode for the same material. The same ordering of eigenvalues can be seen with respect to the zeroes for the Bessel function J_1 and its derivative, J'_1. The attenuation for the liner is shown in Figure 4.9. Again, there are clear distinctions between the attenuation for successive radial modes except near the cut-off frequencies for a hard-walled duct.

The treatment was intended to show the basic behavior of successive eigenvalues for two types of materials with the impedance characteristics given in Section 4.1. No conclusions can be drawn from this analysis about general eigenvalues for materials with arbitrary impedance characteristics. The general behavior of eigenvalues for arbitrary impedance is given by the Morse Charts (8). To obtain the exact eigenvalues, it is best to obtain solutions directly from Equation 2.32.

A complete set of eigenvalues were determined for each material throughout the frequency range of generation for each mode.

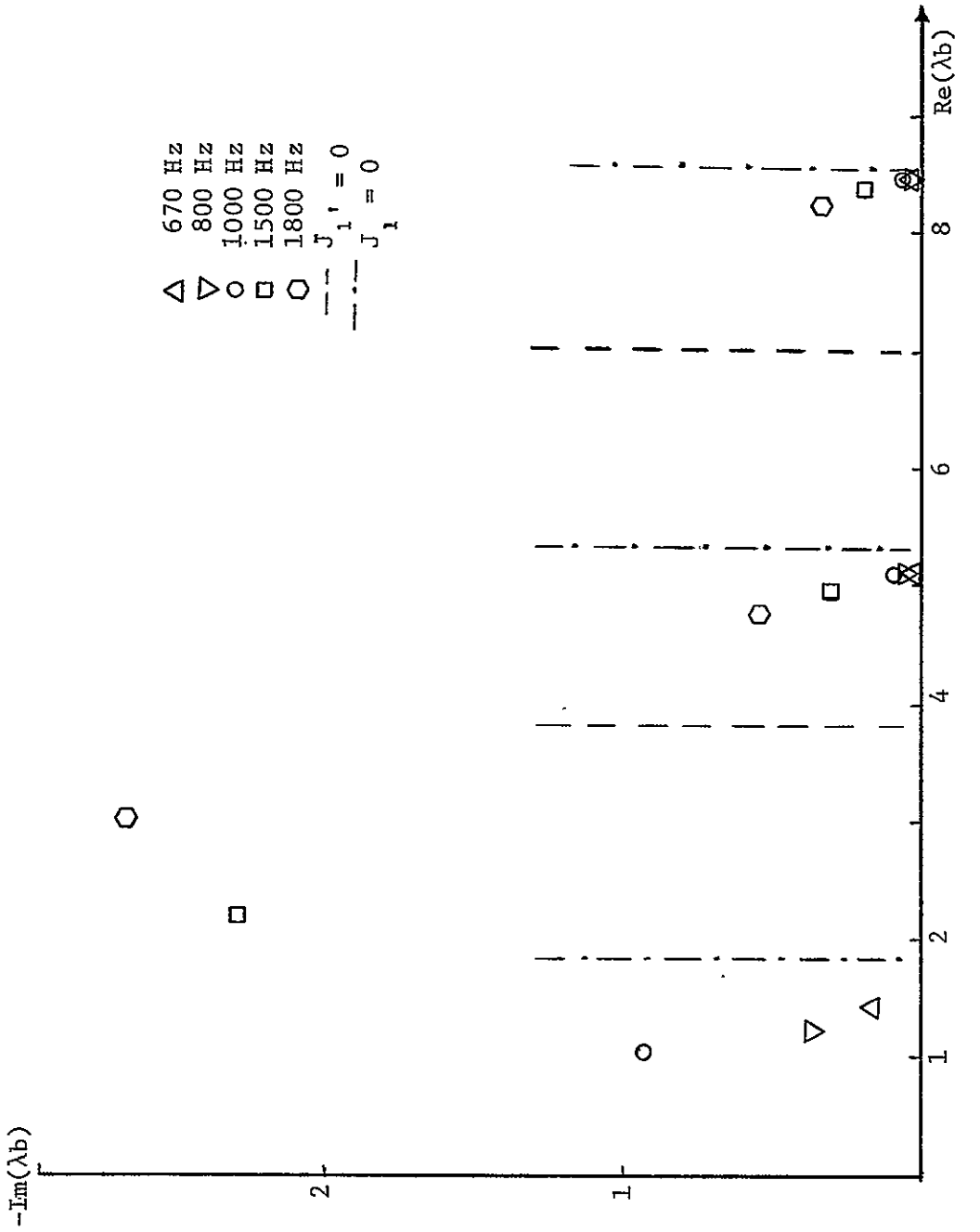

Figure 4.8 Ordering of Eigenvalues for FM 1 Liner, m = 1

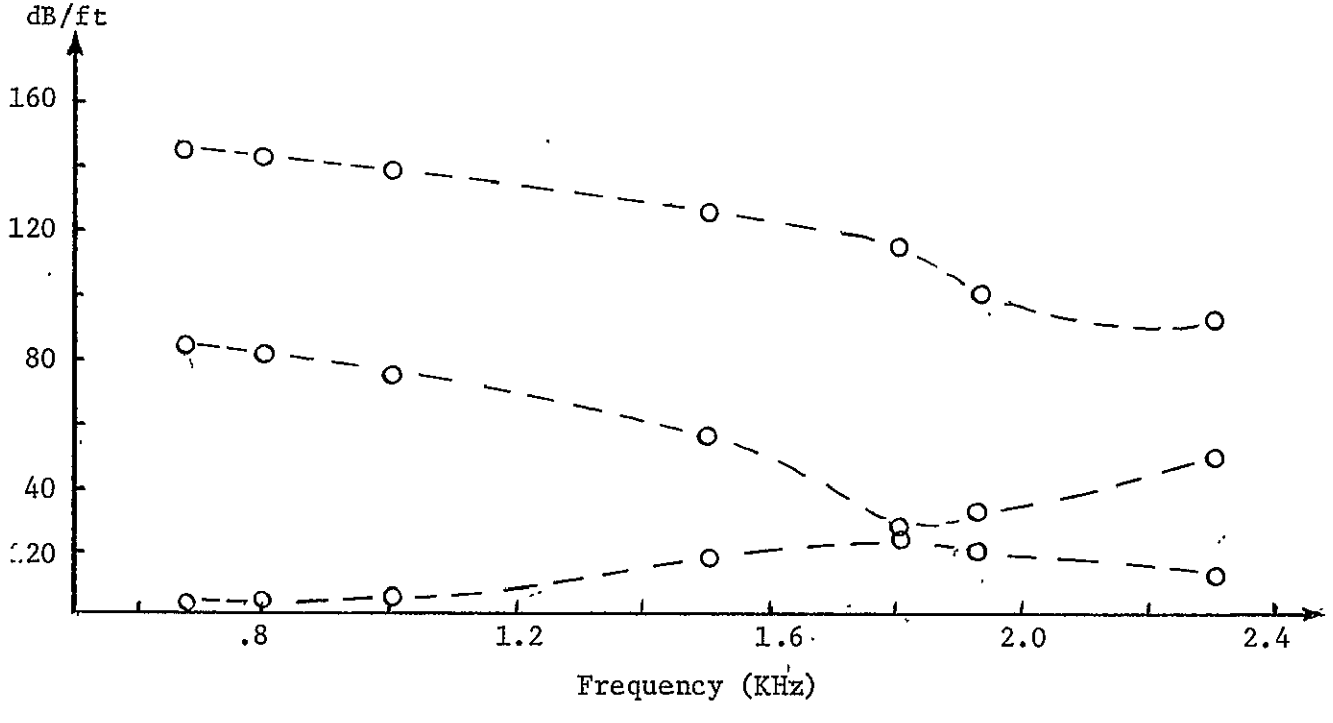

Figure 4.9 Attenuation of Successive Radial Mode for FM 1 Liner, m = 1

4.3 Multisectioned Duct Model

The analysis of a multisectioned duct system was presented in Section 2.5. This analysis will now be modified to consider an anechoically terminated duct with three sections. Figure 4.10 shows the duct system and the appropriate interfaces between each section. The resulting matrix equation for the system is given by Equation 4.1.

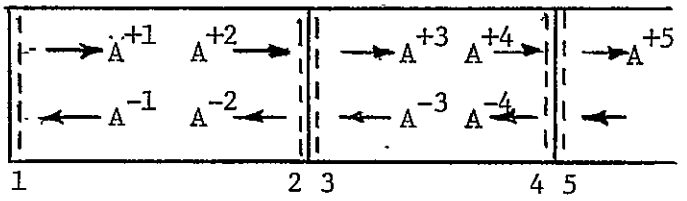

Figure 4.10 Multisectioned Duct Mode

A computer program was developed to analyze the mathematical model of the experimental duct system. The admittance and eigenvalues for each section were assigned to the proper interface and were used to calculate the transmission and reflection matrices between each section. The real eigenvalues for the hard-walled section are known (4) and the complex eigenvalues for the lined section were determined from measured impedance characteristics and the search technique described previously.

The source distribution and Equation 2.72 must be modified to account for the experimental source array. For generation of a circumferential mode of order M, the equation becomes

$$V(r) = \frac{Q_1\,\delta(r)}{r} + \frac{2\pi Q_2\,\delta(r-r_1)}{r} \sum_{n=1}^{4} \delta\left(\theta - \frac{\pi n}{2}\right) e^{i\frac{\pi}{2}nM} + \frac{2\pi Q_3\,\delta(r-r_2)}{r} \sum_{n=1}^{8} \delta\left(\theta - \frac{\pi}{4}n\right) e^{i\frac{\pi}{4}nM} \qquad (4.2)$$

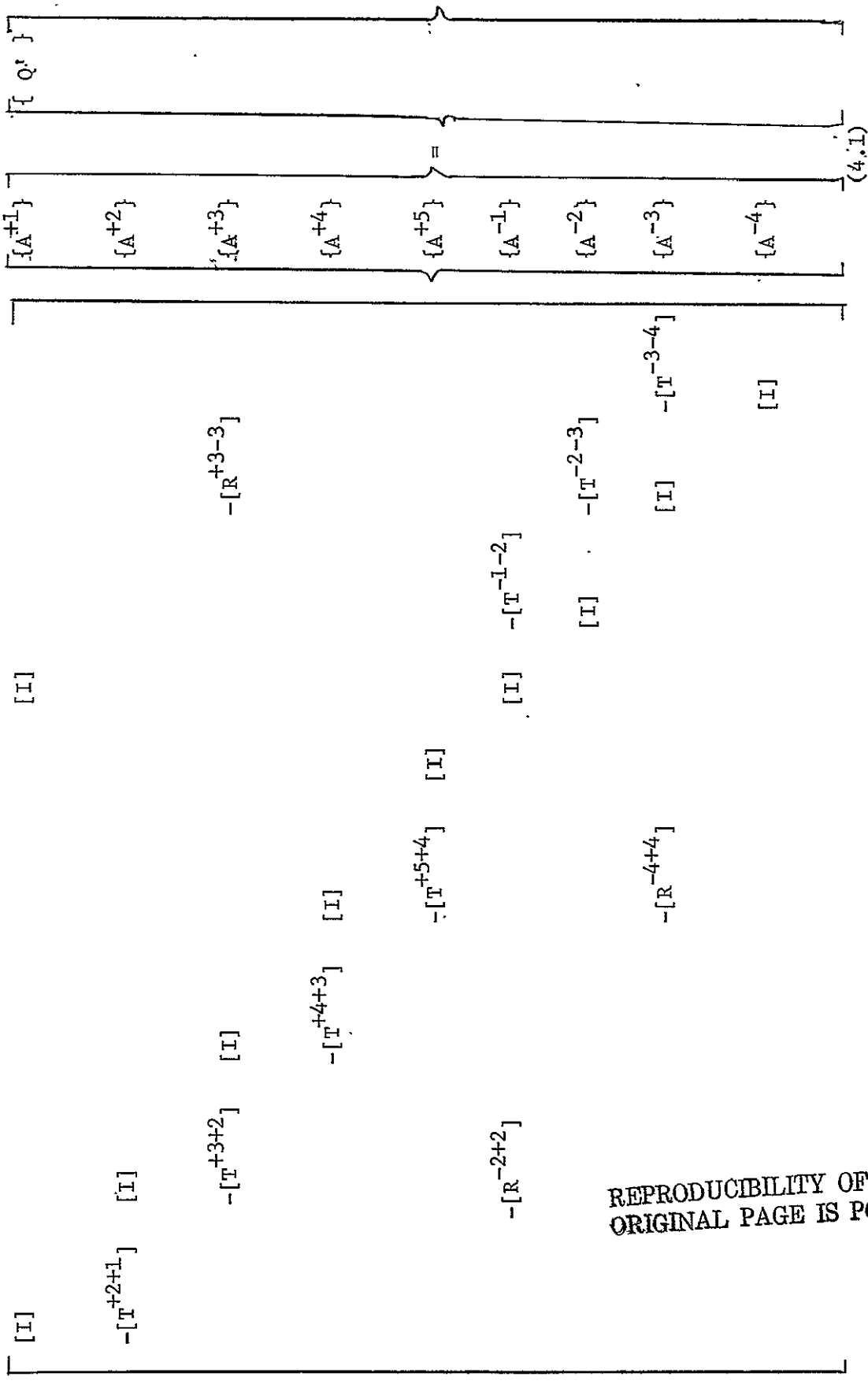

The relative amplitudes of the source strengths are related to their radial positions and the radial pressure distributions as presented in Figures 2.2 and 2.3. Using the momentum equation and the modal orthogonality conditions, the source equation becomes

$$\{A_\mu^{+1}\} + \{A_\mu^{-1}\} = \{Q'\} \tag{4.3}$$

where

$$\{Q'\} = \left\{\frac{Q_1 \Psi_\mu^{+1}(0) + 4 Q_2 \Psi_\mu^{+1}(r_1) + 8 Q_3 \Psi_\mu^{+1}(r_2)}{\Omega_\mu^{+1}}\right\}.$$

Each coefficient in the matrix equation is now specified. The matrix equation was developed into a system of 9 x μ_m linear equations where μ_m is the number of finite terms included in the summation over μ. These linear equations relate individual modal amplitudes at each interface to the reflection and transmission coefficients. The modal amplitudes were evaluated using a computer subroutine to solve the set of simultaneous linear equations.

Once the modal amplitudes are determined, the pressure field everywhere throughout the duct can be defined. Furthermore, the transmission and insertion loss of a liner can be calculated from these amplitudes.

The number of radial modes μ_m considered by this analysis at each frequency, was limited to all propagating modes and the next two higher order cut-off modes. There was no significant improvement in results when additional cut-off modes were included.

4.4 Multisectioned Duct Measurements

McDaniel (25) has performed an experimental study of the propagation of higher order modes through a duct containing a finite length liner. Mode shapes throughout the duct were measured for two liner materials. However, there was no effort to compare theoretical calculations with these results. In addition, the liners were simply inserted with a hollow duct, causing an abrupt reduction in the cross-sectional area within the lined section.

This study provides a significant improvement over the initial work of McDaniel. Progress was made to investigate acoustic propagation in a multisectioned duct through both experimental and theoretical techniques. An improved source array was developed to generate higher order acoustic modes within duct liners. These liners were inserted so that there was no change in cross-sectional area throughout the duct. This configuration thus provides a more realistic application of duct liners as acoustic treatment. An attempt was made to theoretically evaluate acoustic propagation in a multi-sectioned duct by determining the eigenvalues for a lined duct section and developing a mathematical model for the system. Finally, sources of error and discrepancies between measurement and theory were explained.

The soruce array was used to generate higher order modes throughout a range of frequencies in the multisectioned duct system. These modes included a plane wave, (0, 0) mode, the (0, 1) non-spinning mode, and the (1, 1) and (2, 1) spinning modes. The propagation of these modes was investigated for each of the liner materials described in Section 3.6. Measurements of the sound pressure level and radial mode shapes were taken at stations throughout the duct. These results were compared

with the levels and mode shapes calculated from the mathematical model for the multisectioned duct. In addition, the propagation of the (0,2) and (1,2) higher order modes was investigated with the fiber metal liner FM 1.

There are two distinct sources for error in the resulting duct measurements. First, the slight variation in cross section throughout the duct will cause errors in measured mode shapes. A change of only 1/2 inch in the duct diameter becomes significant at high frequencies where this change is of the order of the free space wavelength. In some sections of the 12 inch diameter duct, there is an increase of 1/2 inch in the diameter in one direction and a corresponding decrease of the same order at right angles to this. Thus, the duct is somewhat more eliptical in cross section than round. No estimate of the error produced by these non-uniformities can be made other than the fact that these variations in circular cross section will tend to redistribute the acoustic energy in the radial direction as well as shift the location of nulls in the radial pressure distribution. This variation seems to have greater effect on the propagation of spinning modes. This is not unexpected since the majority of acoustic energy is concentrated near the outer wall for all spiralling waves. Second, the individual phase differences between elements of the source array generate additional spurious modes together with the desired modes. These spurious modes can include plane waves and non-spinning modes as well as circumferential modes in both the clockwise and counterclockwise directions. Although they are generated at a much lower amplitude than the desired mode, their presence will often affect the radial mode shapes. The contribution of these modes is discussed in Appendix A.

In the following figures, the radial mode shapes were measured at the stations shown in Figure 3.1. The duct system contains a finite length liner inserted between the upstream and downstream hard-walled sections. Measurement positions at two upstream locations were chosen to investigate the radial mode shape generated by the source array and the presence of a standing wave. The standing wave is the result of reflections at the impedance discontinuity between different duct sections. These reflections cause conversion of energy between modes and often alter the radial pressure distribution of the generated mode. The measurement station at the middle of the liner was chosen to investigate the change in radial mode shapes due to the complex eigenvalues for this section. Since the anechoic termination eliminates reflection from the end of the duct, only one measurement station was chosen in the downstream section. In this section, the eigenvalues are the same as for the upstream section and the mode shape resorts to the form of the incident waves.

In some cases, the mode shape at the downstream station has no relationship at all to the generated mode, despite the fact that the eigenvalues are the same as for the upstream duct section. There are two reasons for this. First, there are components from other radial modes of the same circumferential order which make up the pressure distribution at this position. These components are the result of modal conversion of energy at each interface before this section. Second, the spurious modes contributed by the source array can appear downstream. Their presence at upstream positions is not evident since these modes are generated at a much lower level than the desired mode. However, since the transmission loss of the liner for individual modes is

different, these modes are often evident at downstream positions because they are not attenuated to the same extent as the desired mode. This result is particularly noticeable at high frequencies where several lower order modes can propagate. Therefore, when spurious modes exist and the major component of the propagating mode is attenuated, an unrecognizable mode shape which is the combination of several residual modes results.

In order to see the relationship between the mode shapes and levels at stations throughout the duct, the mode shapes will all be presented in one figure. Selected mode shapes at several frequencies for different modes will be presented for one liner, FM 1. Also, modes for different liners which exhibit interesting behavior will be presented.

The source strengths of individual elements of the array can be used to calculate the sound pressure levels throughout the duct. However, these levels will be normalized to the maximum level in the upstream section and plotted as relative levels in the following figures.

The lowest order mode in a duct is the plane wave. It is possible to generate this mode up to the cut-off frequency for the first non-spinning radial mode. Within this frequency range, the first spinning mode can also propagate but is suppressed due to source symmetry and phasing of the array. Mode shapes measured for a plane wave generated at 500 Hz are shown in Figure 4.11 when an FM 1 liner is inserted in the test section of the duct system. At this frequency, the plane wave is the only mode that can propagate without exponential attenuation in the hard-walled section. The relative sound pressure levels and mode shapes as calculated from the multisectioned duct analysis are also

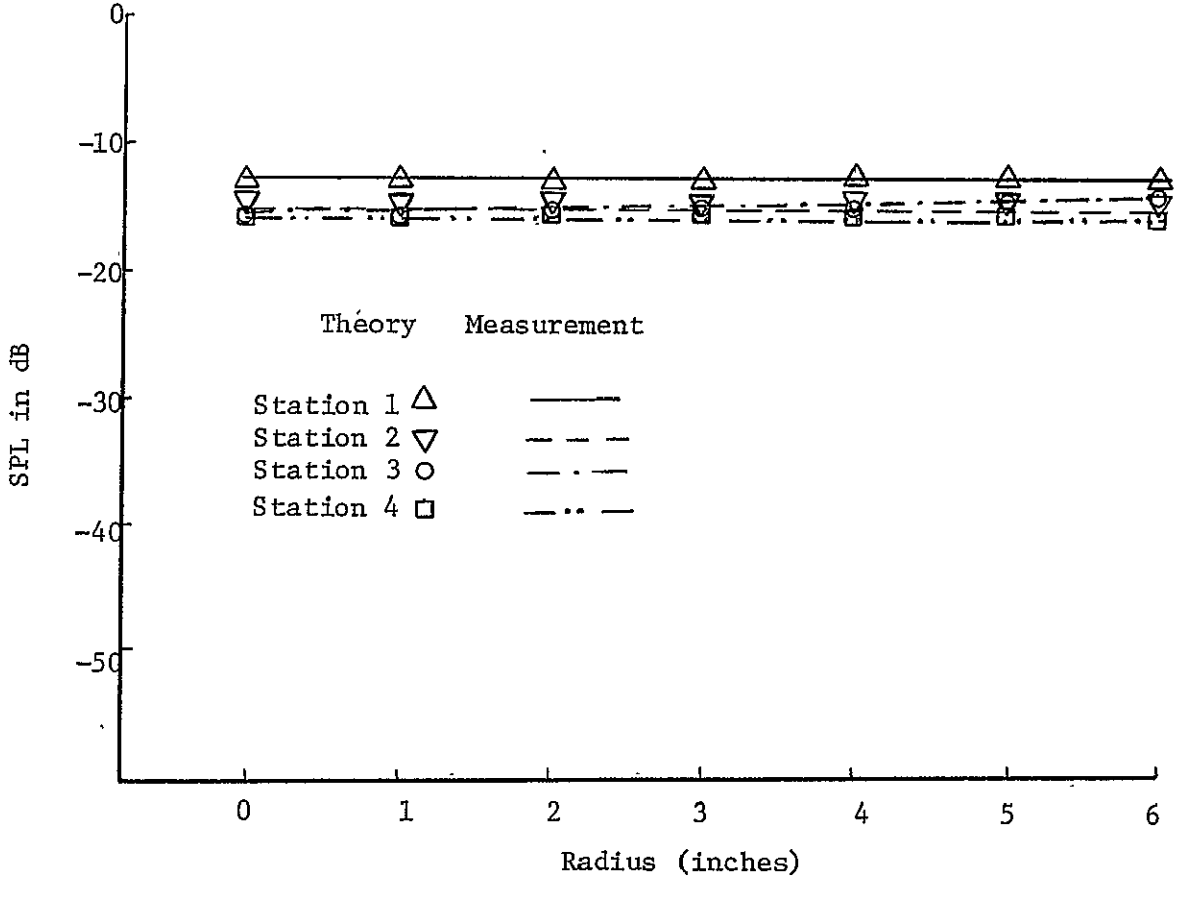

Figure 4.11 Radial Mode Shapes for (0,0) Mode, 500 Hz - EM 1 Liner

presented. Despite the presence of plane waves at upstream and downstream positions, a plane wave does not exist within the liner section. This result is in agreement with Morse (33) who showed that a plane wave could not exist within the lined section of a duct. The deviation from plane wave behavior in the liner is further emphasized in Figure 4.12 where a plane wave is generated at 800 Hz. Again, a well defined plane wave exists both above and beyond the liner but not in the liner. In both cases, there is good agreement between measurement and theory for both the acoustic levels and the mode shapes at each of the duct stations. Plane wave propagation at 1250 Hz, which is just below the cut-off frequency for the first non-spinning radial mode, is shown in Figure 4.12. In this case, the levels upstream and within the liner are fairly well predicted but there is an indication of a standing wave in the downstream section.

The first non-spinning radial mode (0, 1) can be generated at frequencies well above its cut-off frequency. Furthermore, this mode is being generated in a frequency range where the (1, 1) and (2, 1) spinning modes can also propagate. The propagation of these modes is restricted by the shading and phasing of the source array. Mode shapes at 1390 Hz at the four duct stations are shown in Figure 4.14. The nulls in the mode shapes exhibit a noticeable shift in radial position which is predicted by theory. This shift is due to the modal conversion of energy at the interface of each section. Also, the standing wave pattern is emphasized by the difference in levels between positions 1 and 2. Furthermore, this standing wave is predicted by theory with the station closest to the liner having a higher level. The mode shapes at 1600, 2000 and 2500 Hz, well above the cut-off frequency, are shown in

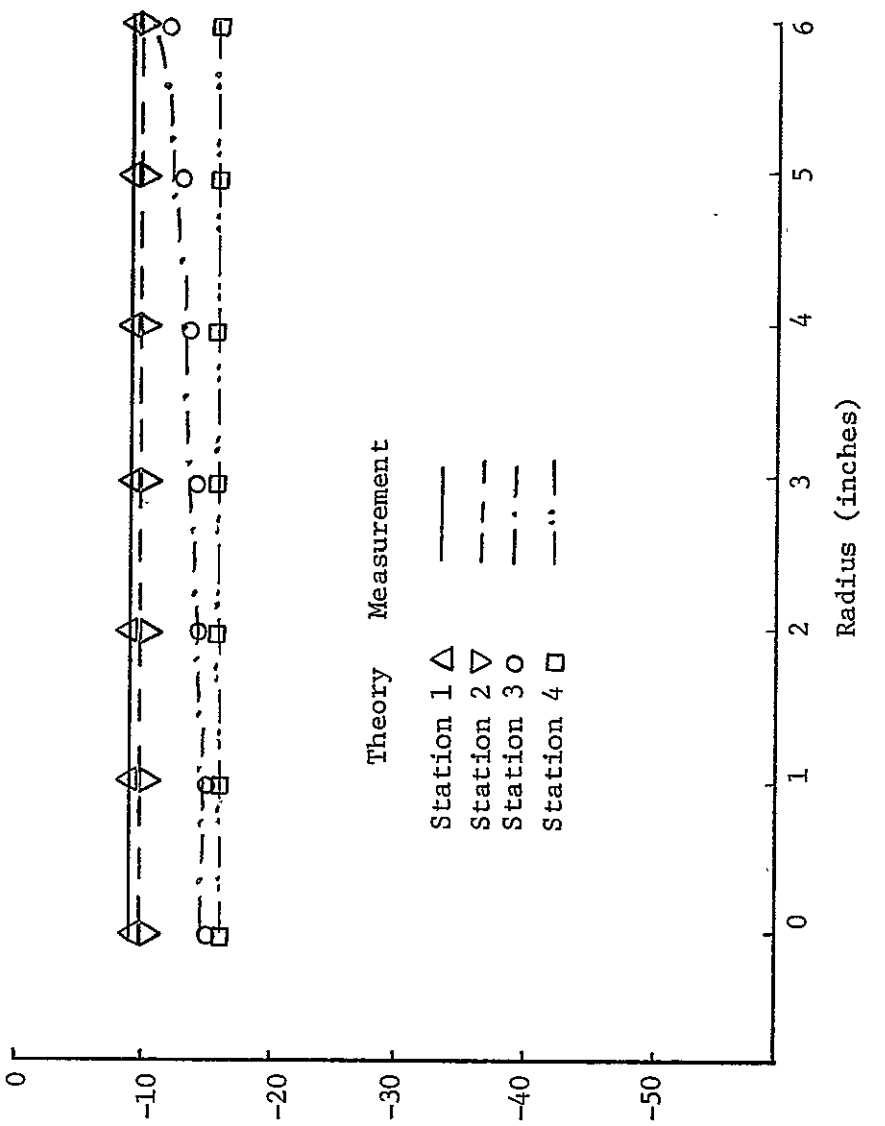

Figure 4.12 Radial Mode Shapes for (0,0) Mode, 800 Hz - FM 1 Liner

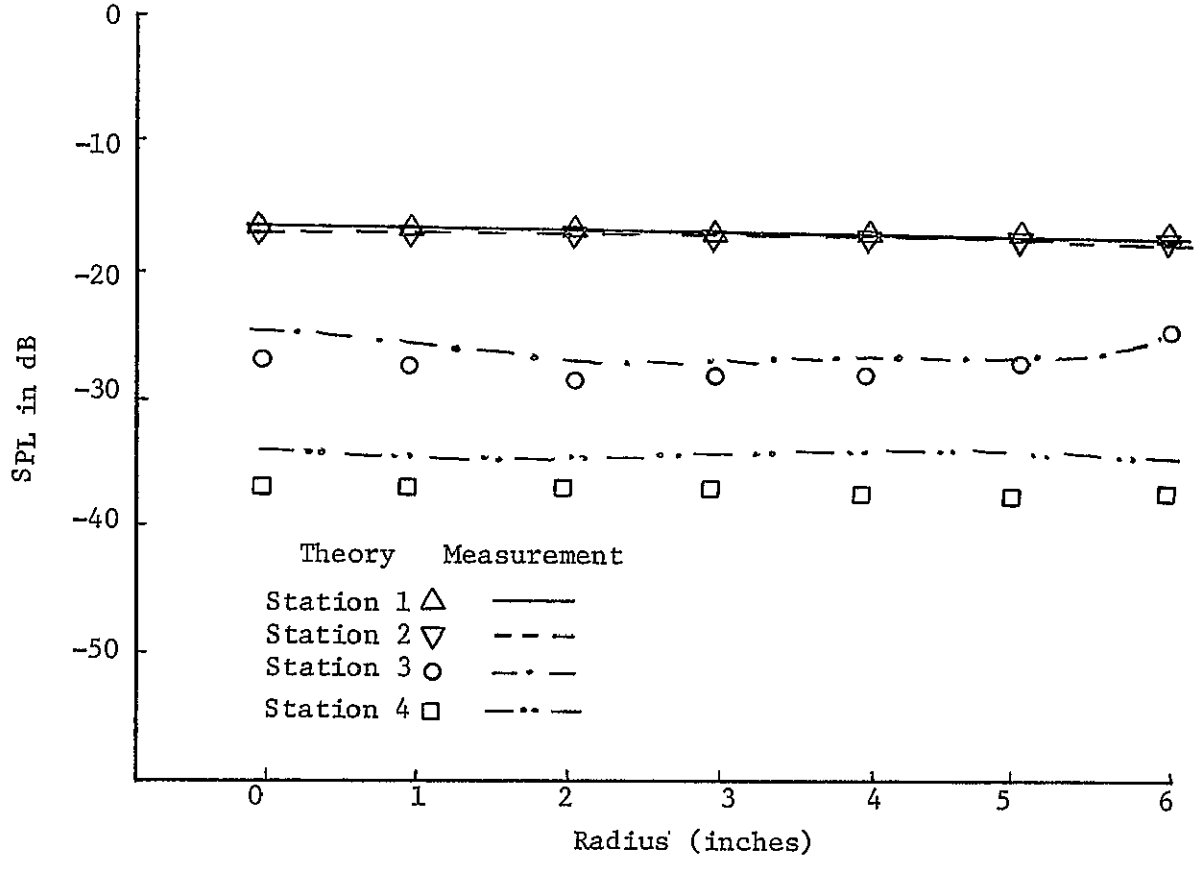

Figure 4.13 Radial Mode Shapes for (0,0) Mode, 1250 Hz - FM 1 Liner

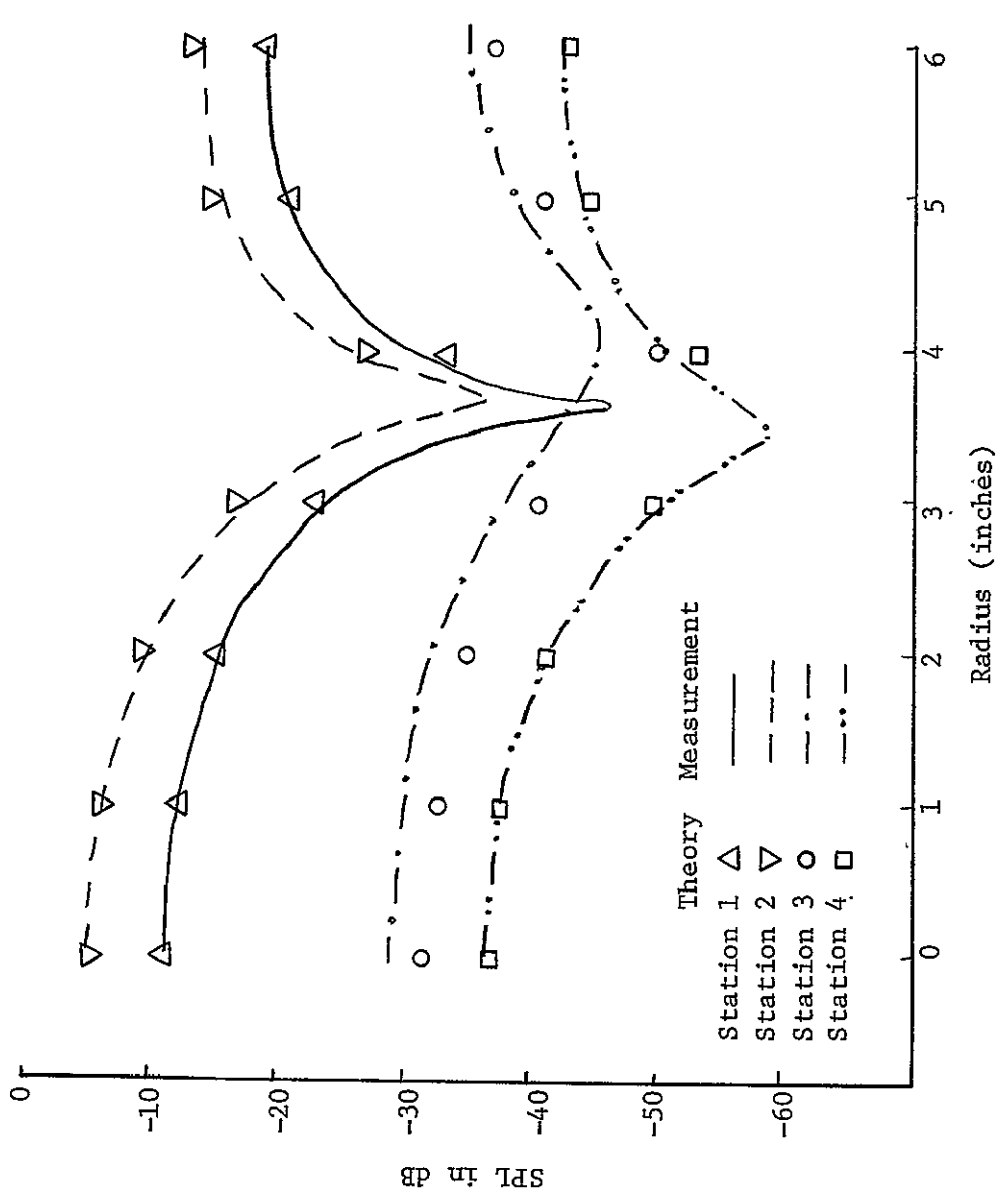

Figure 4.14 Radial Mode Shapes for (0,1) Mode, 1390 Hz - FM 1 Liner

Figures 4.15, 4.16 and 4.17. Again, similar results for the shift in nulls are noticed. Despite the well defined mode shapes upstream, the mode shapes in the downstream section show considerable distortion in each case. This is a result of the conversion of energy between the (0, 1) mode and the (0, 0) mode or plane wave, both of which can propagate without exponential attenuation at this frequency. The mode shapes within the liner are fairly well predicted, indicating that the local reaction boundary condition is a valid assumption. It is interesting to note the differences between mode shapes within the liner as a function of frequency. Although the eigenvalues for the liner at a particular frequency are dependent on the impedance, these modes are similar in shape. This is because the impedance does not exhibit any rapid variations within this frequency range and is only slowly changing in value.

By properly adjusting the phase and amplitude of each element in the source array, the first spinning mode can be generated in the multi-sectioned duct. Radial mode shapes throughout the duct are shown in Figure 4.18 for the (1, 1) mode at 670 Hz. Although the mode shapes are fairly well defined, there is a discrepancy between the predicted levels at each station. This can be explained by the presence of a significant standing wave due to the anechoic termination which exists near the cut-off frequency. Improved agreement between measurement and theory is seen in Figure 4.19 for this same mode at 1000 Hz. The higher level of the station nearer the liner is predicted by theory as well as the modes shapes in each section. Mode shapes at 1500 Hz are shown in Figure 4.20. The upstream mode shapes are fairly well defined and are in reasonable agreement with theory. The absence of a clearly defined null at the

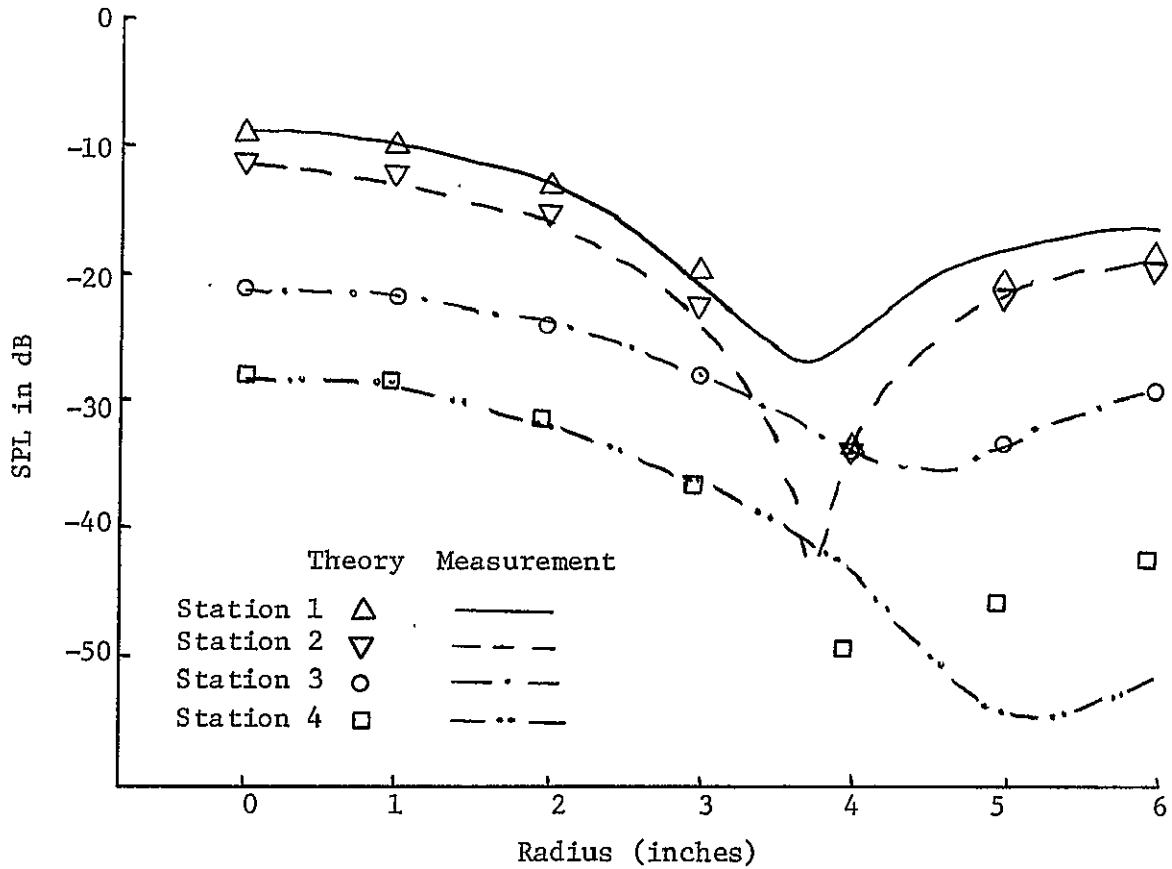

Figure 4.15 Radial Mode Shapes for (0,1) Mode, 1600 Hz - FM 1 Liner

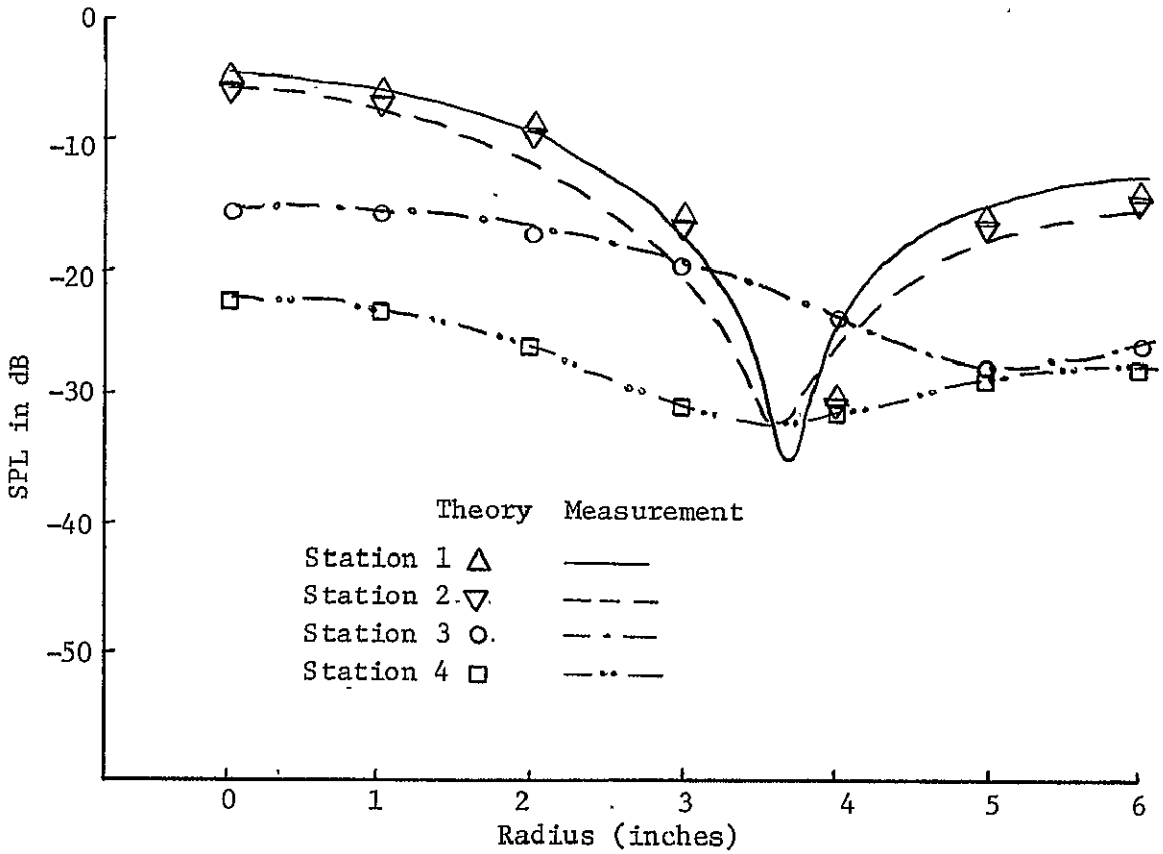

Figure 4.16 Radial Mode Shapes for (0,1) Mode, 2000 Hz - FM 1 Liner

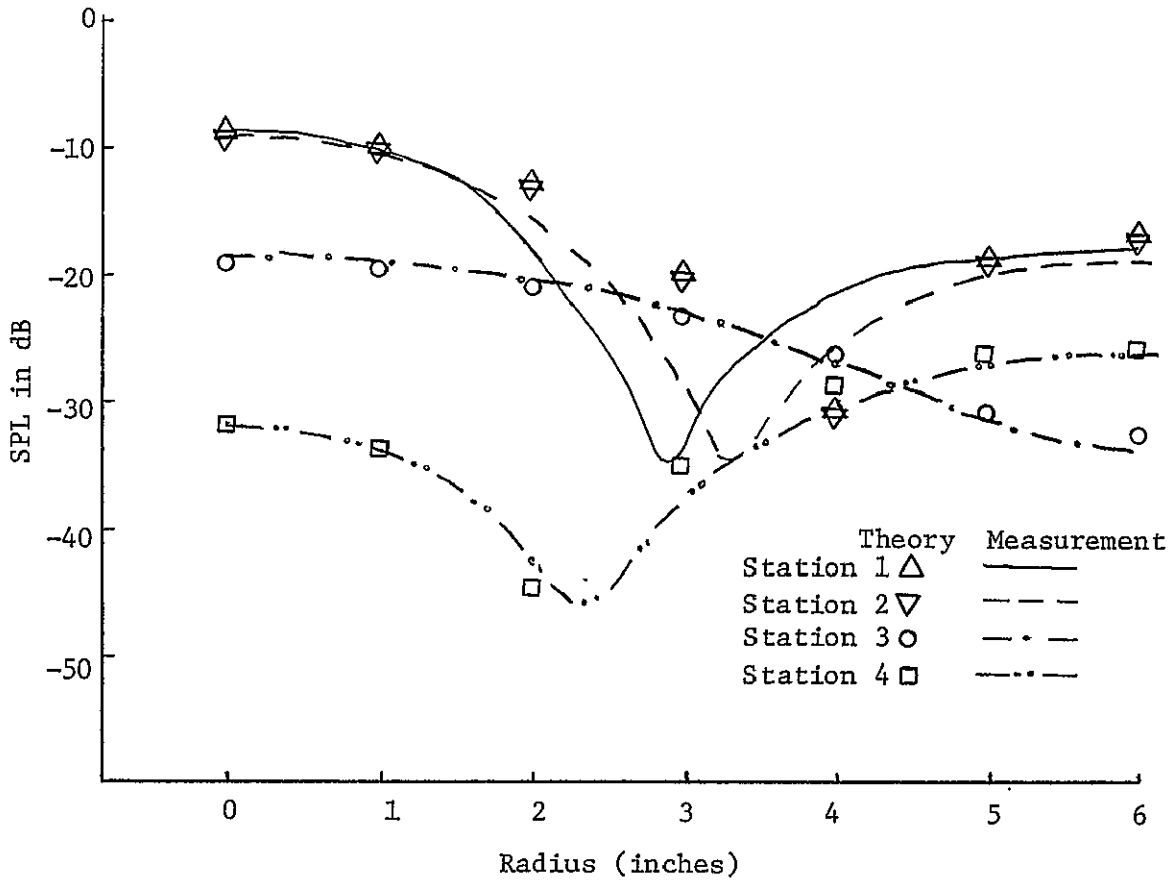

Figure 4.17 Radial Mode Shapes for (0,1) Mode, 2500 Hz - FM 1 Liner

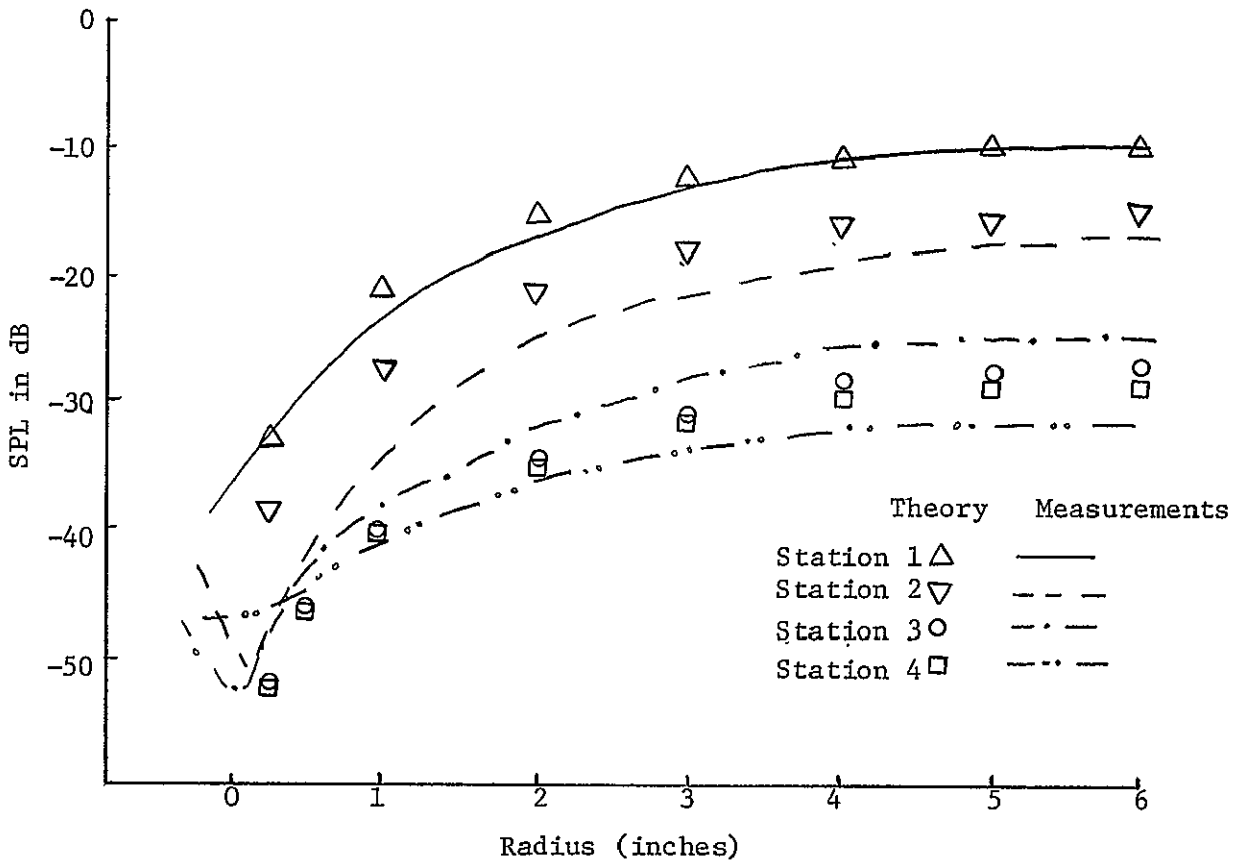

Figure 4.18 Radial Mode Shapes for (1,1) Mode, 670 Hz - FM 1 Liner

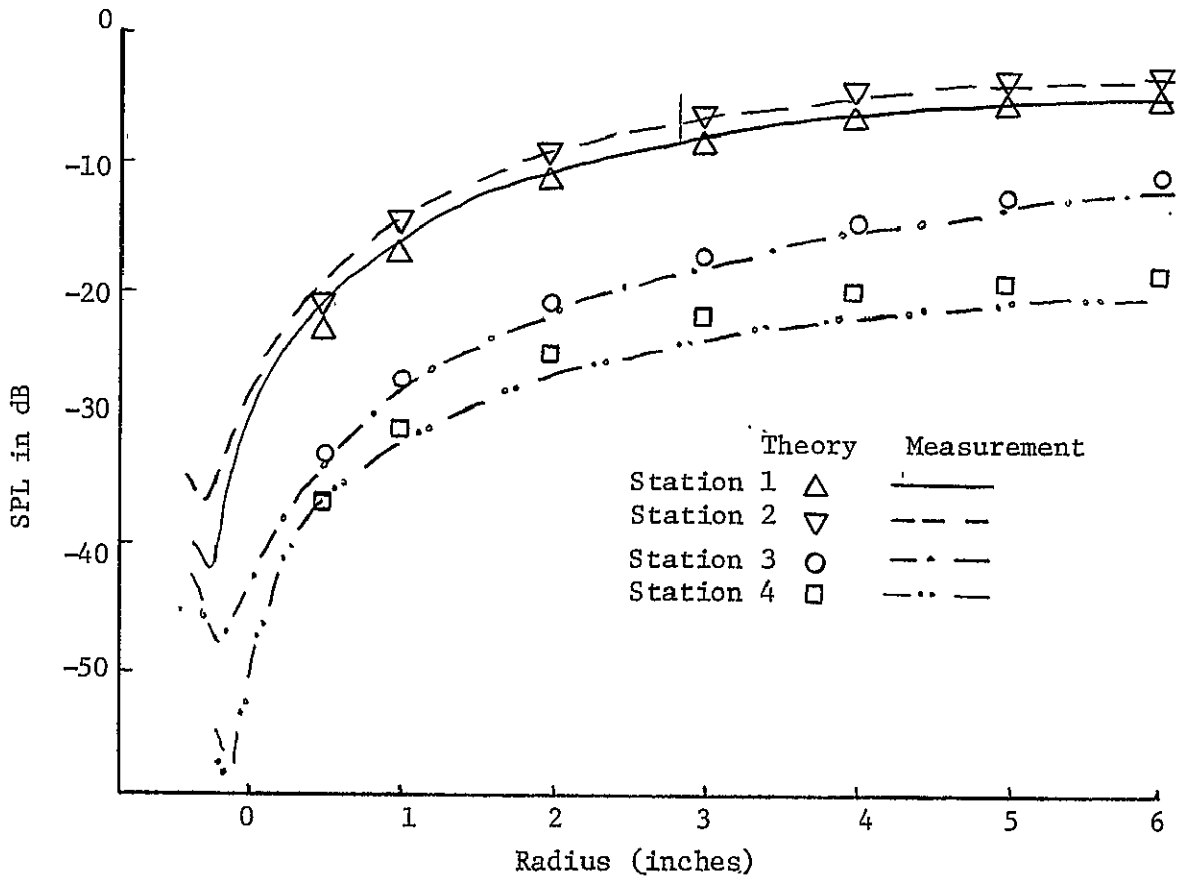

Figure 4.19 Radial Mode Shapes for (1,1) Mode, 1000 Hz - FM 1 Liner

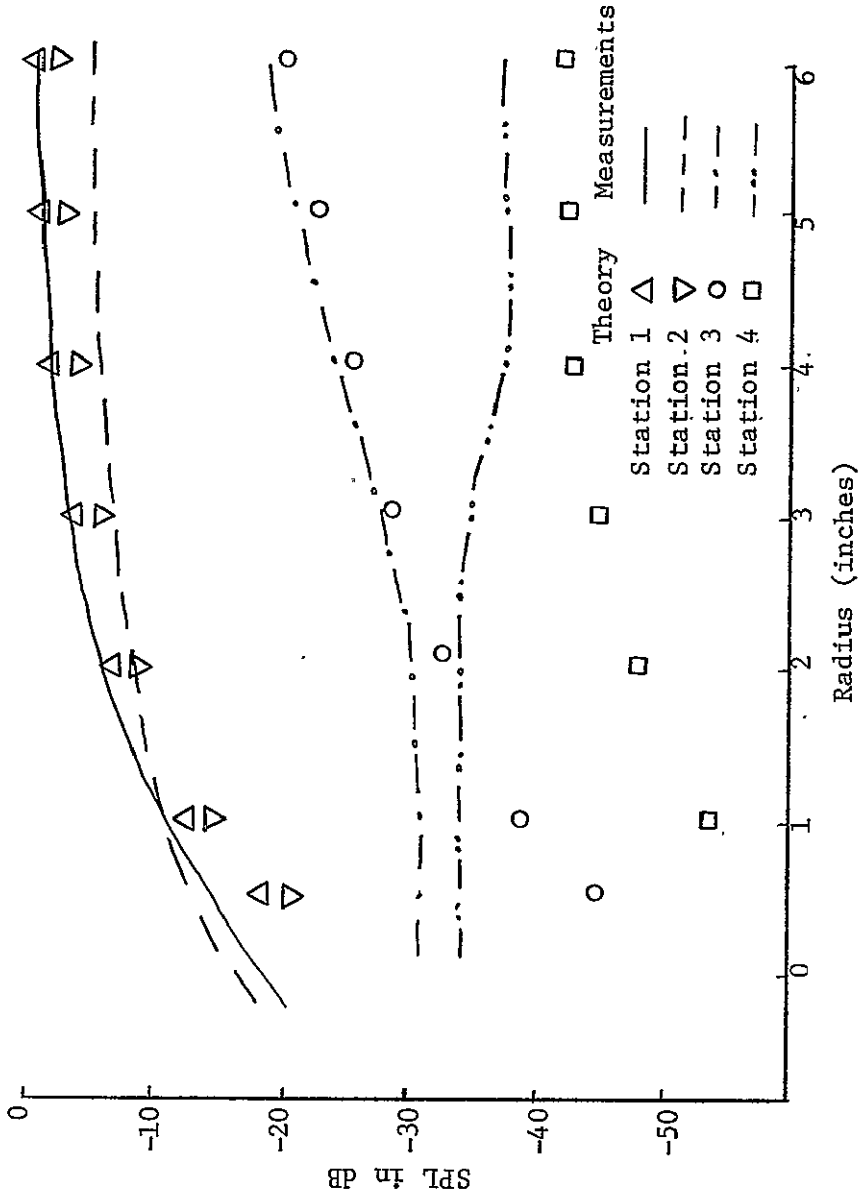

Figure 4.20 Radial Mode Shapes for (1,1) Mode, 1500 Hz - FM 1 Liner

center indicates contamination from additional non-spinning modes. Within the liner, the mode shape is accurately predicted over the majority of the radius. Near the center, there is a complete absence of a null. Thus the total acoustic pressure at this position contains the generated spinning mode at a reduced level and contributions from non-spinning modes. In the downstream section, the mode shape has no resemblance to the spinning mode which should have a null at the center. The measured mode shapes would seem to be a combination of a plane wave and (0, 1) mode. This is not unexpected since both the plane wave and (0, 1) mode can propagate at this frequency without exponential attenuation. In addition, the downstream level is much higher than predicted by theory. This is because the total upstream acoustic pressure contains components of non-spinning modes which are not attenuated to the same extent by the liner as the generated spinning mode.

To generate a spinning mode of order m = 2, only the outer ring of speakers was used. The use of additional speakers is restricted by Equation 3.1. As a result of using only the eight outer speakers to generate this mode, the modal purity suffers considerably. Mode shapes at 1250 Hz are shown in Figure 4.21. The nulls at the center of the duct are obscured by the presence of additional modes. Again, the mode shapes upstream and in the liner are fairly well predicted by theory. The downstream component appears to be a residual plane wave and has no relationship to the spinning modes characteristic of upstream propagation. The transmission loss of nearly 40 dB across the liner for circumferential modes of order m = 2, removes the major components of the (2, 1) spinning mode and leaves only a pressure distribution which is the sum

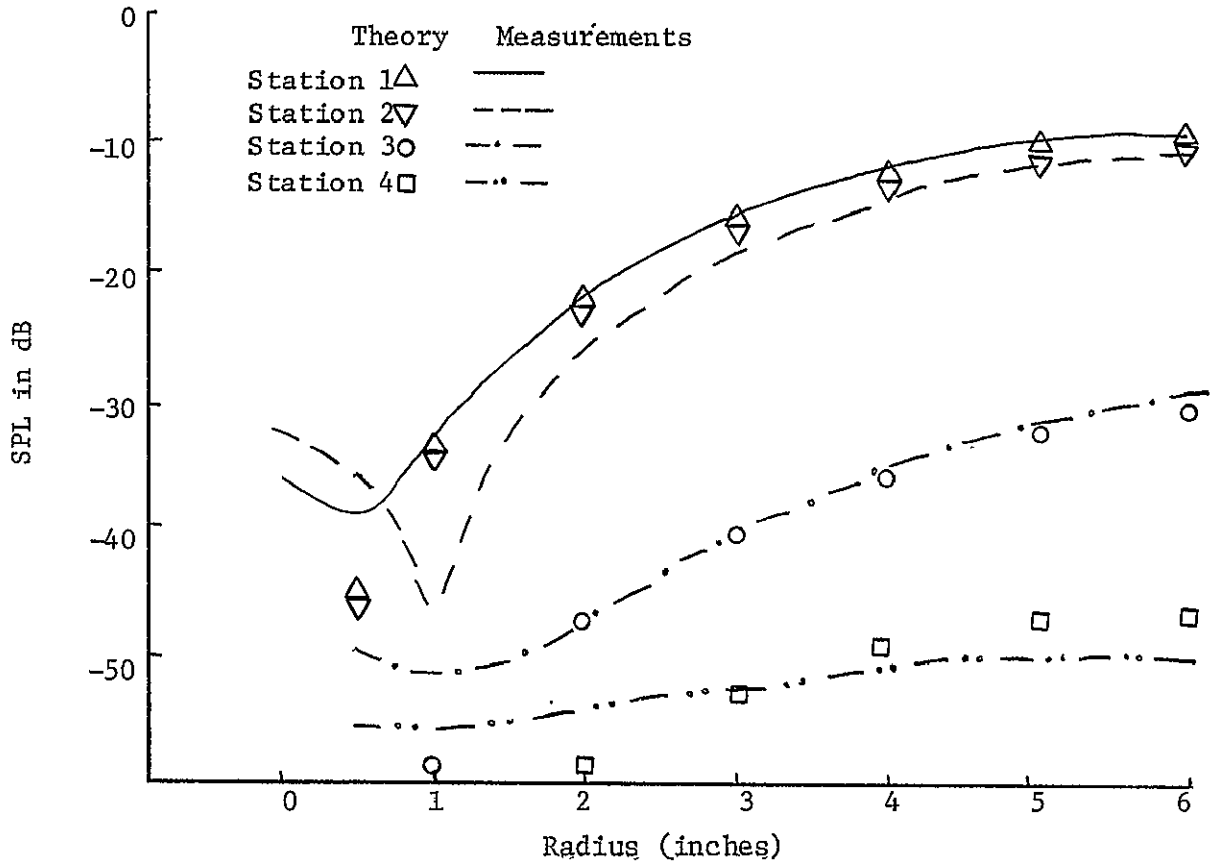

Figure 4.21 Radial Mode Shapes for (2,1) Mode, 1250 Hz - FM 1 Liner

of components of several residual modes. At a higher frequency of 1600 Hz, the modal purity begins to deteriorate, not only downstream, but within the liner. The upstream mode shapes show contamination from other modes because of the absence of the null at the center. The (2, 1) component of the acoustic pressure is attenuated as it passes through the liner leaving an unrecognizable mode shape downstream. This mode vaguely resembles (0, 1) mode with a pressure maximum at the center of the duct. This mode is one of the least attenuated modes by the liner at this frequency. The reversed levels of the upstream positions is also predicted in this case. Due to the noticeable contamination at position 2, little agreement with theory can be expected within the liner and in the downstream section.

The propagation of several additional higher order modes was studied for the same fiber metal liner. In Figure 4.23 the (0, 1) mode is being generated at 3000 Hz, which is significantly above its cut-off frequency as well as the cut-off frequency of the second radial mode (0, 2). The (0, 1) mode shapes are well defined in the upstream section and there is no indication of the (0, 2) mode. The levels and mode shapes throughout the duct are reasonably predicted by theory. It is not unexpected that the agreement for this mode would not be as good as for the previous lower order modes since three radial modes of the same circumferential order can propagate at this frequency. Furthermore, the slight variation in duct geometry and duct diameter mentioned earlier would have a greater effect on acoustic propagation at high frequencies where the wavelength is small and of the same order as the non-uniformities in the duct.

The (0, 2) mode is shown in Figures 4.24 and 4.25. At 2700 Hz,

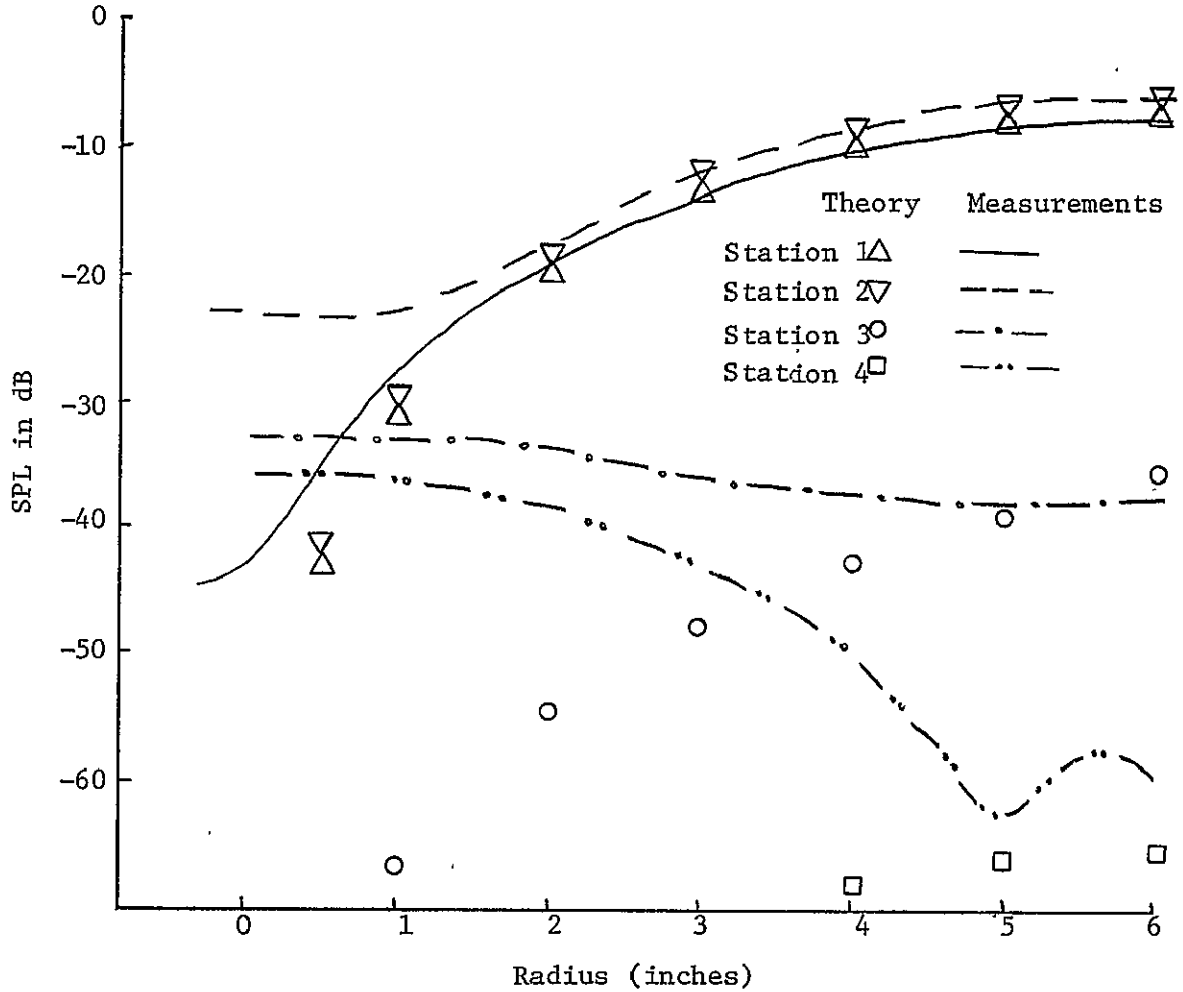

Figure 4.22 Radial Mode Shapes for (2,1) Mode, 1600 Hz - FM 1 Liner

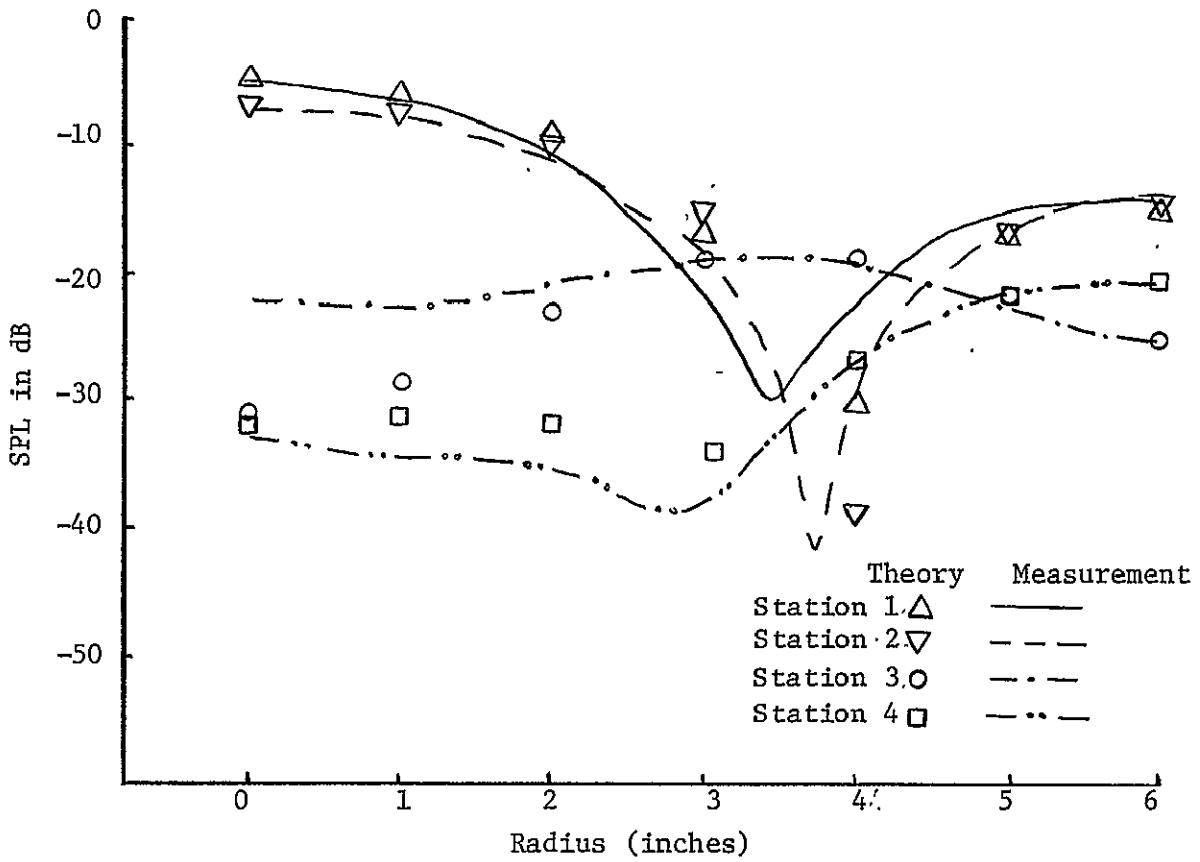

Figure 4.23 Radial Mode Shapes for (0,1) Mode, 3000 Hz - FM 1 Liner

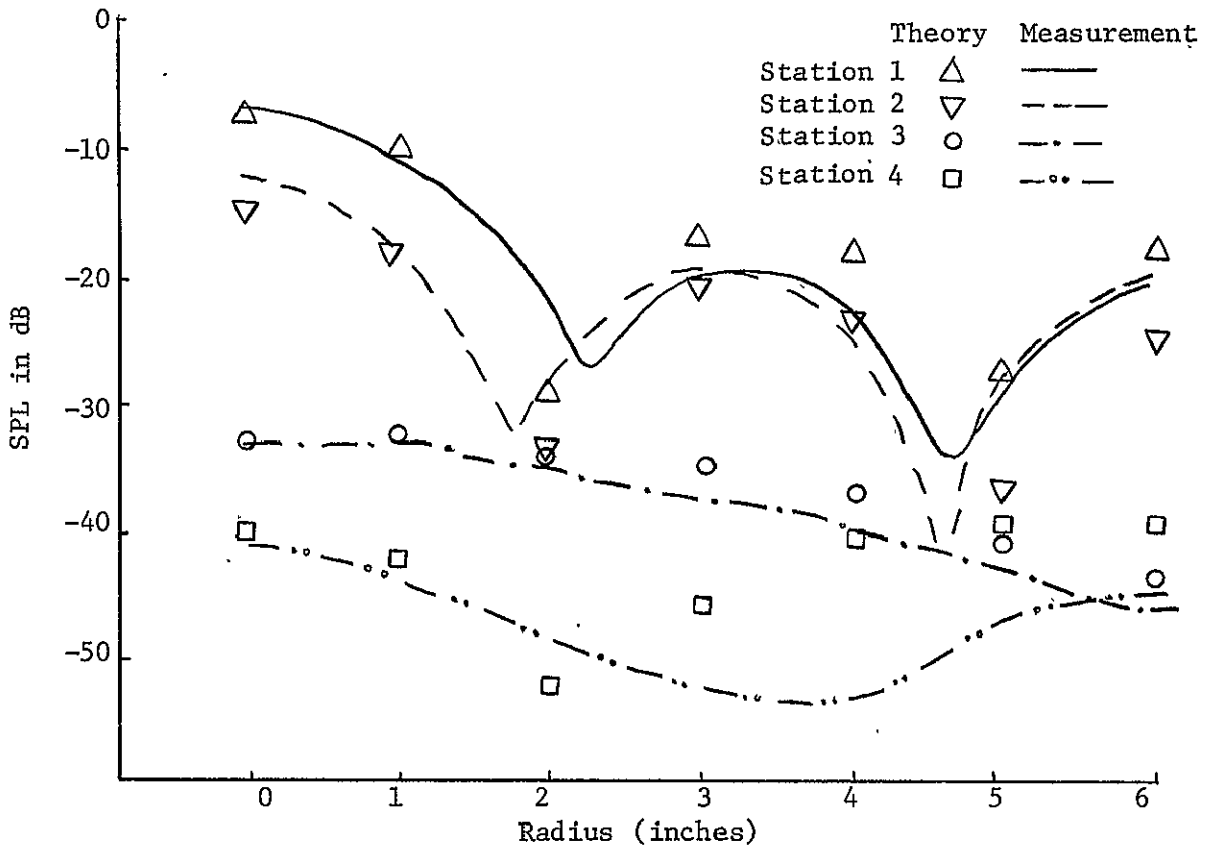

Figure 4.24 Radial Mode Shapes for (0,2) Mode, 2700 Hz - FM 1 Liner

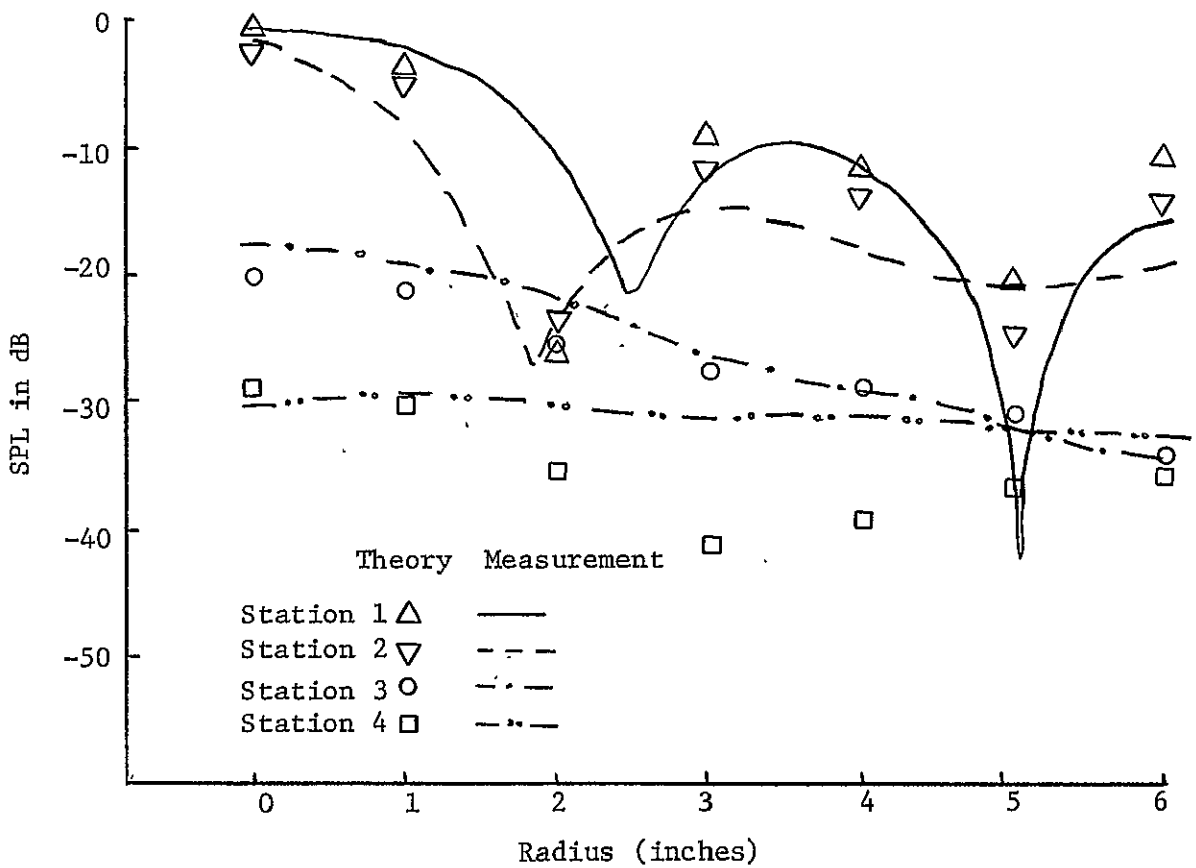

Figure 4.25 Radial Mode Shapes for (0,2) Mode, 3100 Hz - FM 1 Liner

the upstream mode shapes are in fairly good agreement with theory. Within the liner, the mode shape begins to deviate from the form predicted by theory and at the downstream position, the mode shape is distorted considerably. At 3100 Hz, there is further deterioration in the modal purity at upstream positions which is reflected throughout the duct. Nevertheless, the mode shape in the liner is fairly well predicted for the resulting boundary conditions and eigenvalues. The downstream component indicates contamination from plane waves and the level is accordingly higher than predicted by theory for the (0, 2) mode.

The (1, 1) spinning mode is shown in Figure 4.26 at a frequency of 2499 Hz. This mode is generated at a frequency above the cut-off frequency for the second radial mode. Although this mode is not as clearly defined upstream as for previous cases at lower frequencies, the relative levels at the two stations are predicted. The mode shape in the liner and in the downstream section are in good agreement with predicted mode shapes.

The second radial mode with circumferential order of m = 1 is shown in Figure 4.27 at 2300 Hz. The null at the center is well defined for both upstream mode shapes. There is a difference between the levels at the wall and the radial position of the nulls. This could occur as the result of the non-uniformities and changes in the circular cross-section throughout the duct. The measurements within the liner and downstream section agree with theory for both the levels and the mode shapes.

Mode shapes for an incident plane wave, (0, 0) mode, were investigated for each of the remaining liner materials. The relative levels and mode shapes at stations in the duct system are shown in

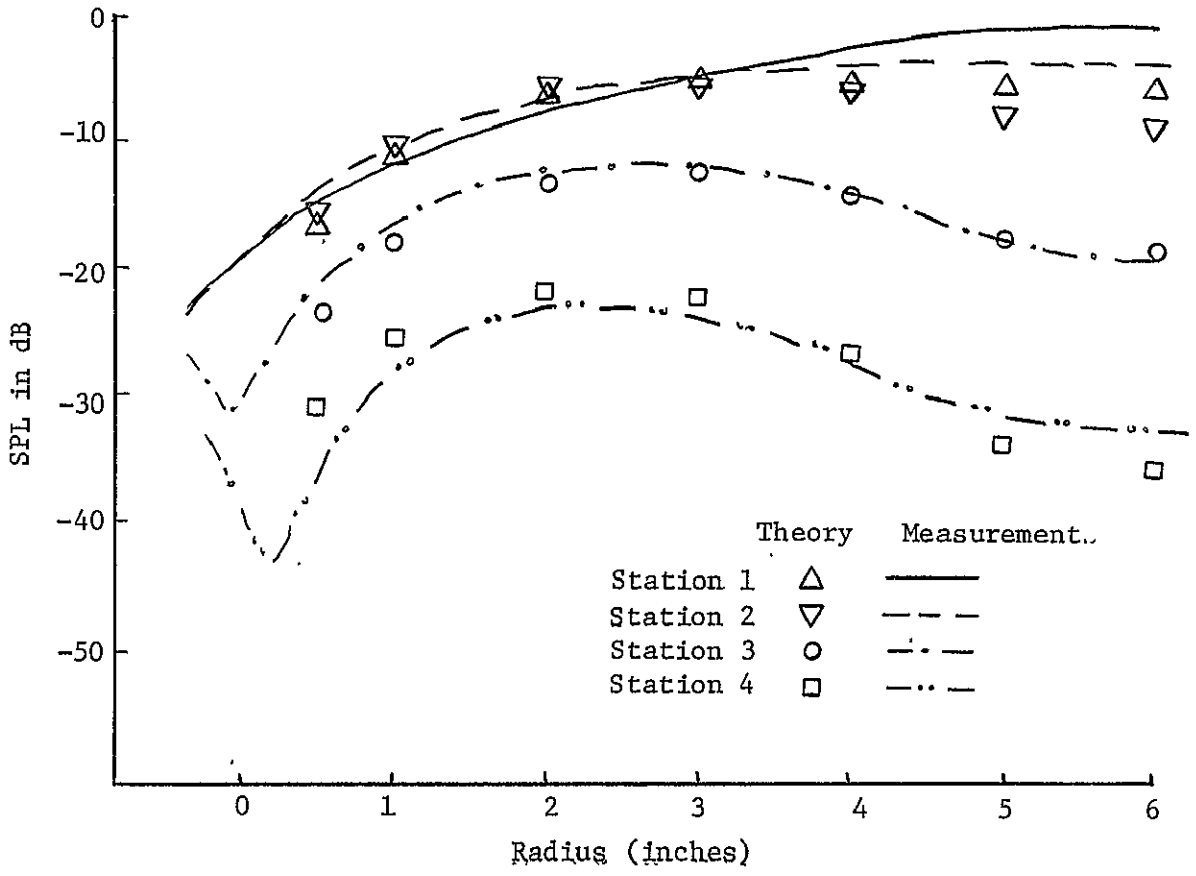

Figure 4.26 Radial Mode Shapes for (1,1) Mode, 2400 Hz - FM 1 Liner

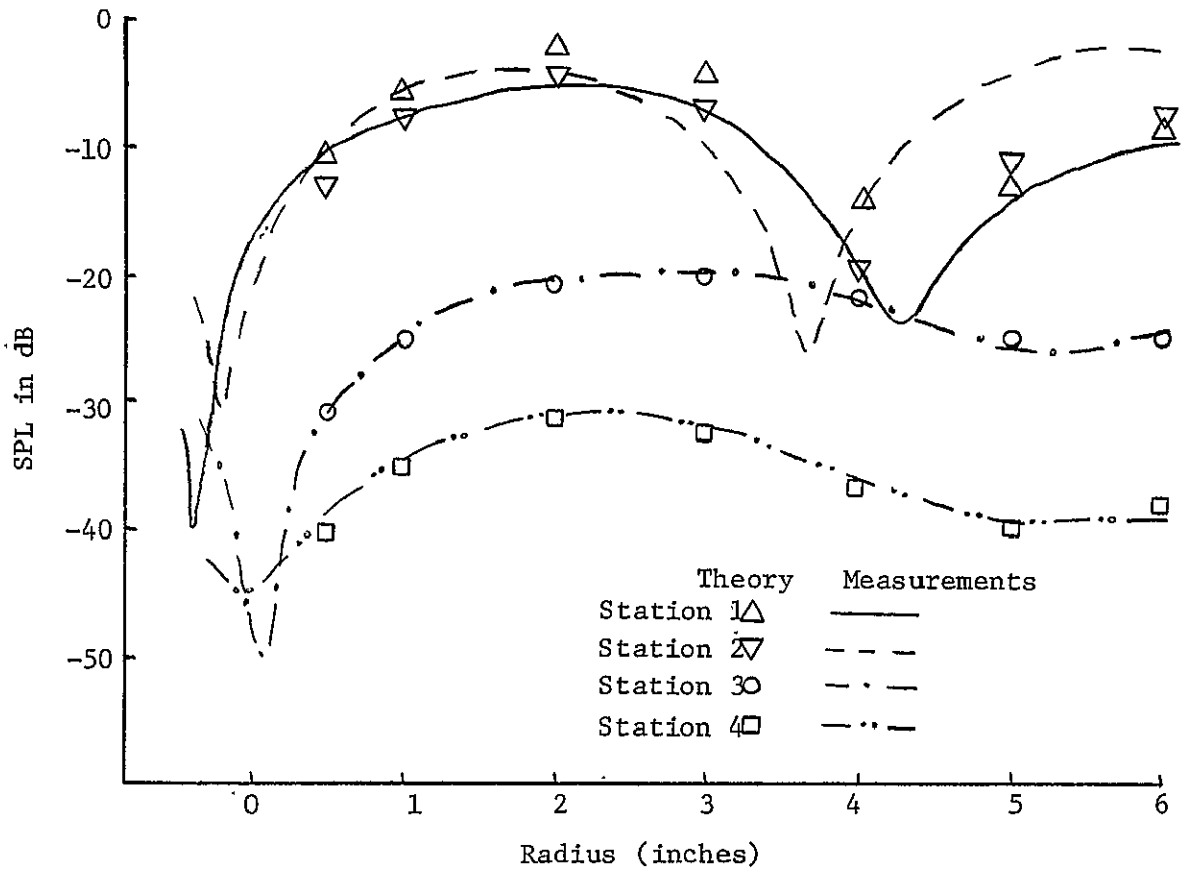

Figure 4.27 Radial Mode Shapes for (1,2) Mode, 2300 Hz - FM 1 Liner

Figure 4.28 for a plane wave at 800 Hz and the liner Perf 1. Similar results are shown at the same frequency for the liner FM 2 in Figure 4.29. The increased attenuation for the fiber metal liner as compared to the perforated panel liner can be seen in this figure. The difference in attenuation between a one foot and two foot glass fiber liner for a plane wave at 800 Hz is shown in Figures 4.30 and 4.31. The agreement with theory is good in all cases. The radial mode shape within each liner has the same general form despite the different eigenvalues for each material. This is because the plane wave is the only circumferential mode of order m = 0 that can propagate at this frequency without exponential attenuation. There is no conversion of energy by reflection and transmission at each interface to lower order radial modes and little, if any, conversion to higher order modes. This is evident by plane wave behavior at positions on each side of the liner. The mode shapes at each station for a one foot glass fiber liner at 1250 Hz are shown in Figure 4.32. There is still reasonable agreement between measurement and theory. This indicates that the local reaction boundary condition is valid for the glass fiber material for the attenuation produced by a plane wave.

The first non-spinning radial mode, (0, 1) was investigated next for the different liners. At 1600 Hz, the radial mode shapes for the liners Perf 2 and FM 2 are shown in Figures 4.33 and 4.34. The mode shapes throughout the duct are well defined. Due to the small attenuation of the perforated metal liner for the (0, 1) mode, it is difficult to clearly see the radial mode shape within the liner which is by the eigenvalues. This mode shape is shown in Figure 4.35 and compared with theory. The shift in the radial position of the null is probably

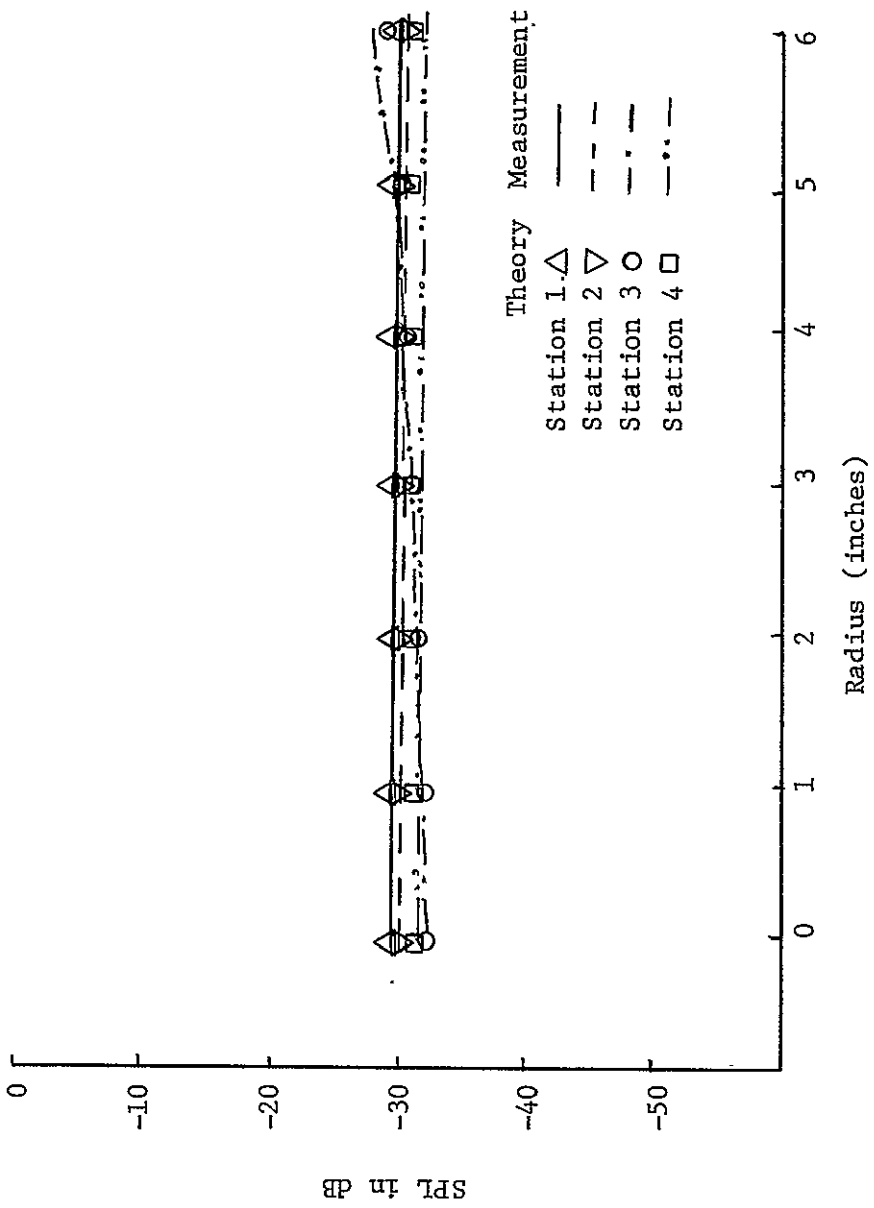

Figure 4.28 Radial Mode Shapes for (0,0) Mode, 800 Hz - Perf 1 Liner

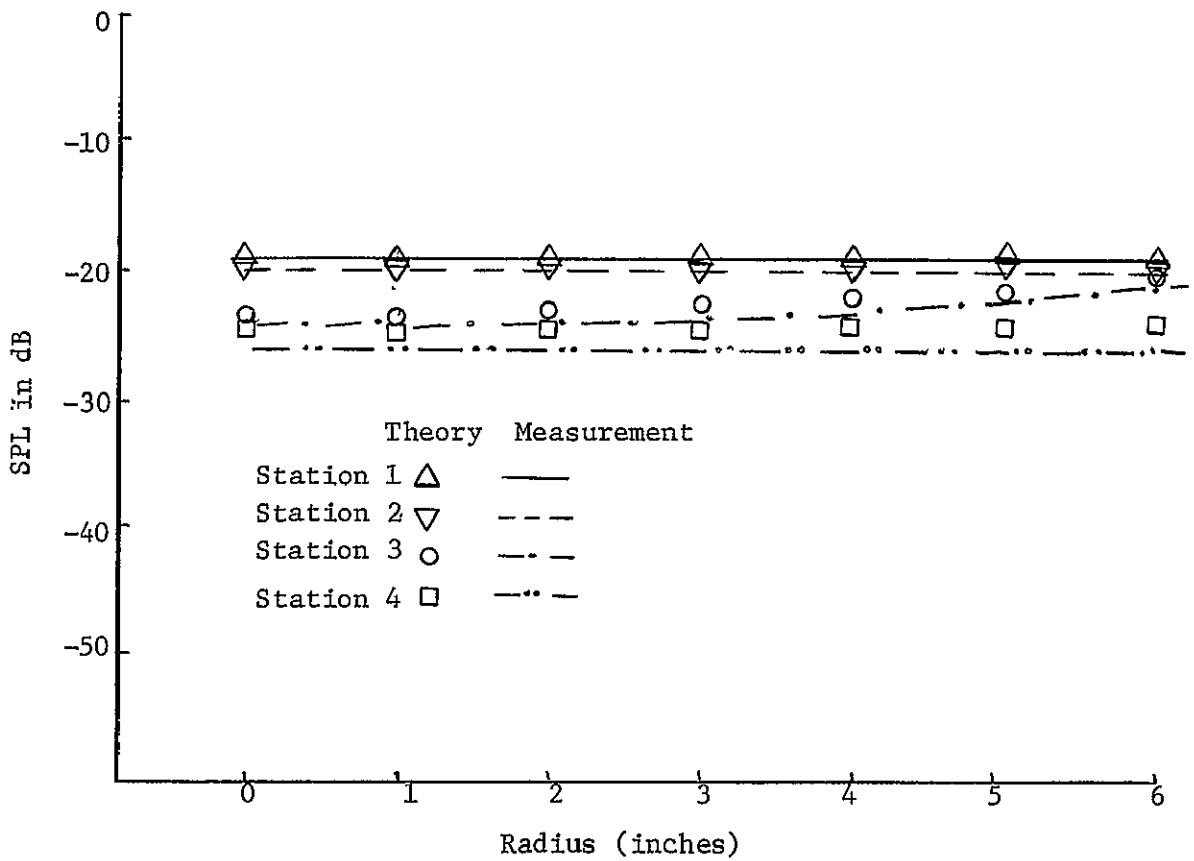

Figure 4.29 Radial Mode Shapes for (0,0) Mode, 800 Hz - FM 2 Liner

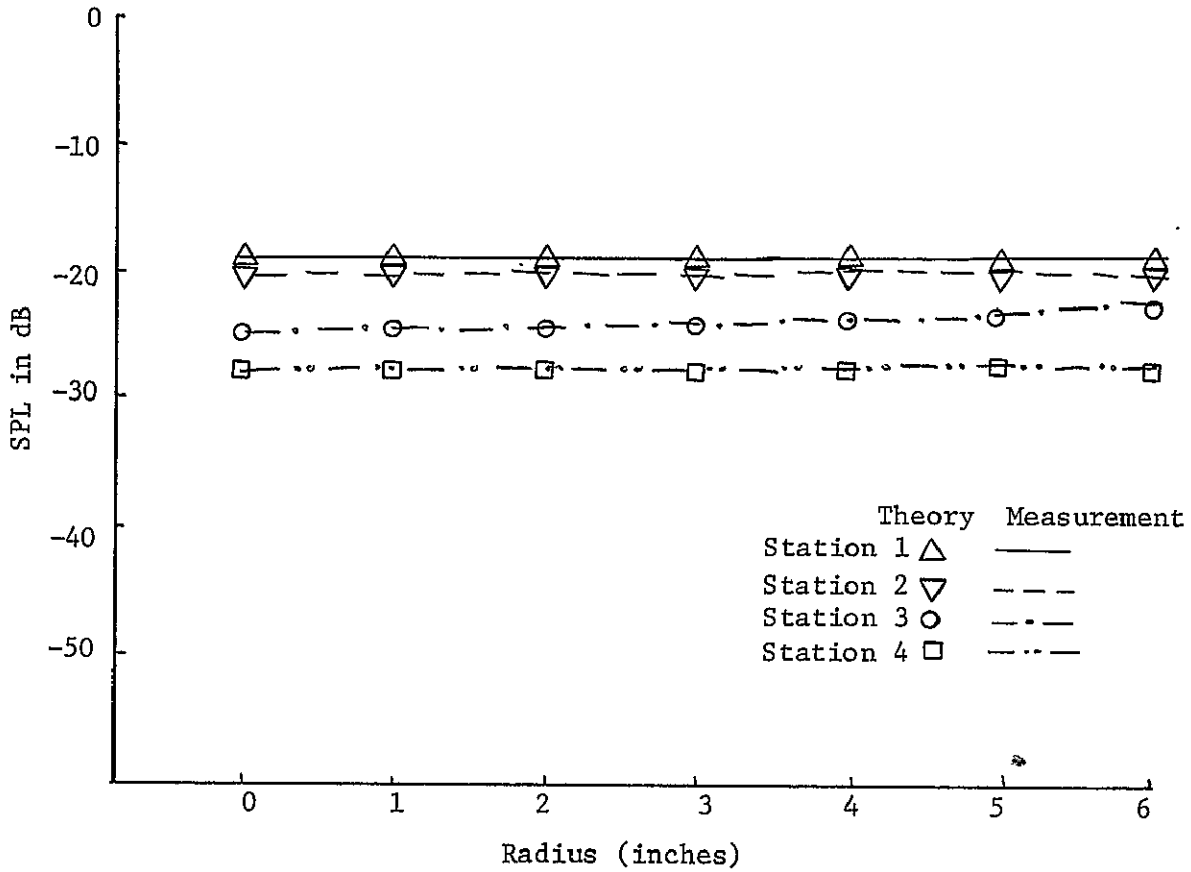

Figure 4.30 Radial Mode Shapes for (0,0) Mode, 800 Hz - One Foot Glass Fiber Liner

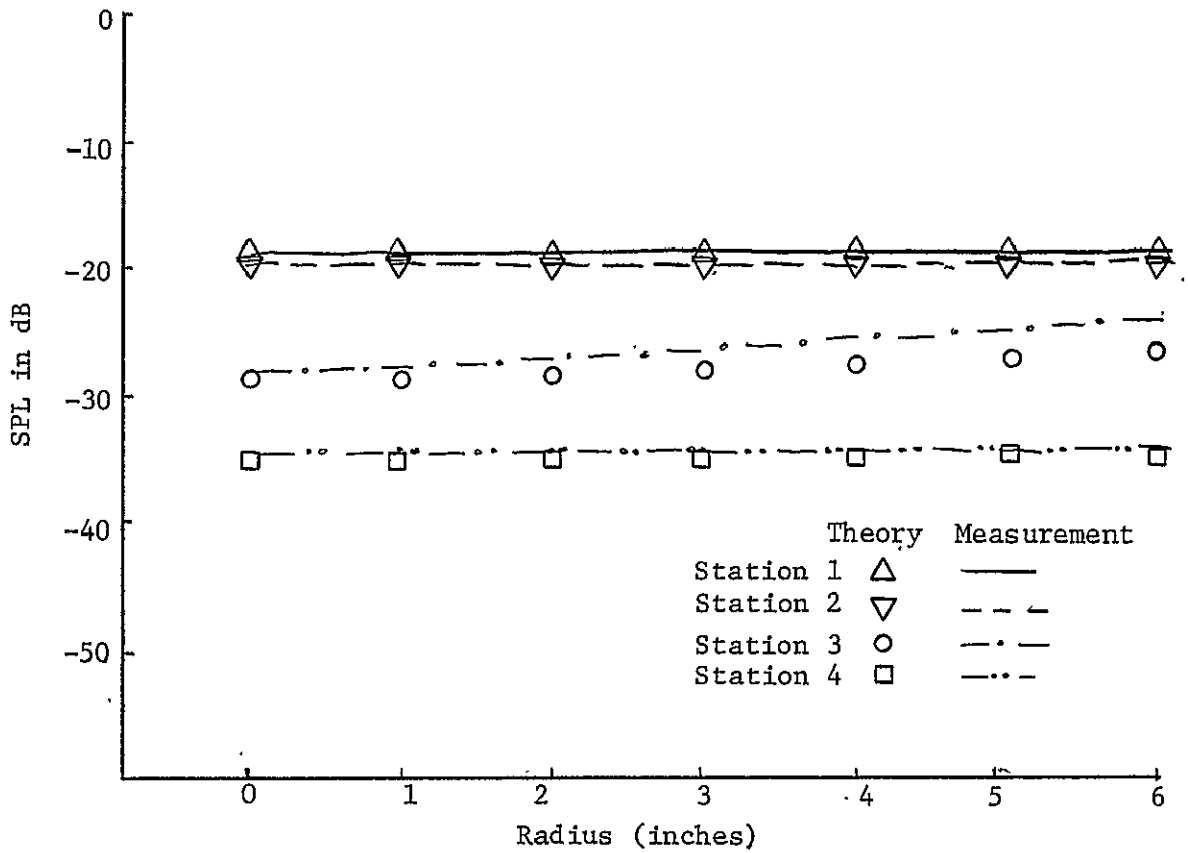

Figure 4.31 Radial Mode Shapes for (0,0) Mode, 800 Hz - Two Foot Glass Fiber Liner

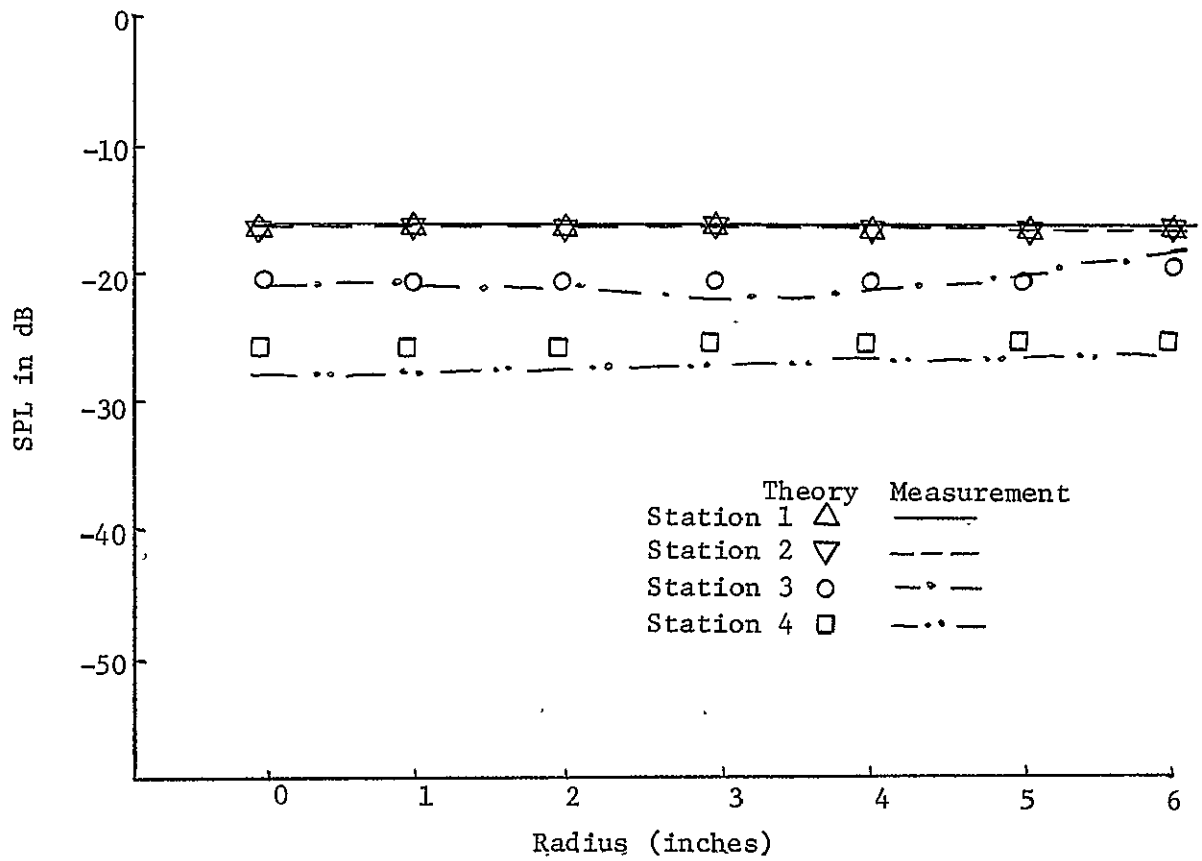

Figure 4.32 Radial Mode Shapes for (0,0) Mode, 1250 Hz - One Foot Glass Fiber Liner

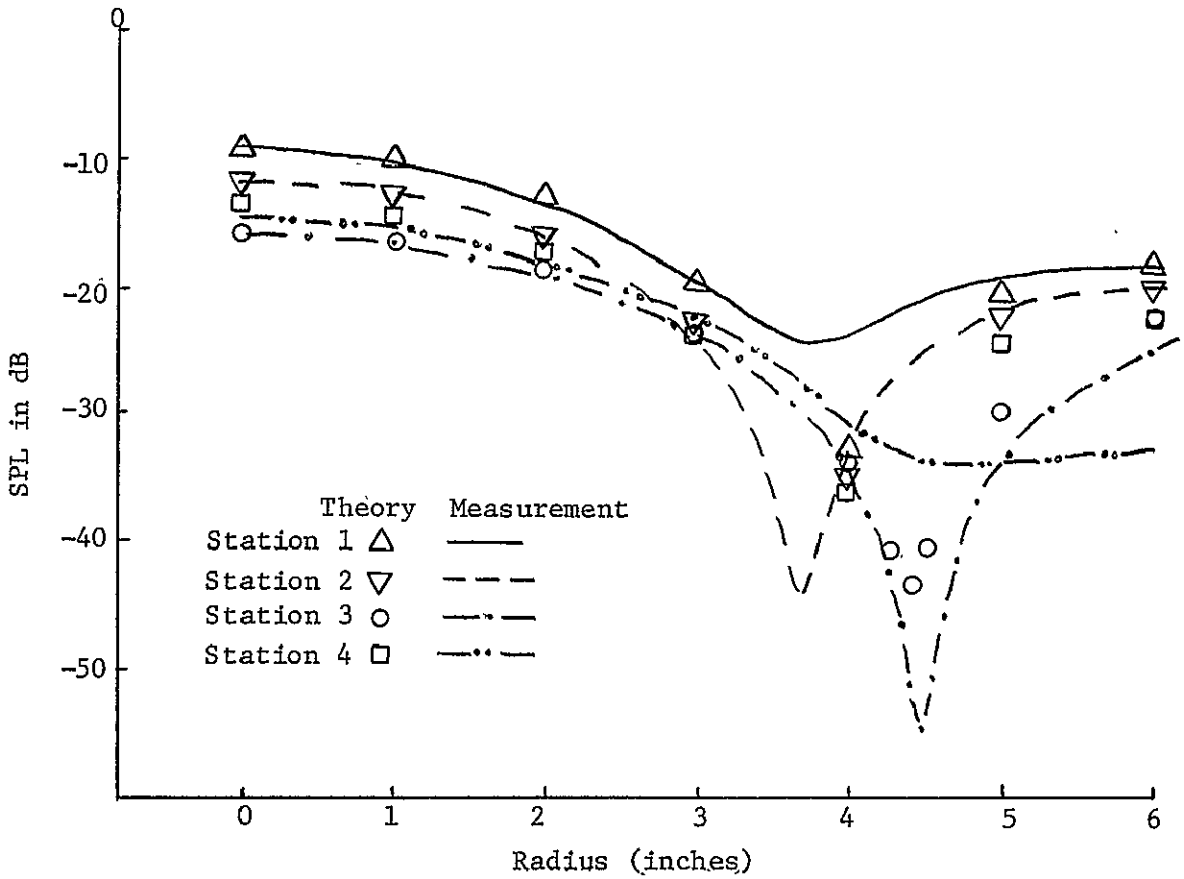

Figure 4.33 Radial Mode Shapes for (0,1) Mode, 1600 Hz - Perf 2 Liner

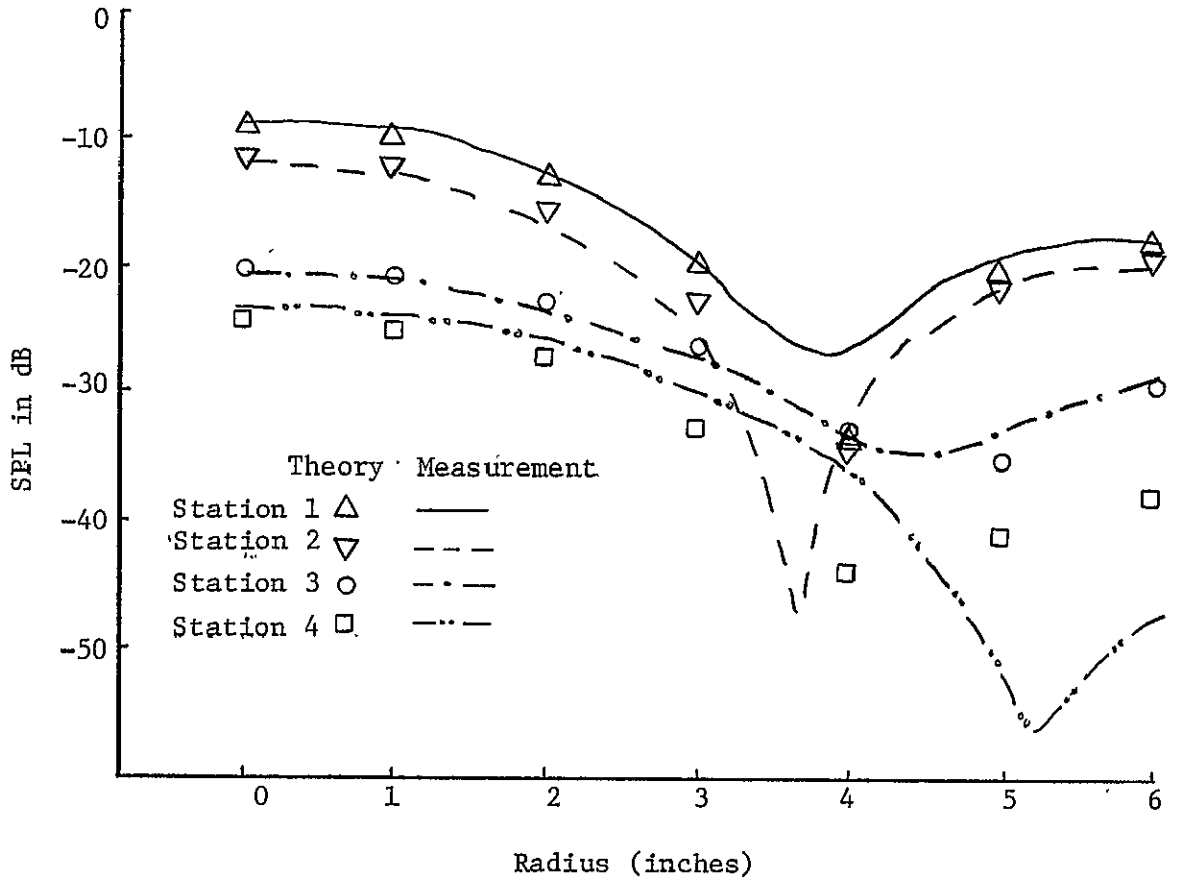

Figure 4.3.4 Radial Mode Shapes for (0,1) Mode, 1600 Hz - FM 2 Liner

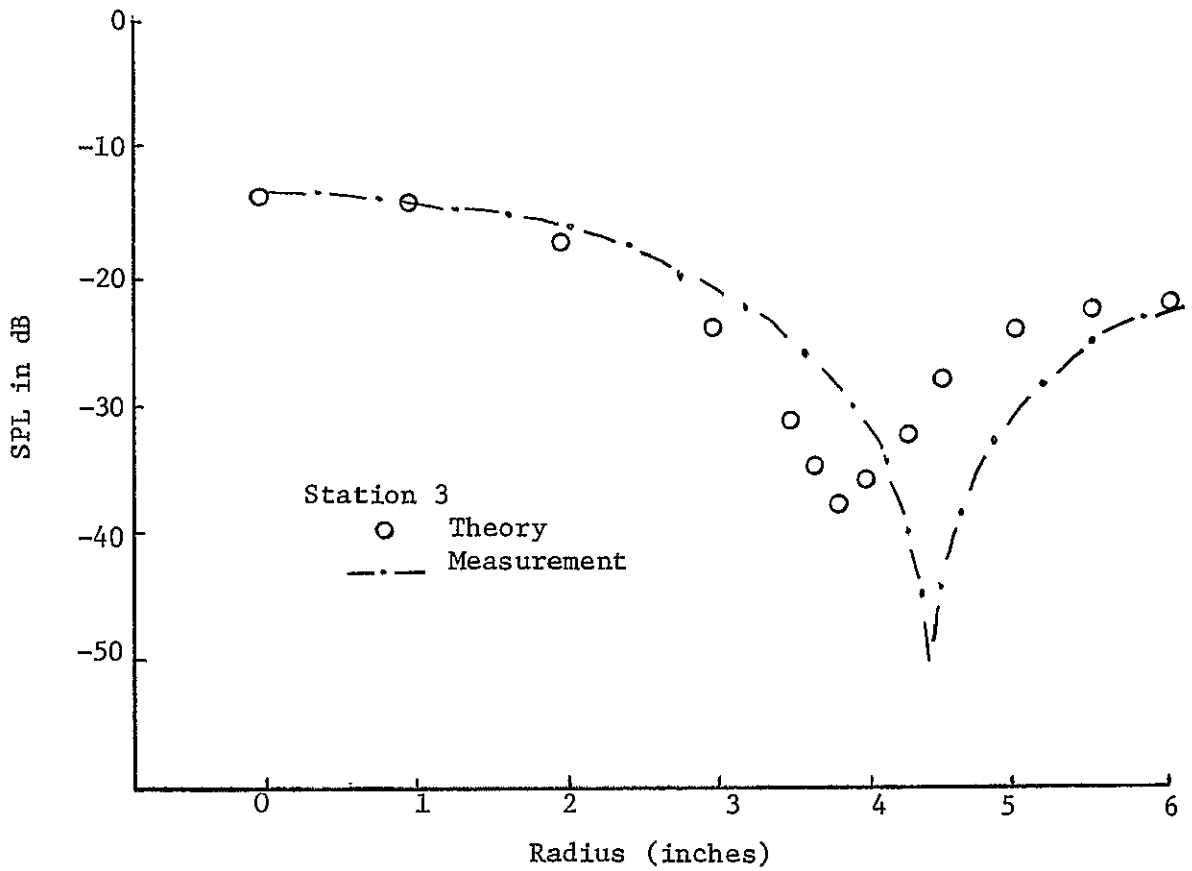

Figure 4.35 Radial Mode Shape in Perf 2 Liner, 1600 Hz

due to duct non-uniformities. The mode shape within the fiber metal liner can be explicitly seen and is fairly well predicted by the eigenvalues for this material. Mode shapes at the same frequency are shown for the one foot glass fiber liner in Figure 4.36. There is reasonable agreement with theory for the mode shapes and levels at upstream and downstream positions. The general form of the mode shape within the liner is defined. It is interesting that despite the reasonably pure (0, 1) mode in the upstream section for all previous cases, the mode shapes within each liner are completely different. These separate mode shapes are predicted by the eigenvalues for each material. Furthermore, since the plane wave can also propagate at this frequency, there can be conversion of energy between these modes for reflection and transmission at each interface before and after the liner. Mode shapes at 2000 Hz for the liners FM 2 and Perf 1 are shown in Figures 4.37 and 4.38. Again, these different mode shapes within each liner are predicted by theory. There is reasonable agreement between measurement and theory at all positions. The (0, 1) mode at 2500 Hz is shown in Figure 4.31 for the liner Perf 2. The agreement with theory is fair but since there is little attenuation for the perforated panel, the distinction between mode shapes is not clearly defined. Therefore, the mode shape within the liner is shown in Figure 4.40 and compared with theory. The null measured near the outer wall is exactly predicted by the eigenvalues for this liner.

The first spinning mode was next investigated for each of the liners. The (1, 1) mode at 670 Hz is shown in Figure 4.41 for the one foot glass fiber liner. The significant attenuation of this mode can be seen from the difference between upstream and downstream levels.

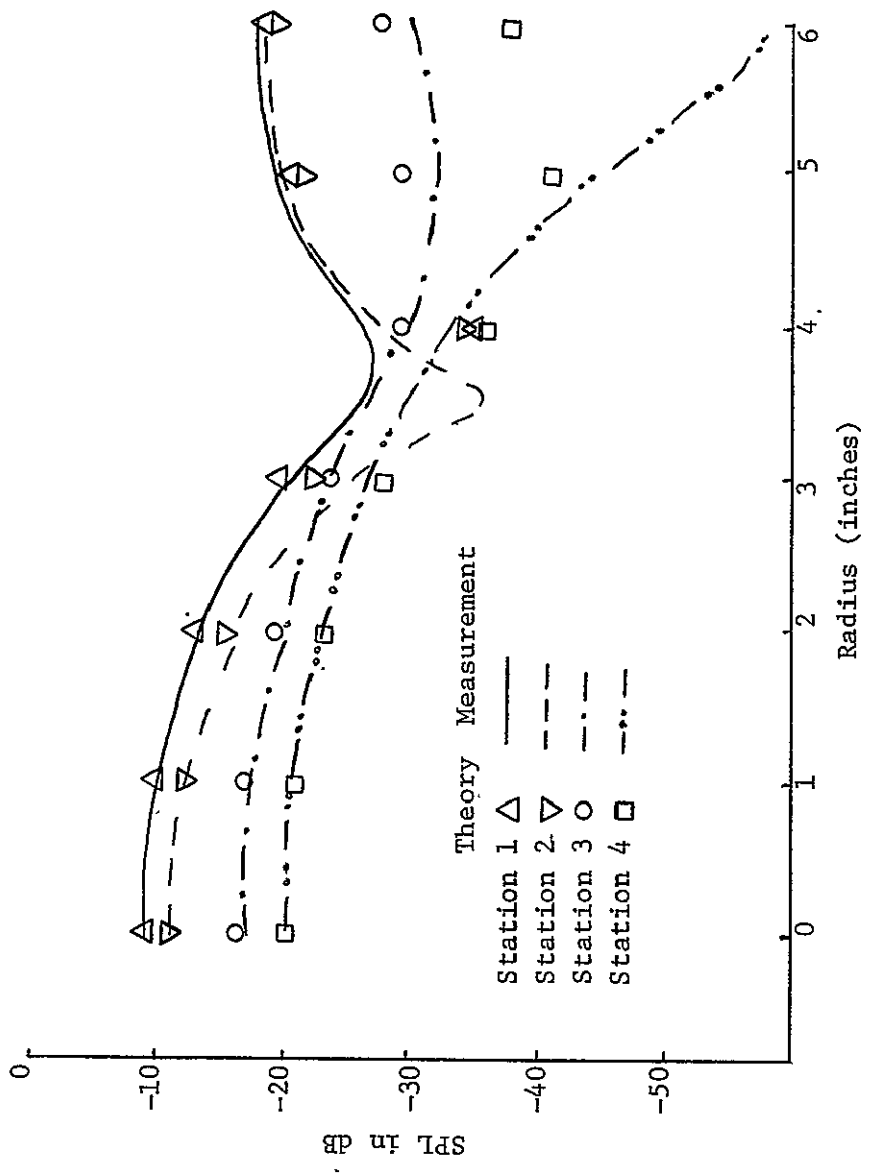

Figure 4.36 Radial Mode Shapes for (0,1) Mode, 1600 Hz - One Foot Glass Fiber Liner

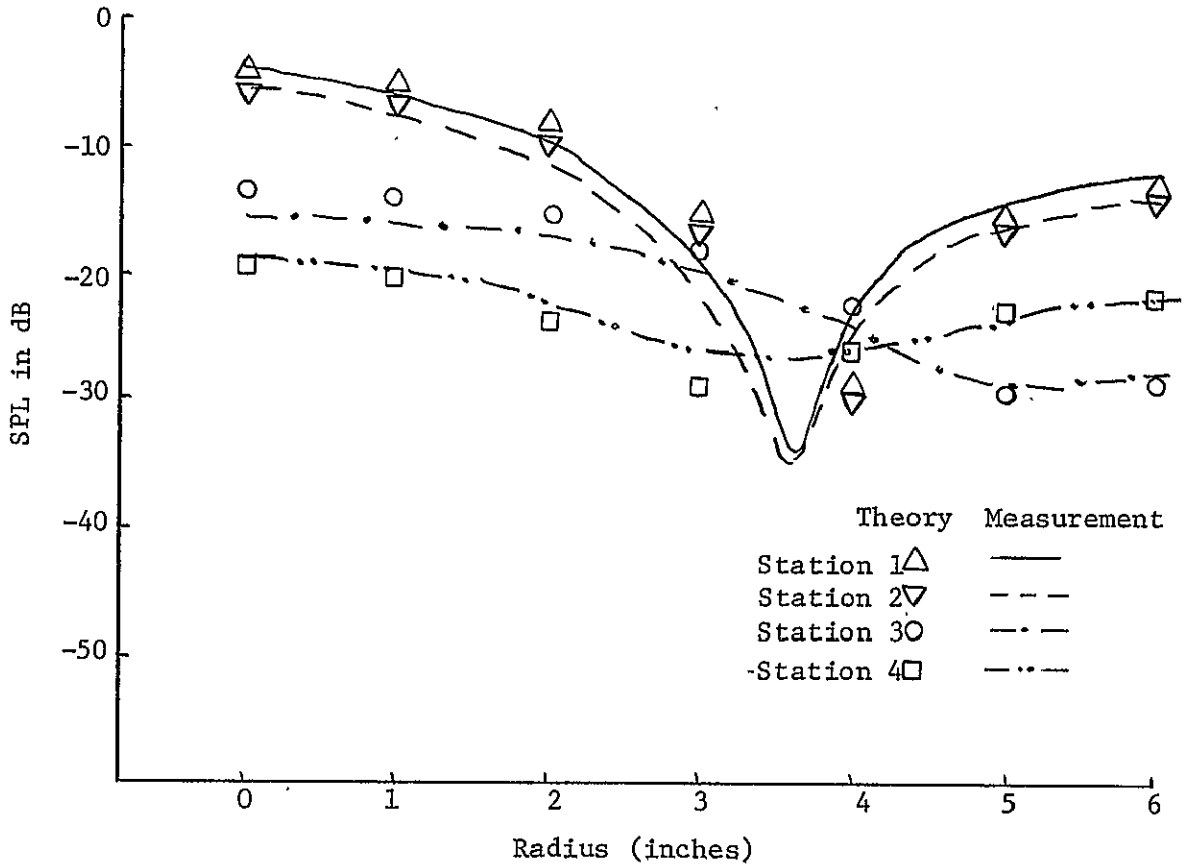

Figure 4.37 Radial Mode Shapes for (0,1) Mode, 2000 Hz - FM 2 Liner

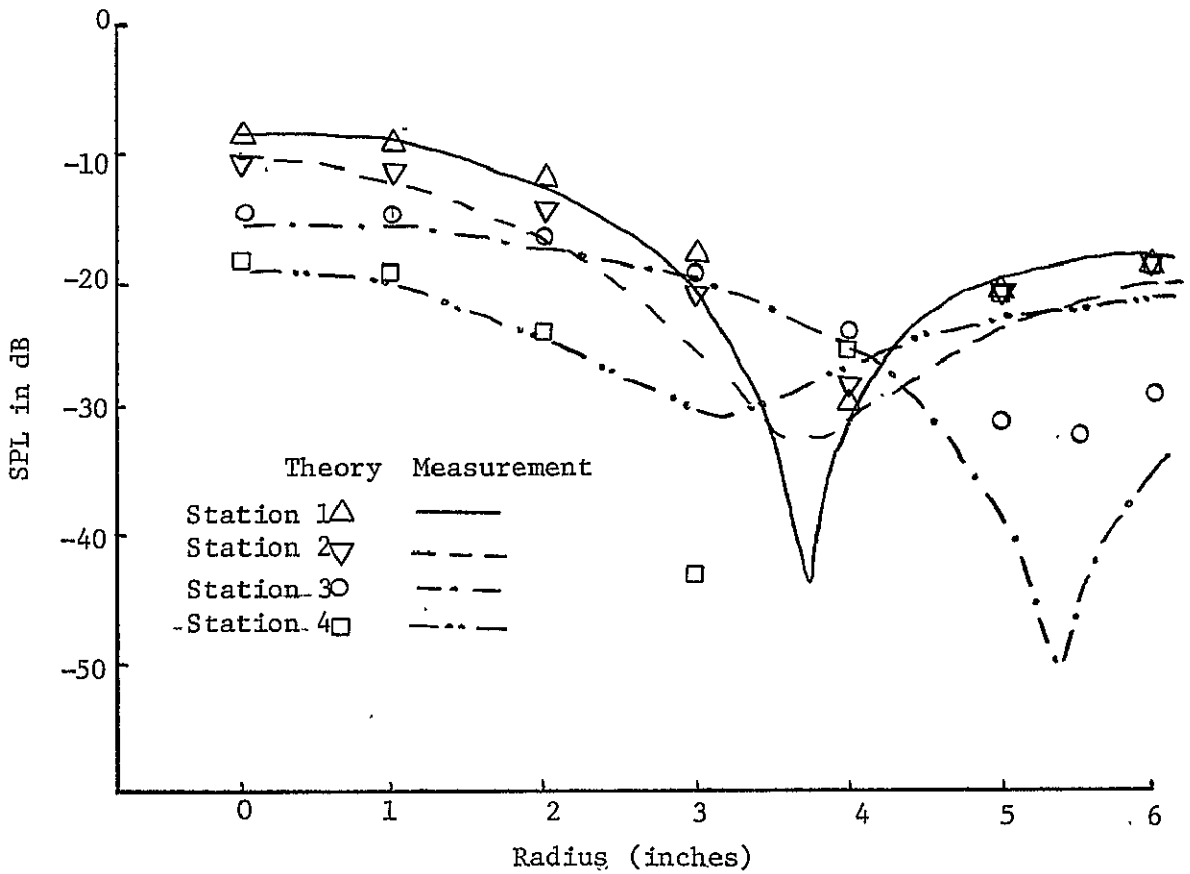

Figure 4.38 Radial Mode Shapes for (0,1) Mode, 2000 Hz - Perf 1 Liner

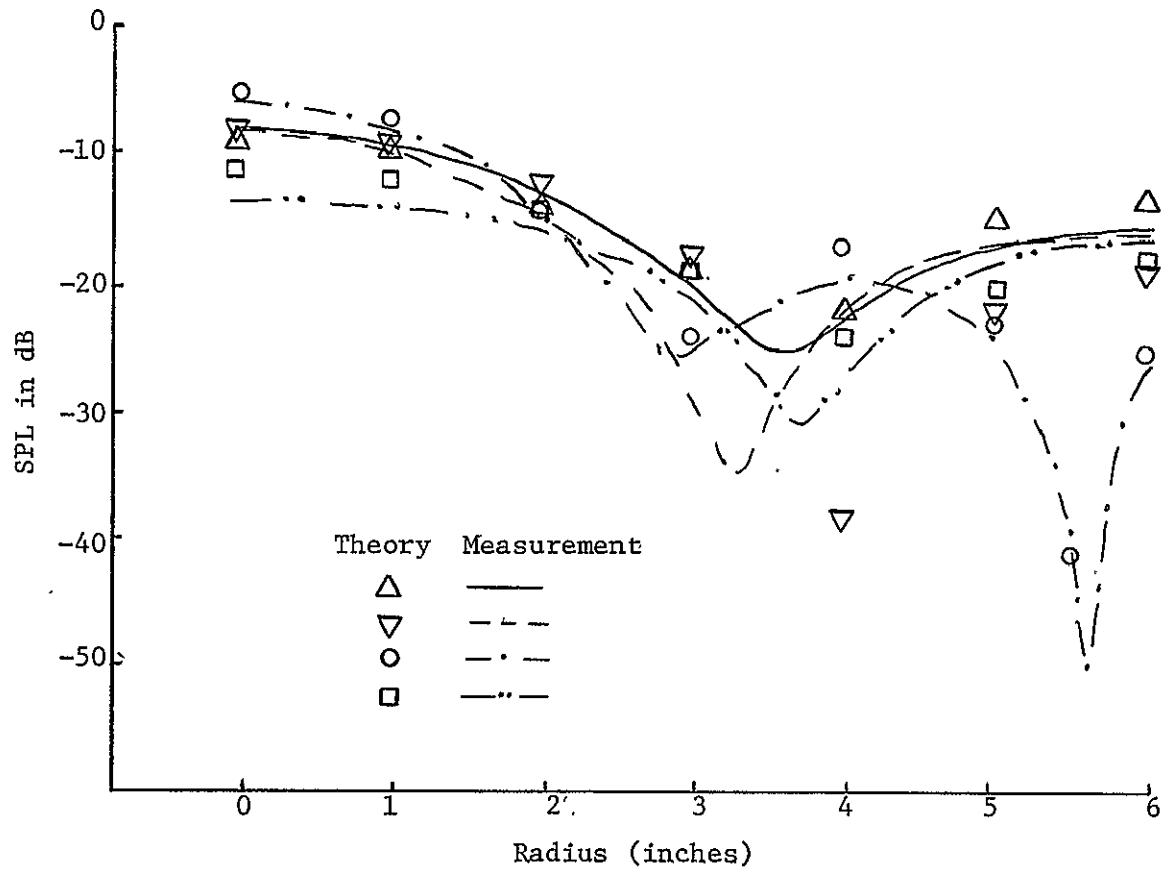

Figure 4.39 Radial Mode Shapes for (0,1) Mode, 2500 Hz - Perf 2 Liner

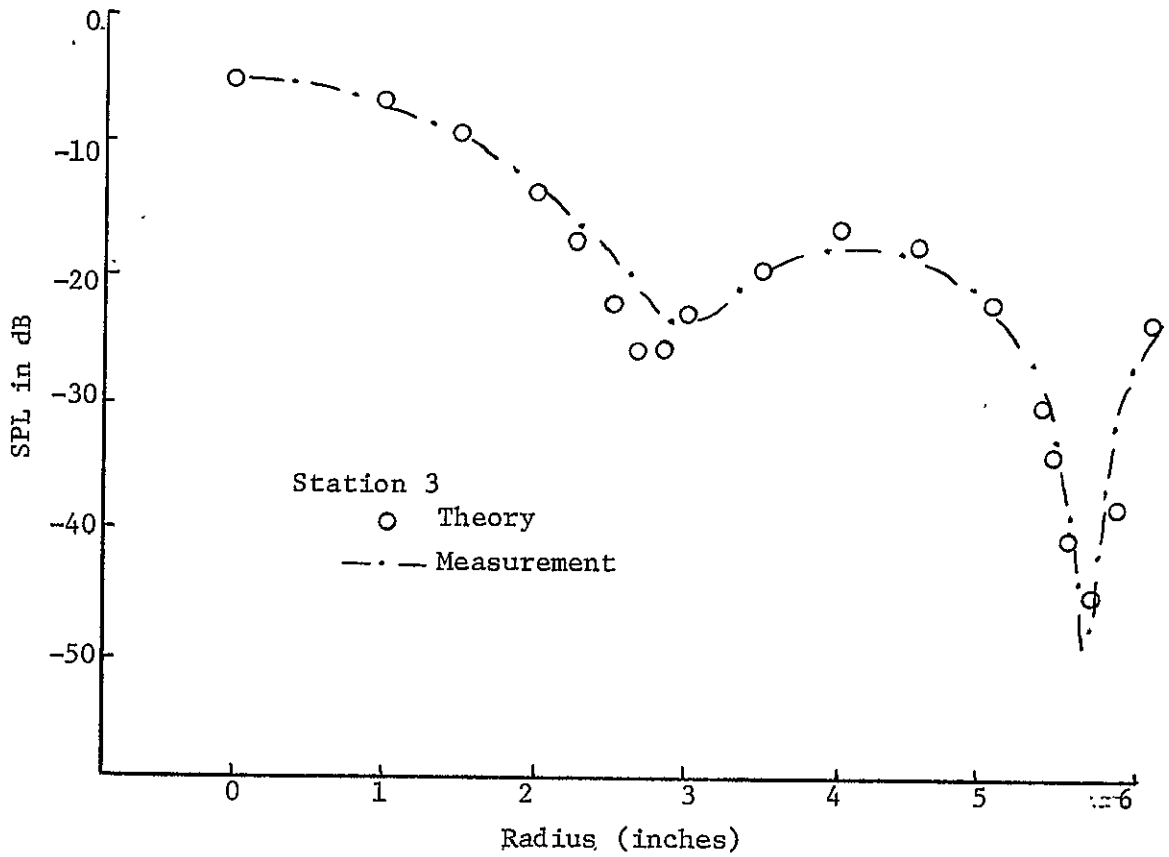

Figure 4.40 Radial Mode Shape in Perf 2 Liner, 2500 Hz

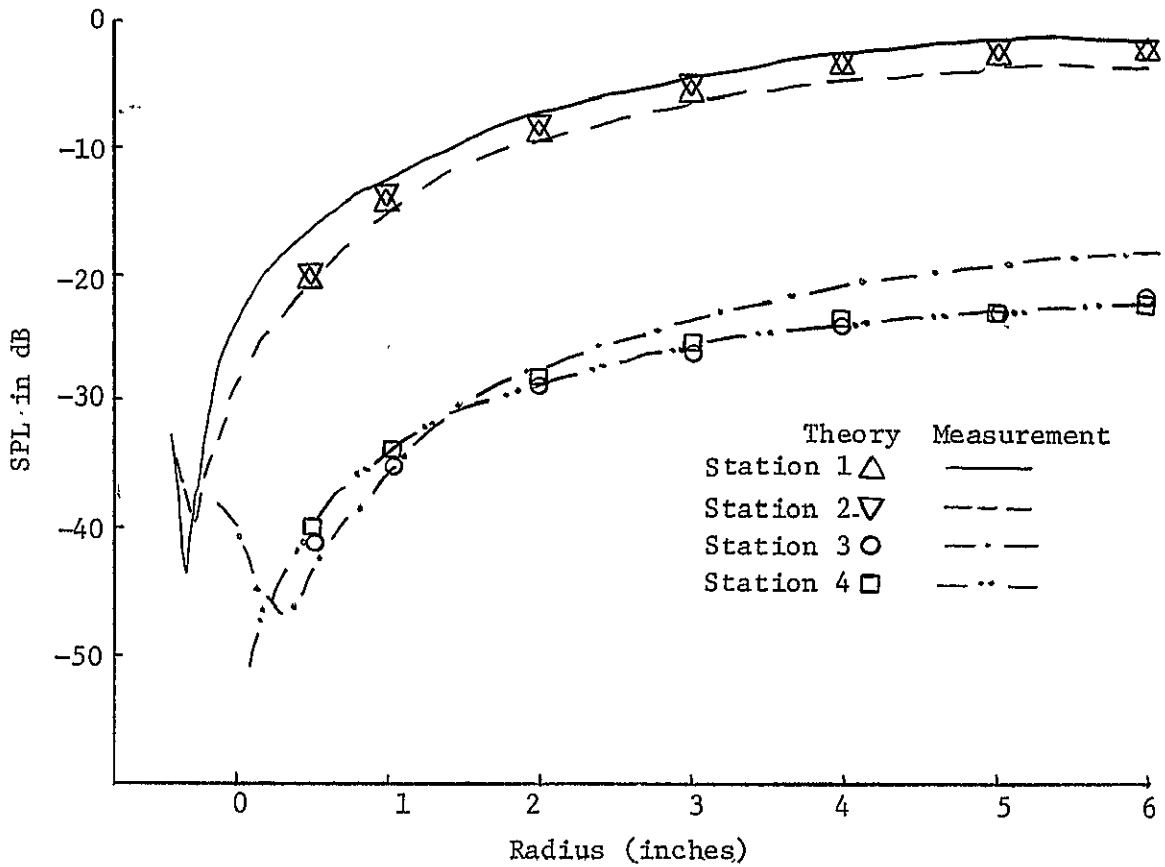

Figure 4.41 Radial Mode Shapes for (1,1) Mode, 670 Hz - One Foot Glass Fiber

The highest level at the upstream station nearest the liner is predicted by theory. The levels within the liner and in the downstream section are also fairly well predicted by theory. Mode shapes at 1000 Hz are compared in Figure 4.42 for the one foot glass fiber liner and in Figure 4.43 for the liner, Perf 2. In both cases, there is good agreement between measurement and theory at all positions. The mode shapes within each liner have the same general form despite the different eigenvalues for each material. This is because the (1, 1) mode is the lowest radial mode of circumferential order m = 1 and there is little conversion of energy to the exponentially attenuated higher order radial modes. For the (1, 1) mode at 1500 Hz in Figure 4.44, there is very little modal purity in the upstream mode shapes. The absence of the null at the center indicates contamination from non-spinning modes. Evidence of this is confirmed for downstream mode shapes which have the form of (0, 0) modes or plane waves. Finally, an interesting mode shape within the liner, Perf 1, is shown in Figure 4.45 for the (1, 1) mode at 1800 Hz, just below the cut-off frequency for the next higher radial mode. There is good agreement for the upstream mode shapes and the radial mode shape in the liner is reasonably predicted. At high frequencies, the agreement between measurement and theory was good for the fiber metal and perforated panel liners but was poorer for the glass fiber materials.

Finally, the (2, 1) spinning mode was investigated. Since only the outer ring of speakers could be used in generating this mode, there was a corresponding decrease in the modal purity for the generated mode.

Mode shapes for the (2,1) mode at 1250 Hz are shown in Figures 4.46 and 4.47 for the one foot glass fiber liner and the liner FM 2 respectively. The lack of modal purity is evident from the radial

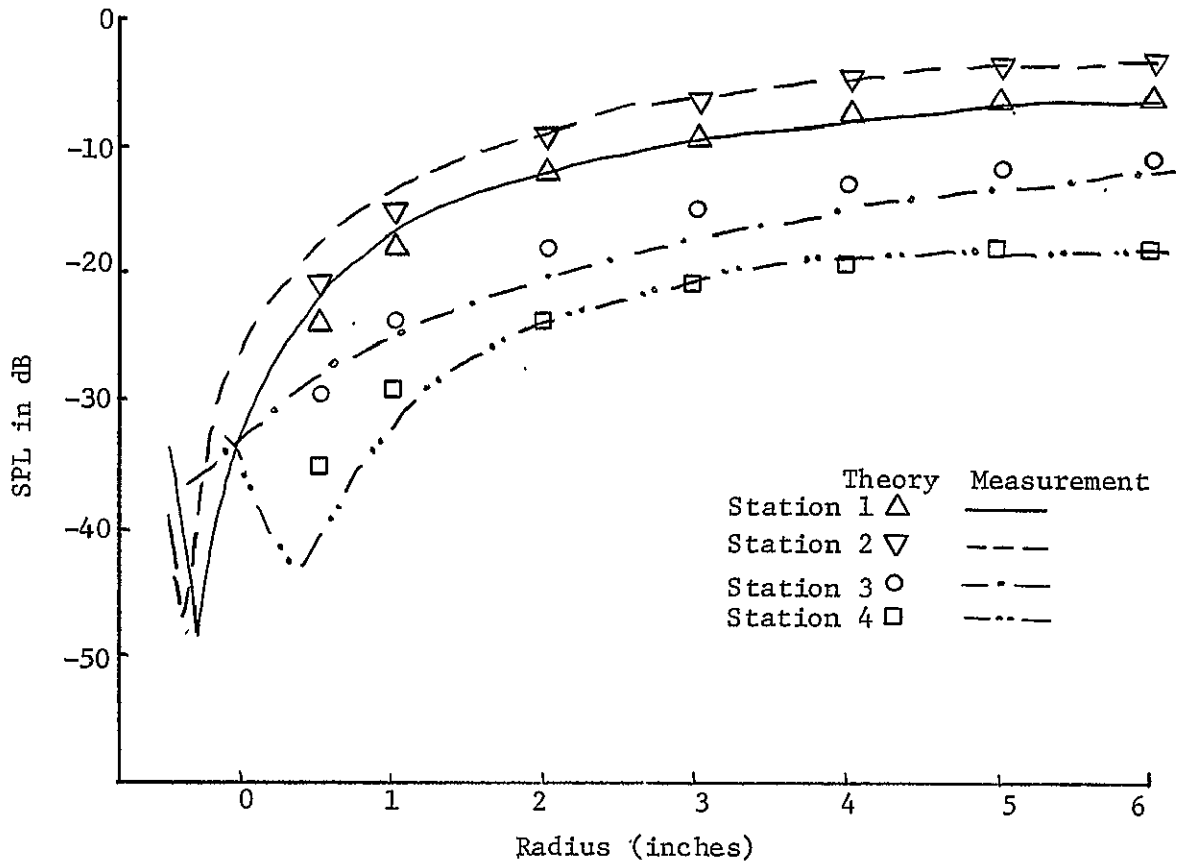

Figure 4.42 Radial Mode Shapes for (1,1) Mode at 1000 Hz - One Foot Glass Fiber Liner

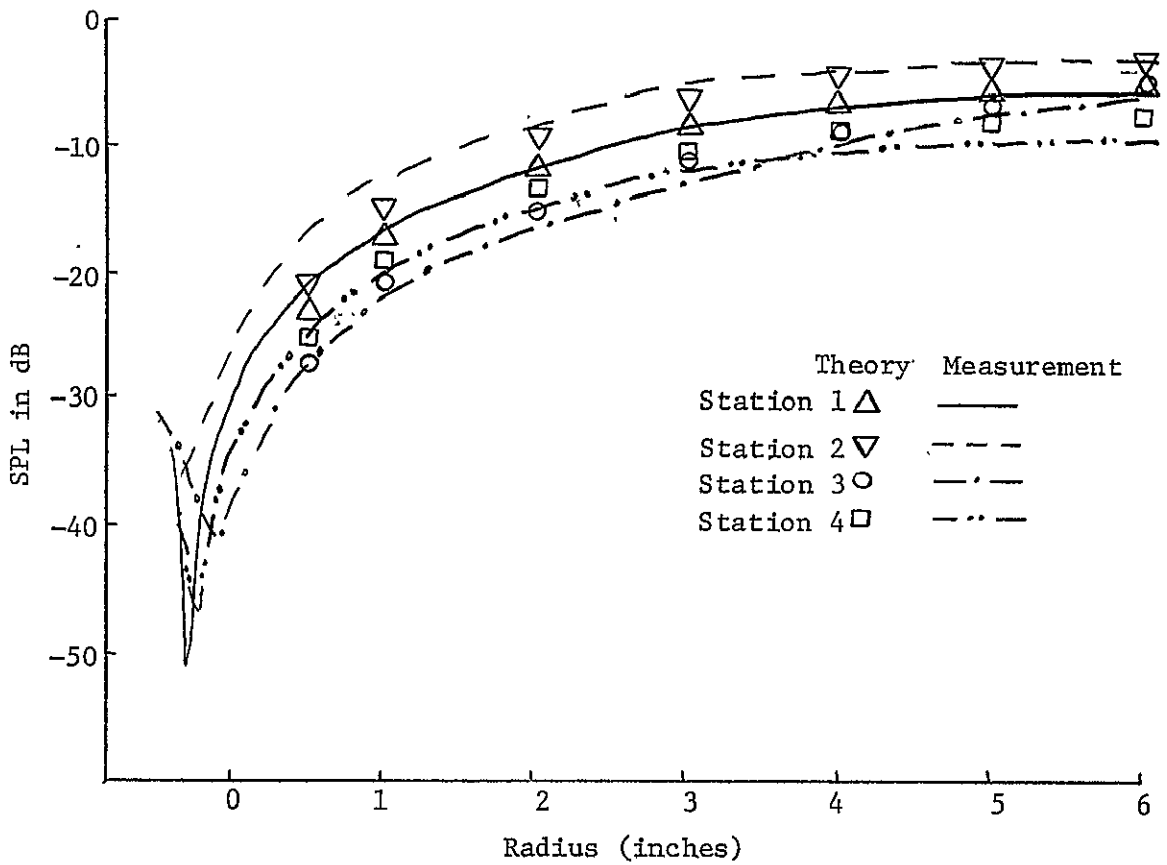

Figure 4.43 Radial Mode Shapes for (1,1) Mode, 1000 Hz - Perf 2 Liner

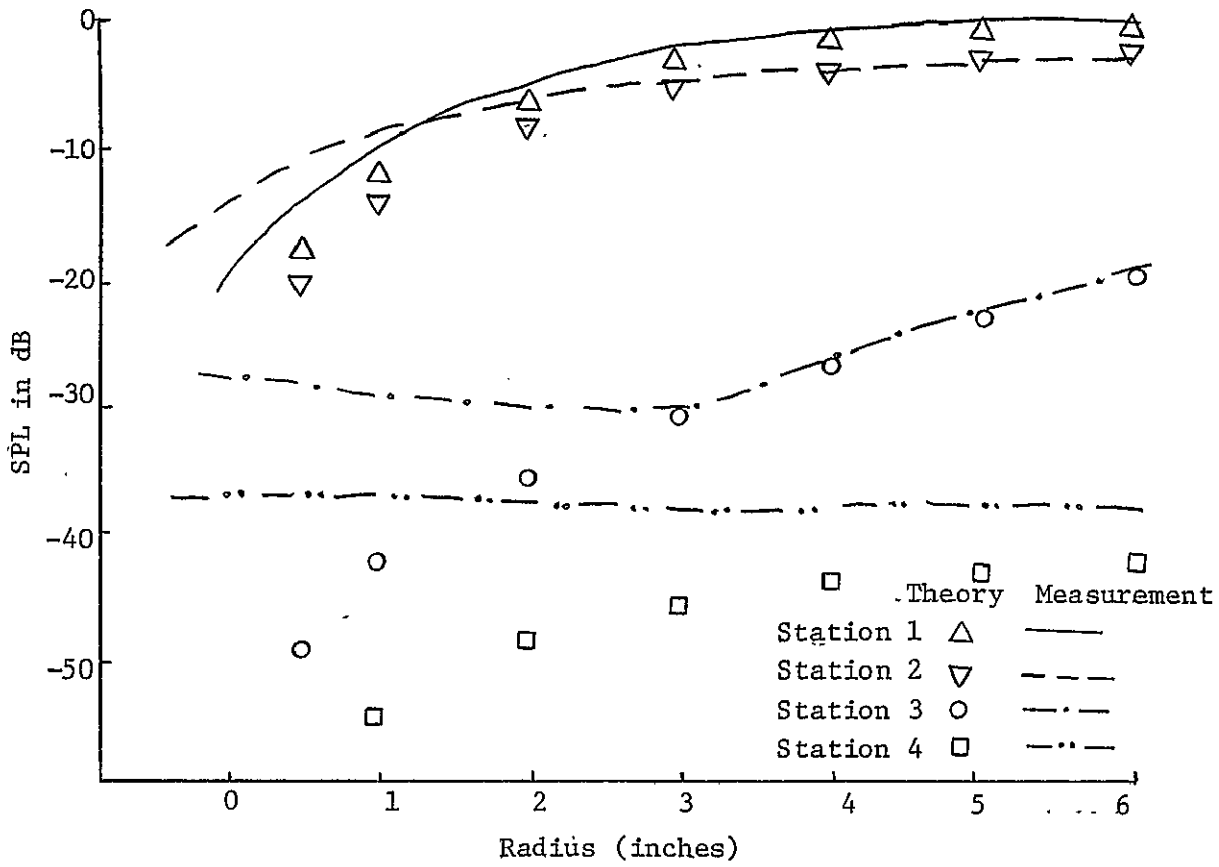

Figure 4.44 Radial Mode Shapes for (1,1) Mode, 1500 Hz - FM 2 Liner

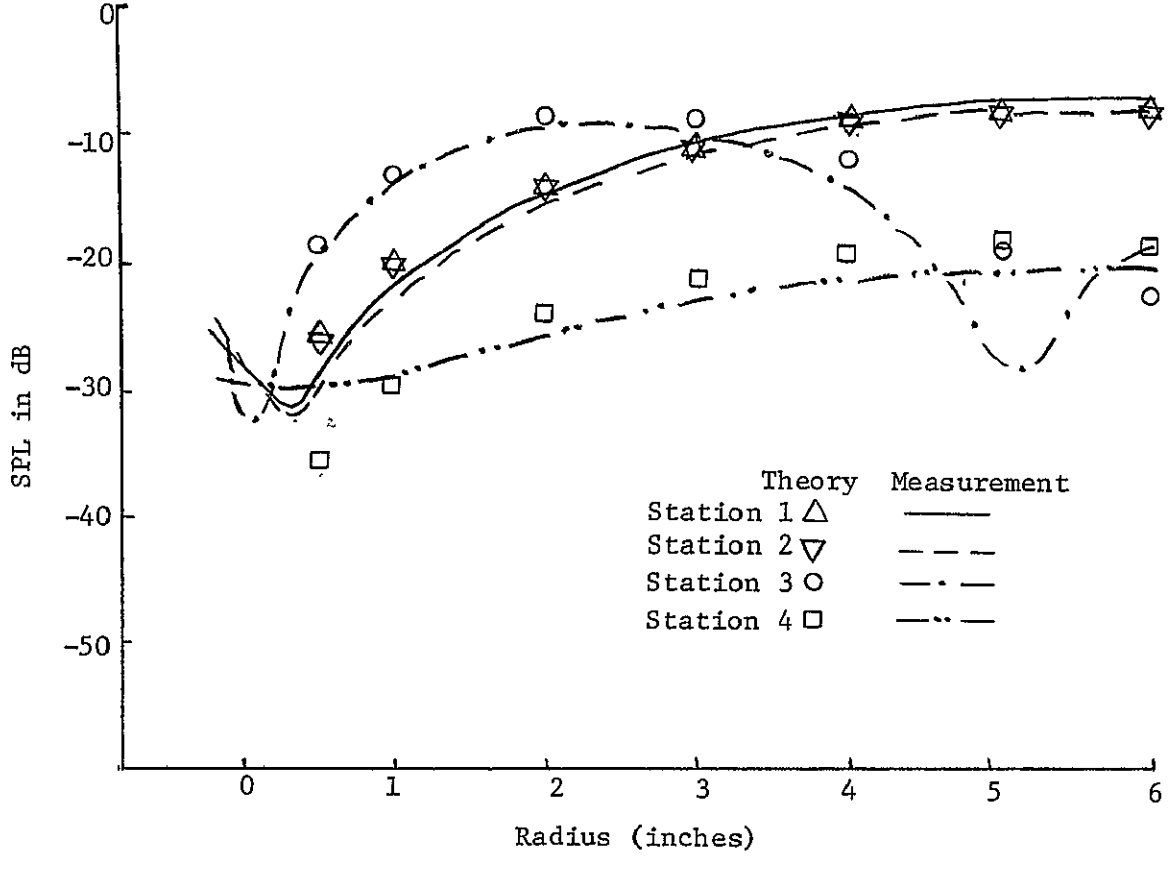

Figure 4.45 Radial Mode Shapes for (1,1) Mode, 1800 Hz - Perf 1 Liner

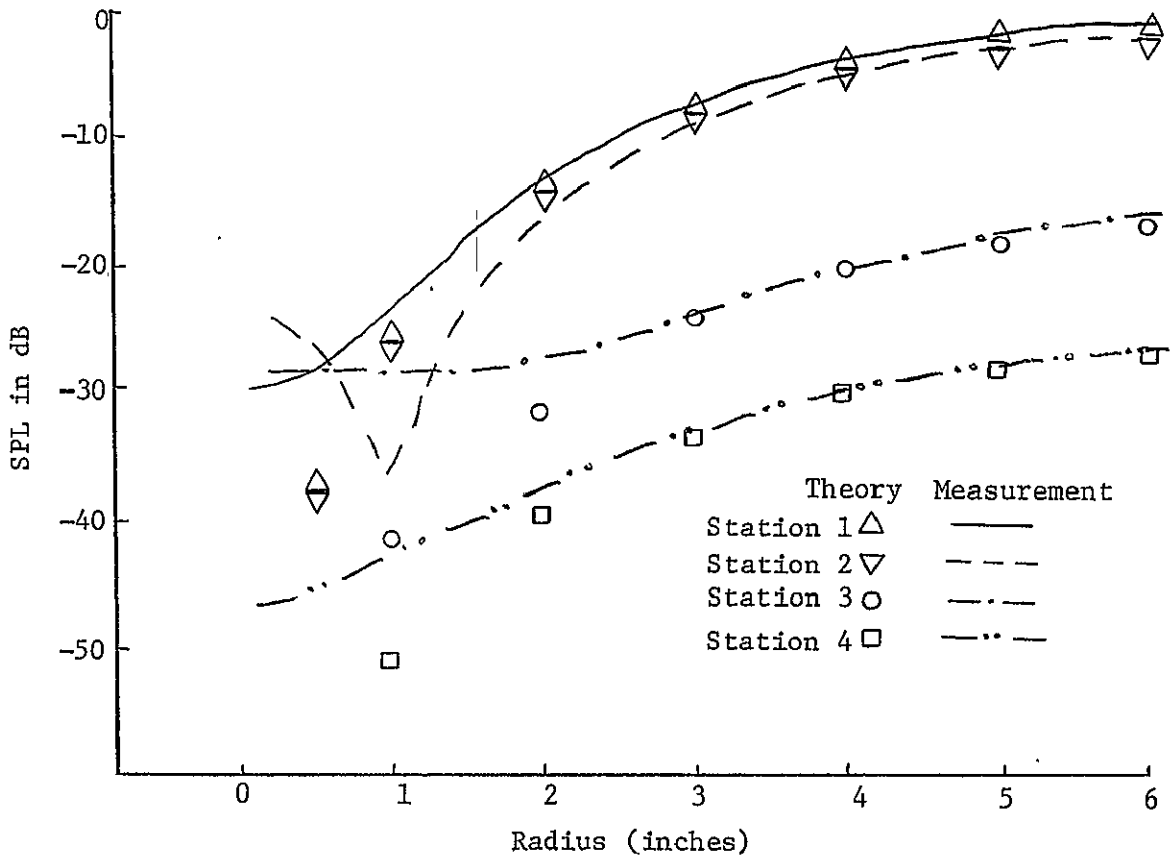

Figure 4.46 Radial Mode Shapes for (2,1) Mode, 1250 Hz - One Foot Glass Fiber Liner

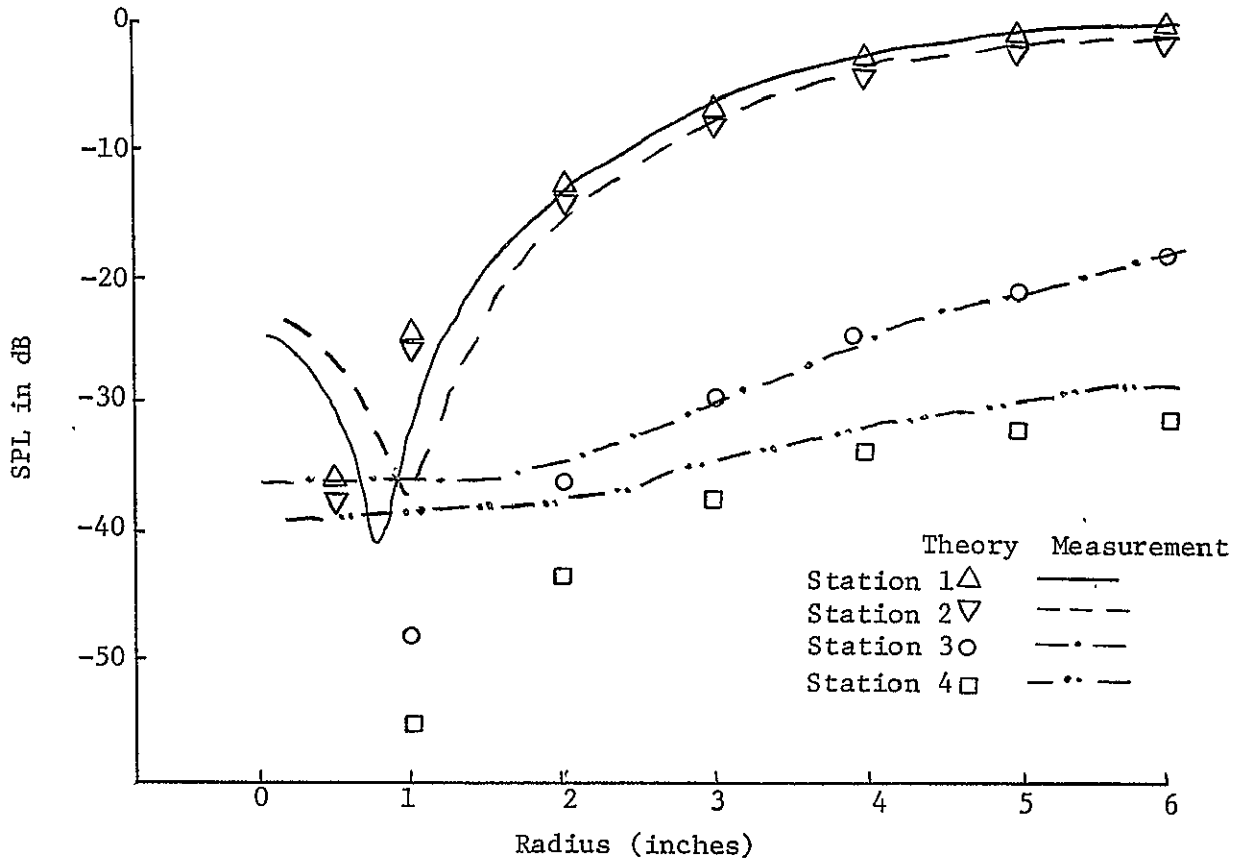

Figure 4.47 Radial Mode Shapes for (2,1) Mode, 1250 Hz - FM 2 Liner

pressure distribution near the center. The presence of non-spinning circumferential order modes obscures the null at the center. Components of residual plane waves are evident at downstream locations and even within the liner. Nevertheless, in both cases, the general form of the mode is preserved throughout the duct and the agreement with theory is reasonable. At higher frequencies, the modal purity for the (2, 1) mode deteriorates even more and there were corresponding differences between measurement and theory.

For each of the liner materials considered, the agreement between theory and measurement of mode shapes and levels in the multisectioned duct for both spinning and non-spinning modes was generally good. However, this agreement was often poorer nearer the cut-off frequencies of individual modes. Despite the ease of generation of higher order modes near their cut-off frequencies, a significant standing wave is present which obscures the results, especially for spinning modes. Even in cases when the agreement with theory was poor, the mode shapes and the relative levels of acoustic pressure at each station were fairly well defined by theory.

In the preceeding figures, discrepancies between measurement and theory cannot be attributed solely to either experimental errors or to assumptions for the mathematical model. This is because a complex process is involved to finally calculate the levels and mode shapes in a multisectioned duct. For example, a measured impedance is used to calculate eigenvalues which are then used in the multisectioned duct model to predict acoustic levels throughout the duct. These predicted levels are then compared to experimental measurements in the duct system. Sources of error for experimental measurements were discussed

earlier. It is obvious that any error along this path would contribute to errors between final measurements and theory.

Assuming that the average impedance values determined from standing wave tube measurements were representative of the entire liner, the complex eigenvalues calculated from the local reaction boundary condition should predict the mode shapes and attenuation throughout the duct. The results indicate that the local reaction boundary condition is a valid assumption for both the fiber metal liners and the perforated panel liners. For a glass fiber material, this assumption is not always true. In cases where there is moderate sound attenuation, this boundary condition can, however, be applied. When the attenuation for a mode increases to a point where it becomes comparable to the attenuation within the bulk material, the local reaction boundary condition is invalid for the reasons discussed in Section 2.4. The propagation constant would then be better predicted by the extended reaction boundary condition.

4.5 Acoustic Performance of Duct Liners

The acoustic performance of a duct liner for individual modes can be determined from the transmission loss and the insertion loss. These parameters were described in Section 2.5.

The use of these parameters provides a significant improvement over the experimental work of McDaniel (25) for evaluating the acoustic performance of finite length duct liners. McDaniel measured radial mode shapes at positions in front of and behind the liner. The average of upstream levels was compared with the downstream levels to determine the attenuation of the liner. This method was an improvement over previous test methods since the propagation of individual higher order modes at discrete frequencies was analyzed. However, the presence of a standing wave in front of the liner could yield little true information about liner attenuation when upstream levels were averaged for comparison with downstream levels.

A comparison between the transmission loss and insertion loss for a 28+1/- inch length of FM 1 is presented in Figure 4.48 for the first higher order non-spinning and spinning modes respectively. There is little difference between the transmission loss and insertion loss for an individual mode at the upper limit of its frequency range. Since the insertion loss describes the difference in sound power level with and without a liner, this parameter will be used to compare the performance of different acoustic materials.

The insertion loss of each liner was studied throughout a range of frequencies for an individual mode. The length of the liners were all chosen to be 28-1/2" long so that relative comparisons can be made between the attenuation of different materials. Figure 4.49 shows the

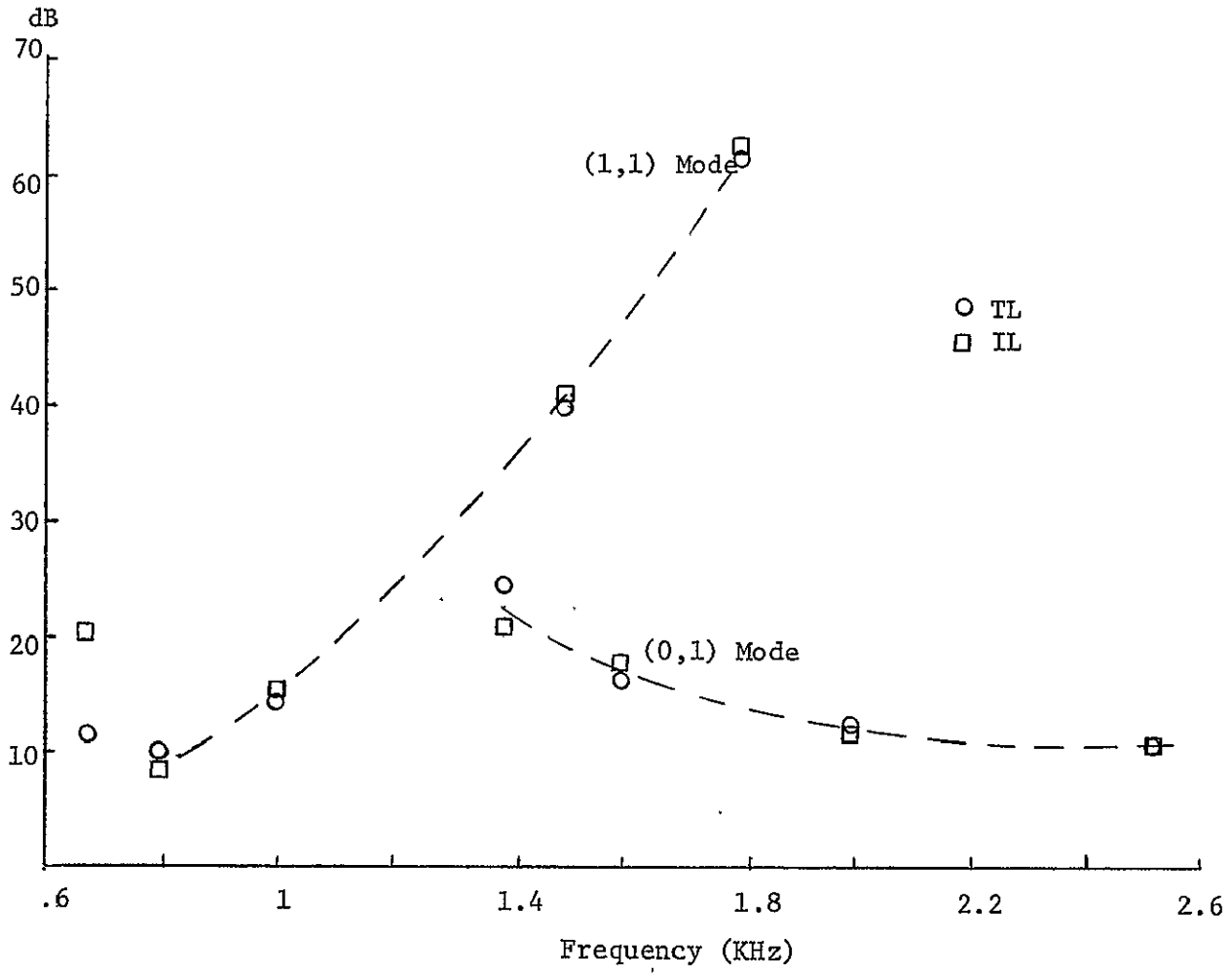

Figure 4.48 Comparison Between Transmission Loss and Insertion Loss for FM 1 Liner

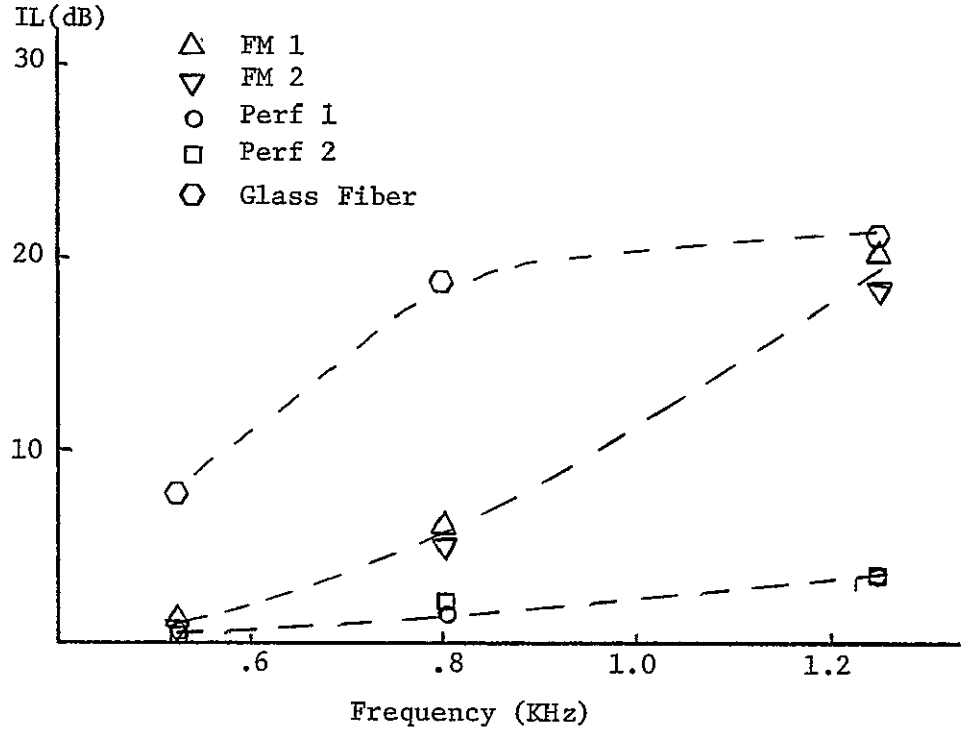

Figure 4.49 Insertion Loss for (0,0) Mode

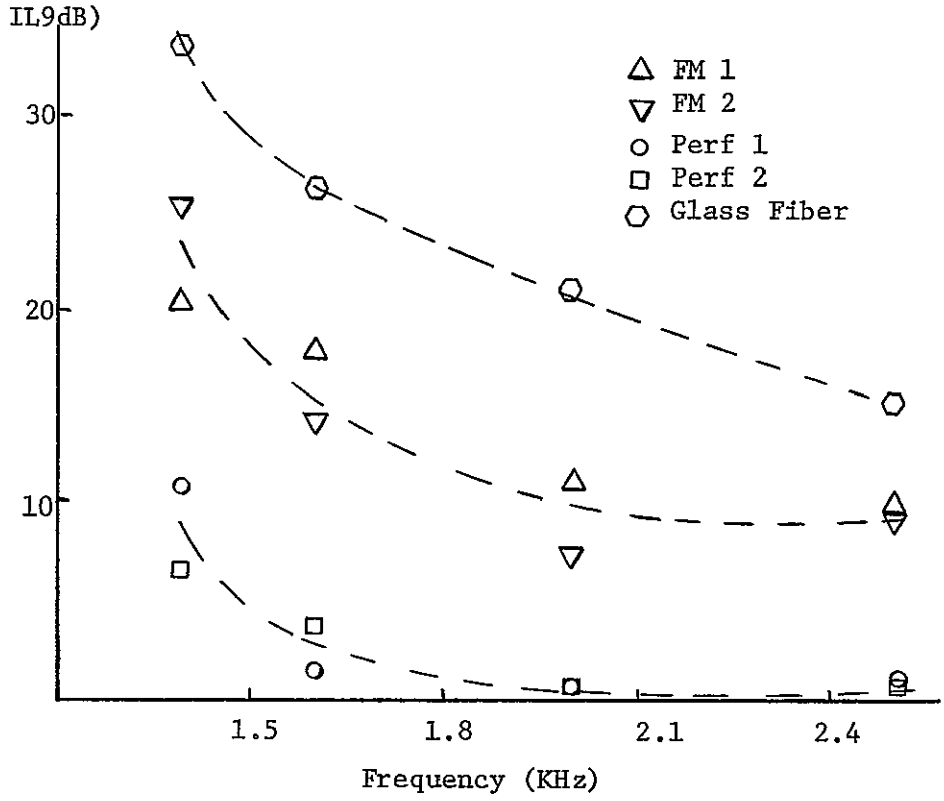

Figure 4.50 Insertion Loss for (0,1) Mode

insertion loss throughout the frequency range for generation of a plane wave. The attenuation for each material increases with frequency. In Figure 4.50, the insertion loss of the (0, 1) mode decreases initially with frequency and remains relatively constant for each material. The insertion loss for the (1, 1) and (2, 1) spinning waves are shown in Figures 4.51 and 4.52 respectively. In both cases, there is considerable attenuation throughout the frequency range for each mode. This is not unexpected since for spinning modes, the majority of energy is located near the outer duct wall next to the liner material. There is an increase in attenuation near the cut-off frequency at the beginning of each frequency range. This is because the group velocity of the wave is zero at the cut-off frequency and the energy effectively remains within the duct. Thus, the "dwell time" of the wave within the duct is longer near cut-off and serves to produce greater attenuation.

The attenuation of the non-spinning modes complicates the problem of having residual modes downstream of the liner in a multisectioned duct. Since these modes are not attenuated by the liner to the same extent as the spinning modes, their presence is frequently noticed in mode shapes at positions beyond the liner.

The frequency dependence of the insertion loss for individual modes is shown in Figure 4.53 for a 28-1/2 inch length of FM 1. Even at the same frequency, the attenuation for individual modes differs. Thus, it becomes difficult to assign a single number rating to a liner as a measure of its effectiveness in attenuating sound. Further information regarding source characteristics and modal content are necessary to give an estimation of the effectiveness of an acoustic liner.

The attenuation for individual modes is not directly proportional

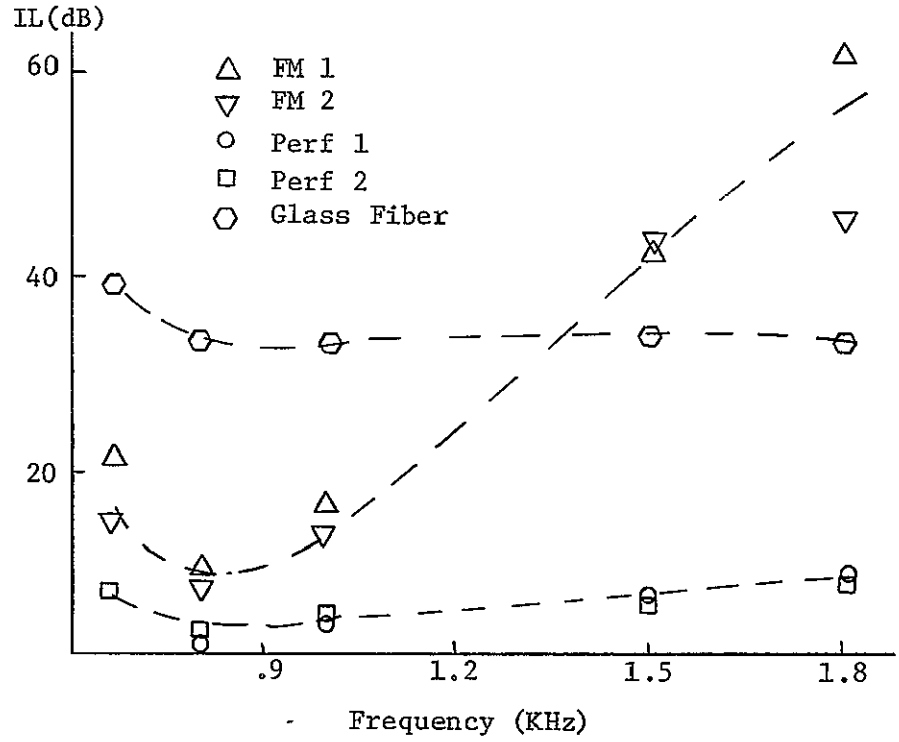

Figure 4.51 Insertion Loss for the (1,1) Mode

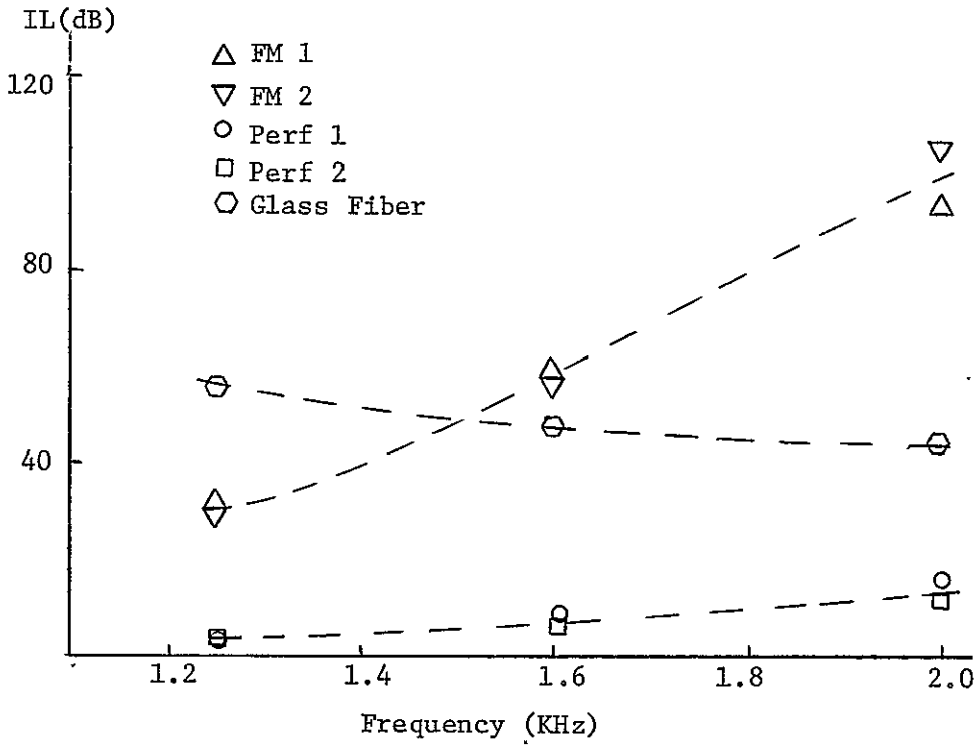

Figure 4.52 Insertion Loss for the (2,1) Mode

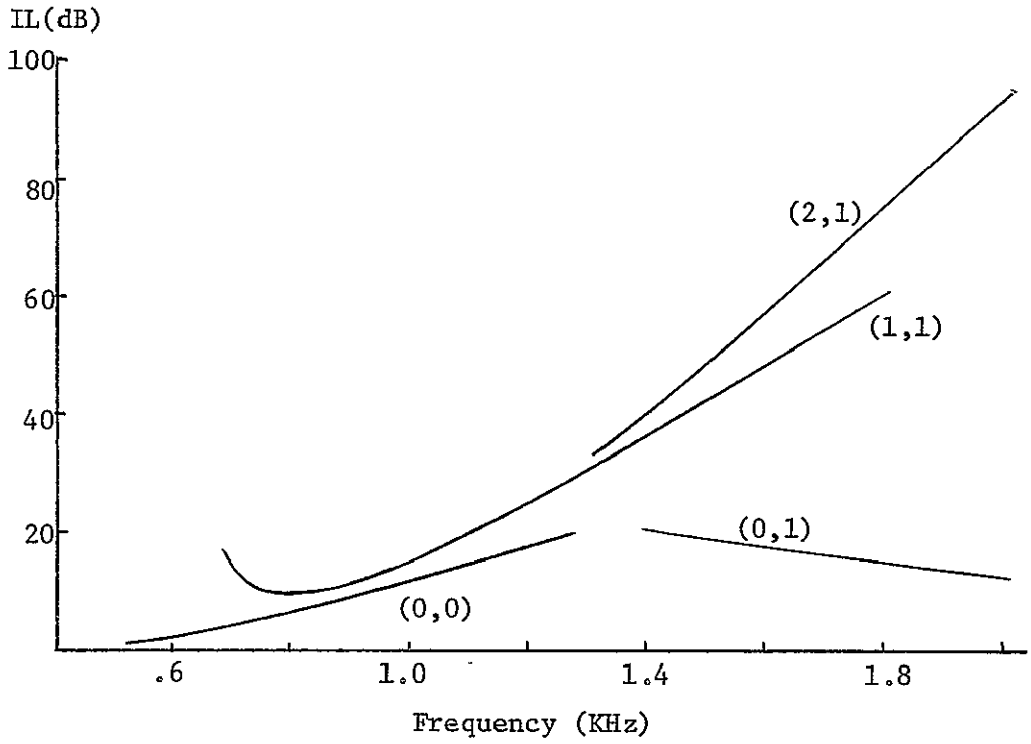

Figure 4.53 Insertion Loss for FM 1

to the length of the liner. The insertion loss of different modes for one foot and two foot lengths of glass fiber material are compared in Figures 4.54 through 4.55 to illustrate this point. The insertion loss is not exactly doubled for the longer liners and is sometimes greater and sometimes less than twice the attenuation for the shorter liner. This is because the attenuation is a result of the reflection at the impedance discontinuity between the ends of the liner and the hard-walled duct as well as the transmission effects through the liner.

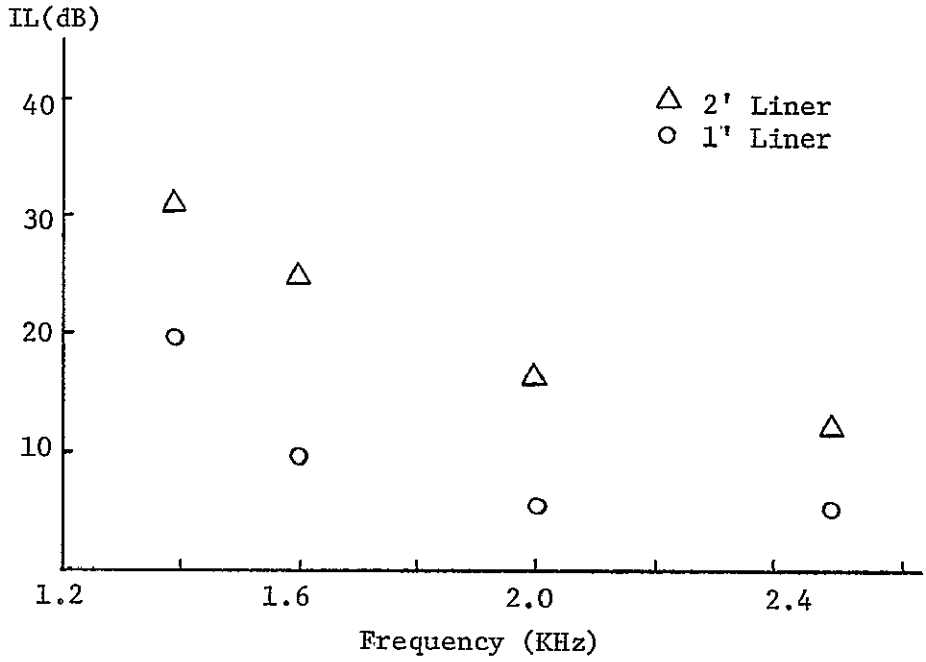

Figure 4.54 Insertion Loss for Two Lengths of Glass Fiber Material, (0,1) Mode

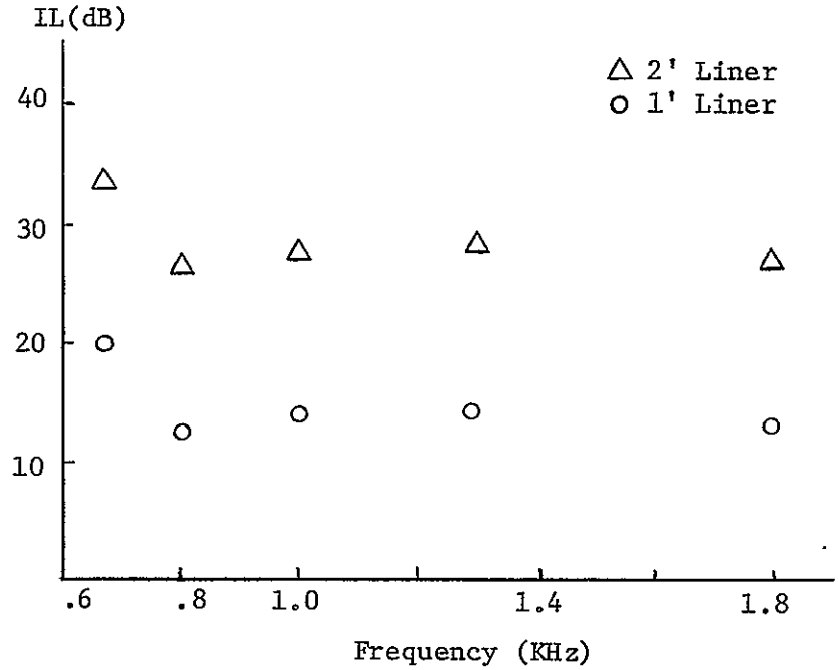

Figure 4.55 Insertion Loss for Two Lengths of Glass Fiber Materials, (1,1) Mode

CHAPTER V

SUMMARY, CONCLUSIONS AND RECOMMENDATIONS

This research program has achieved its goal of understanding the behavior of acoustic propagation in multisectioned ducts. In addition, materials used in the study were evaluated. Developments in both experimental and analytical techniques were achieved as a result of this work and will be described in this section. Furthermore, interesting topics for future research are outlined.

The propagation of plane waves and higher order modes in an infinite hard-walled circular duct was first described. An understanding of this process is necessary for study of more complex cases of acoustic propagation. This effort was then expanded to consider propagation in ducts lined with different acoustic materials.

The fundamental acoustic properties of materials representative of three types of duct liners commonly used in different applications were studied. These included a porous glass fiber material, a sintered fiber metal material with an air cavity backing, and a panel of Helmholtz resonators. Expressions were developed to predict their acoustic characteristics and the normal impedance measured by a standing wave tube was compared with values calculated from theory. In all cases, except for the porous material, there was good agreement between measurement and theory throughout the entire frequency range. This ability to model a liner material and predict its impedance is a valuable tool for designing liners with optimum attenuation properties.

The properties of these materials as duct liners were studied with emphasis on determintion of local versus extended reaction boundary conditions. The local reaction boundary condition was valid for the

fiber metal and resonator cavity type material. However, for cases of significant sound attenuation within a duct, the extended reaction boundary condition must be adopted for liners of porous material.

A method using both contour integrations and an iteration technique was developed to find the complex eigenvalues for a liner under the assumption of a local reaction boundary condition. This search technique provided an efficient and reliable means for locating successive eigenvalues in the complex plane for an arbitrary complex admittance.

Once the fundamental properties of acoustic propagation in lined and unlined ducts are understood, these effects may be combined to consider propagation in a duct containing successive lined and unlined sections. Due to the changes in liner impedance for each finite section of the duct, an incident acoustic wave is partially transmitted and partially reflected at the interface between different sections. Using a matrix technique, relationships were developed to account for the acoustic coupling between sections of a hollow circular duct with no flow. The modal amplitudes of the sound field at each interface within the duct are then defined in terms of modal transmission and reflection matrices. For a circular duct with multisection liners, the reflection effects are proportional to the difference in acoustic admittance between adjacent liners. Thus, it is possible to take advantage of the reflection effects between sections as well as the transmission effects of each liner to produce attenuation. Because of this characteristic, a combination of different liners could perform significantly better in attenuating sound than a continuously lined duct. A computer program was developed to model the multisectioned duct based on the admittance and eigenvalues for each section.

A complex source array consisting of two concentric rings of sources was developed to generate plane waves and both spinning and non-spinning higher order modes in a duct. These modes could be generated at their cut-off frequencies and throughout a frequency range extending to the cut-off frequency for the next higher radial mode. Through individual control of the response of each element, the array provided phase and amplitude control in the radial, as well as circumferential, directions. The radial dependence of the measured mode shapes was enhanced considerably by the design of this unique array.

Once it was established that the source array could generate modes with a reasonable degree of purity, the propagation of higher order modes in a multisectioned duct was studied. The duct system consisted of an anechoically terminated duct 12 inches in diameter with 3 sections. Mode shapes generated included the (0, 0) plane wave mode, the (0, 1) non-spinning mode, and the (1, 1) and (2, 1) spinning modes. Measurements of attenuation and radial mode shapes were taken throughout the duct when a finite length liner was inserted between upstream and downstream hard-walled sections. Materials tested as liners included a glass fiber material and both a sintered fiber metal and perforated sheet metal with a honeycomb backing. The experimental measurements were compared with results calculated from the mathematical model of the system. There was generally good agreement between measurement and theory for both non-spinning and spinning modes. The comparison indicates that the multisectioned duct analysis accurately predicts the mode shapes and levels at stations throughout the duct. Furthermore, the local reaction boundary condition is valid for the fiber metal and perforated panel liners. For low to moderate attenuation of sound, this

assumption was valid for the liner of glass fiber material but should be modified in favor of the extended reaction boundary condition for significant attenuation through a duct lined with this material.

Despite the ability of the source array to match the sound field for both the circumferential and radial pressure dependence, the generation of an individual mode is often obscured by contamination from additional spurious modes. These spurious modes are generated as a result of phase variations between individual elements of the array and can include plane waves and circumferential modes in both the clockwise and counterclockwise directions. Although they are very seldom noticed in an unlined duct, their presence is often evident in the downstream section of a lined duct. In this case, the desired mode and each of the spurious modes are attenuated at different rates by the liner. The contribution of these spurious modes was analyzed for various phase differences in the array.

The attenuation characteristics of each of the liner materials was evaluated by the multisectioned duct analysis. For a finite length liner, the acoustic attenuation cannot be specified in terms of an attenuation constant for a particular mode because reflection effects caused by the impedance discontinuity on each side of the liner must be considered.. This introduces a standing wave within each section. Therefore, the transmission loss and insertion loss were used to evaluate liner performance for each material. These characteristics were determined as a function of frequency for each mode.

The results indicate that there is greater attenuation for spinning modes than for non-spinning modes for each of the liner materials. Furthermore, spinning modes of high circumferential order are attenuated

more than spinning modes of low circumferential order. There is up to a 16 dB difference between the increased sound attenuation of a plane wave for a 28-1/2" length of fiber metal liner than for a perforated panel liner and over 40 dB difference between the attenuation of the first spinning mode for these same materials.

The superior acoustic performance of the fiber metal liners is explained by the strong reactive component of the impedance while the perforated panel liners are predominantly reactive materials at low frequencies. The characteristics of these materials could be used to advantage in designing segmented liner configurations of resistive and reactive liners. Such a configuration could take advantage of the reflection effects between successive liners of different admittances and could easily be analyzed by the multisectioned duct theory.

A further significance of multisectioned liners is that modal conditioning may occur and result in increased attenuation as its primary effect. Thus, an incident acoustic wave could be redistributed by an initial liner section into modes which are more readily absorbed by the remaining lining segments. These aspects provide interesting topics for future research.

The results of the study suggest several areas of further research in duct acoustics. Of primary importance is the improved liner performance that may be obtained for a segmented duct configuration of several different liners. The multisectioned duct analysis described in this study could easily be extended to consider configurations of several different duct liners. Furthermore, this analysis could be applied to annular or rectangular ducts as well.

A complete parametric study of acoustic propagation in a multi-

sectioned circular duct would provide useful information for optimizing sound attenuation for both spinning and non-spinning modes. Beckemeyer and Sawdy (2) have performed such an analysis for a two dimensional duct. Their results show that the reflection effects at the interface between two different liner sections may not be as significant a factor in improving sound attenuation as the modal conditioning between sections. An optimum two segment liner has been shown to consist of an initial reactive liner followed by a resistive liner. In this case, the acoustic energy within the first section is converted into modes which are more easily attenuated within the resistive section. Similarly, the optimum configuration for a three segment liner consists of a combined reactive - resistive-reactive configuration. It would be interesting to compare these results for a two dimensional duct to similar configurations in a circular duct for both spinning and non-spinning mode. Furthermore, additional liner combinations for a circular duct should be investigated to optimize sound attenuation for various modes.

A limiting factor in such an optimization scheme is the infinite number of possible liner configurations and the resulting computer time involved to analyze these combinations. Arnold (34) has developed a sparse matrix technique applicable to multisectioned duct analysis which greatly reduces computer time. It would be recommended that this technique be implemented for future studies involving extensive computer work. Since the acoustic characteristics of both fiber metal and Helmholtz resonator type materials can be controlled by the material properties, liners with desired impedance characteristics can be designed. Therefore, the results of optimization studies should be used to design more effective sound absorbing duct liners which can be implemented for

experimental studies. These studies should include duct systems of two or more different liner materials for both annular and hollow circular ducts.

Further investigations should include the effects of mean flow and of various flow profiles on the sound attenuation produced by segmented liners. This situation would then provide a more realistic approximation of the acoustic environment in an actual jet engine inlet duct. When flow is considered, the resulting eigenfunctions are shown by Zorumski (3) to be non-orthogonal. Due to the matrix formulation of the problem, this effect, however, would not seriously complicate the analysis. When flow is included, continuity of particle displacement or particle velocity at the liner becomes the governing boundary condition depending on the flow profile. A discussion of the differences between each boundary condition is given by Lansing and Zorumski (1).

Additional experimental work is warranted to study acoustic propagation and sound attenuation in acoustically lined flow ducts. This work would provide confirmation of the proper boundary conditions in the presence of flow. Since the source array developed in the study is placed at the end of the duct, it could not be used with experiments which include flow. Additional techniques for generating higher order modes with reasonable modal purity would need to be developed in this case.

When a length of porous material is used as a duct liner, the boundary condition at the surface must be modified to consider acoustic propagation within the liner as a separate media. This introduces the extended reaction boundary condition. It would be interesting to compare the successive eigenvalues evaluated for this boundary condition with

eigenvalues for the same material evaluated from the local reaction boundary condition. The conversion of energy between successive modes should also be studied for the extended reaction boundary condition. This analysis might provide information on optimimum segmented liners consisting of a combination of extended reacting and locally reacting liners.

The acoustic characteristics of glass fiber materials, however, could not be as accurately predicted from the fundamental material properties. Therefore, additional work to describe the acoustic characteristics and dissipation mechanisms of these and other porous material in terms of various physical characteristics should be performed. These results would provide a significant improvement over the phenomenological approach of using a structure factor or effective parameters determined from experimental measurements to explain the attenuation characteristics of these materials.

Although acoustic propagation in an anechoically terminated circular duct of three sections with no flow has been the subject of the study, this analysis may be easily extended to consider several different configurations. The multisectioned duct analysis could be applied to annular and rectangular ducts, as well as to other duct geometries. The matrix formulation used in this analysis permits consideration of several different duct sections without undue complications.

To provide a more realistic approximation of the acoustic environment in an actual jet engine inlet duct, flow may also be included in this analysis. The resulting eigenfunctions are shown by Zorumski (3) to be non-orthogonal. Due to the matrix formulation of the problem,

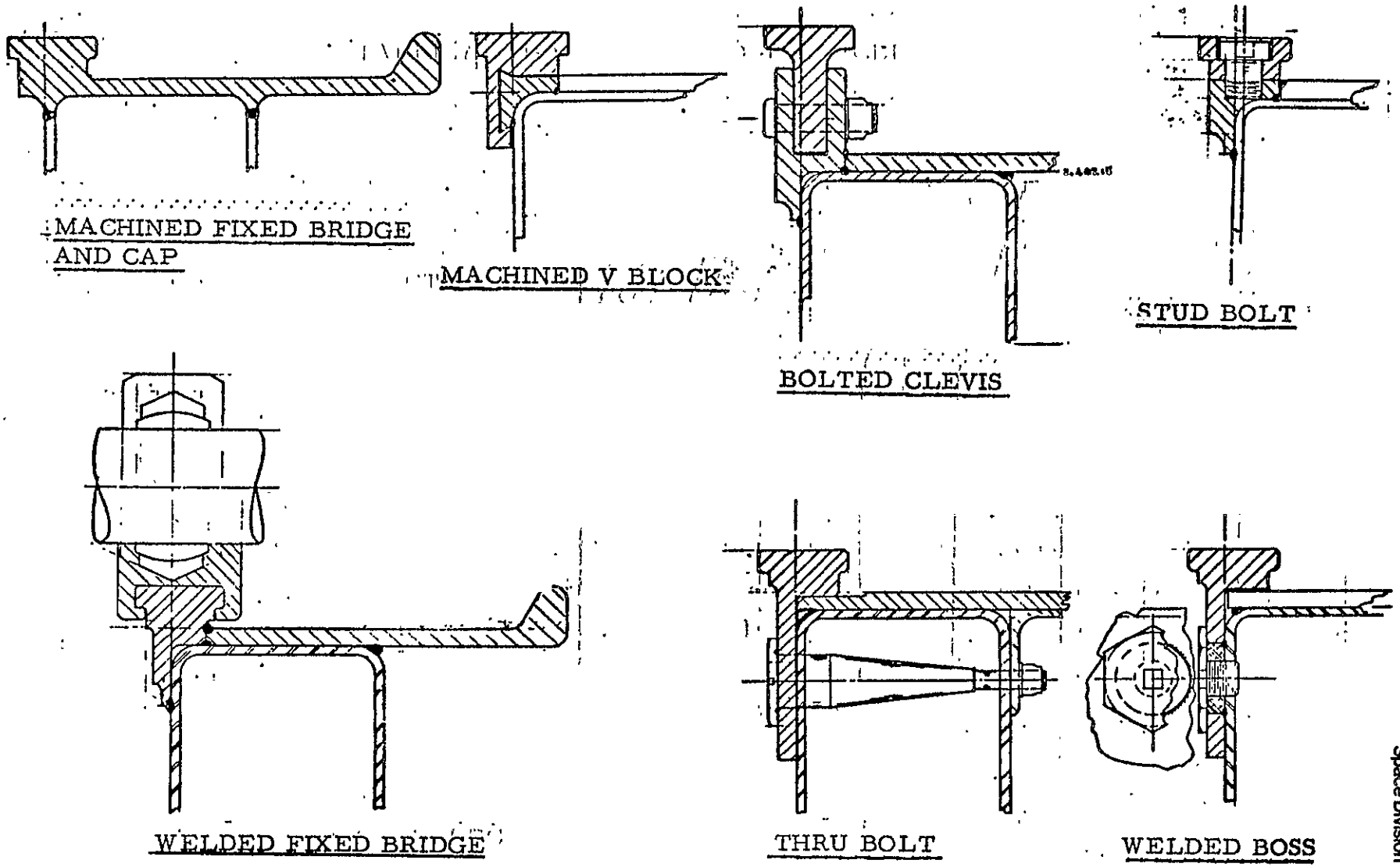

FIGURE 7-7 PAYLOAD LONGERON BRIDGE CONCEPTS

REFERENCES

1. Lansing, D.L. and Zorumski, W.E., "Effects of Wall Admittance Changes on Duct Transmission and Radiation of Sound", Journal of Sound and Vib., Vol. 27, No. 1, pp. 85-100, March 1973.

2. Beckemeyer, Roy J. and Sawdy, David T., "Optimization of Duct Acoustic Liners of Finite Length", Paper Presented at 89th Acoustical Society of America Meeting, Austin, Texas, April 1975.

3. Zorumski, W.E., "Acoustic Theory of Axisymmetric Multisectioned Ducts", NASA TR R-419, 1974.

4. Abramowitz, M. and Stegun, I.A., Eds., Handbook of Mathematical Functions, U.S. Department of Commerce, National Bureau of Standards, Washington DC, 1964.

5. Kilmer, Roger D., "Evaluation and Prediction of the Sound Absorbing Characteristics of Composite Acoustic Absorbers for Normally Incident Plane Waves", Masters Thesis in Mechanical Engineering, The Pennsylvania State University, 1974.

6. Zwikker, C. and Kosten, C.W., Sound Absorbing Materials, Elsevier Publishing Company, Inc., New York, 1949.

7. Kinsler, Lawrence E. and Frey, Austin R., Fundamentals of Acoustics, John Wiley and Sons, New York, 1962.

8. Morse, P.M. and Ingard, K.U., Theoretical Acoustics, McGraw-Hill, New York, 1968.

9. Beranek, Leo L., "Acoustic Impedance of Porous Materials", Journal of the Acoustical Soceity of America, 13, pp. 248-260, 1942.

10. Scott, R.A., "The Absorption of Sound in a Homogeneous Porous Medium", Proceedings of the Physical Society, 58, p. 165, 1946.

11. Pyett, J.S., "The Acoustic Impedance of a Porous Layer at Oblique Incidence", Acustica, 3, pp. 375-382, 1953.

12. Scott, R.A., "The Propagation of Sound Between Walls of Porous Material", Proceedings of the Physical Society, 58, pp. 358-368, 1945.

13. Wyerman, Barry R., "Absorption Characteristics of Glass Fiber Materials at Normal and Oblique Incidence", Masters Thesis in Engineering Acoustics, The Pennsylvania State University, 1974.

14. Zorumski, W.E., "Generalized Radiation Impedances and Reflection Coefficients of Circular and Annular Ducts", Journal of the Acoustical Society of America, Vol. 54, No. 6, pp. 1667-1673, 1973.

15. Lansing, Donald L., "Exact Solution for Radiation of Sound From a Semi-Infinite Circular Duct with Application to Fan and Compressor Noise", Analytic Methods in Aircraft Aerodynamics, NASA SP-228, pp. 323-334, 1970.

16. Fisher, E., "Attenuation of Sound in Circular Ducts", Journal of the Acoustical Society of America, 17, pp. 121-122, 1945.

17. Rice, E.J., "Attenuation of Sound in Soft-Walled Circular Ducts", in Aerodynamic Noise, Proceedings of AFOSR-UTIAS Symposium, Toronto, Canada, May 1968, University of Toronto Press, Toronto, Canada, pp. 229-249, 1969.

18. Molloy, Charles T. and Honigman, Esther, "Attenuation of Sound in Lined Circular Ducts", Journal of the Acoustic Society of America, Vol. 16, No. 4, pp. 267-272, 1945.

19. Benzakein, M.J., Kraft, R.E. and Smith, F.B., "Sound Attenuation in Acoustically Treated Turbomachinery Ducts", ASME Publ. 69-WA/GT-11, 1969.

20. Zorumski, W.E. and Mason, Jean P., "Multiple Eigenvalues of Sound Absorbing Circular and Annular Ducts", Journal of the Acoustical Society of America, Vol. 15, No. 6, pp. 1158-1165, 1974.

21. Copson, E.T., Theory of Functions of a Complex Variable, Clarendon Press, Oxford, pp. 118-119, 1960.

22. Beckett, Royce and Hurt, James, Numerical Calculations and Algorithms, McGraw-Hill Book Company, New York, 1967.

23. Myers, Gale H., "Development of Anechoic Termination Design for an In-Duct Fan Sound Test Facility", Memorandum Report, Carrier Corporation, 1969.

24. Harrington, Walter W., "The Design and Development of an Automatic Control System for the In-Duct Cancellation of Spinning Modes of Sound", Engineering Report, Mechanical Engineering Department, The Pennsylvania State University, 1973.

25. McDaniel, Oliver H., "Propagation of Sound at Moderate and High Intensities in Absorbent and Hard-Walled Cylindrical Ducts", Ph.D. Thesis in Engineering Acoustics, The Pennsylvania State University, 1975.

26. Vajnshtejn, L.A., "The Theory of Sound Waves in Open Tubes", Translated from Russian by J. Shmoys, Research Report No. E M-63, The New York University Institute of Mathematical Sciences, 1954.

27. Levine, Harold and Schwinger, Julian, "On the Radiation of Sound From an Unflanged Circular Pipe", Physical Review, Vol. 73, No. 4, pp. 383-406, 1948.

28. Half-inch Condensor Microphones - Instructions and Applications, Brüel and Kjaer, Copenhagen, 1955.

29. Seiner, John M. and Reethof, Gerhard, "Design and Development of the Spinning Mode Synthesizer", NASA CR02260, 1973.

30. Oslac, Michael J., "A Theoretical and Experimental Study of the Generation and Reduction of Multiple Higher-Order Modes in a Hard-Walled, Anechoically Terminated Cylindrical Duct", Ph.D. Thesis in Engineering Acoustics, The Pennsylvania State University, 1975.

31. "Airflow Resistance of Acoustic Materials", 1970 Annual Book of ASTM Standards, Part 14, American Society for Testing and Materials, Philadelphia, Pennsylvania pp. 223-229, 1970.

32. "Impedance and Absorption of Acoustic Materials by the Tube Method", 1970 Annual Book of ASTM Standards, Part 14, American Society for Testing and Materials, Philadelphia, Pennsylvania pp. 126-138, 1970.

33. Morse, Philip M., Vibration and Sound, McGraw-Hill, New York, 1948.

34. Arnold, W.R., "Sparse Matrix Techniques Applied to Modal Analysis of Multi-Section Duct Liners", Paper 75-514, AIAA Second Aero-Acoustics Conference, Hampton, Virginia, March 1975.

APPENDIX A

THE EFFECT OF PHASE VARIATIONS IN THE SOURCE ARRAY

It has previously been shown that a spinning mode synthesizer can generate higher order duct modes of a particular circumferential order (29). Phase variations between individual elements of the array will contribute additional spurious modes of a different circumferential order but at a much lower amplitude than the amplitude of the desired mode. The contribution of these modes will be analyzed for an array containing a circumferential ring of N equally spaced elements at a radius ro.

The boundary condition for the source array is given by Equation 2.72. If each of the elements has individual phase variations ϕ_n, the boundary condition for generation of a circumferential mode of order M is

$$v(r) = \frac{2\pi\ Q\ \delta(r-ro)}{r} \sum_{n=1}^{N} \delta(\Theta - \frac{2\pi N}{N})\ e^{i(\frac{2\pi nM}{N} + \phi_n)} \qquad (A.1)$$

Applying orthogonality conditions, this equation becomes

$$\int_o^b \int_o^{2\pi} v(r)\ \Psi_\mu(r)\ e^{-im\Theta} r\ dr\ d\Theta = \Psi_\mu(ro) \sum_{n=1}^{N} e^{i[\frac{2\pi n}{N}(M-m) + \phi_n]} \qquad (A.2)$$

If $\phi_n = 0$, Equation (A.2) becomes

$$\sum_{n=1}^{N} e^{i\frac{2\pi n}{N}(M-m)} = N \quad M-m = gN$$
$$= 0 \quad \text{Otherwise} \qquad (A.3)$$

where g is any integer. Therefore, only circumferential modes of order m where

$$m = M + gN \qquad (A.4)$$

can be generated. This includes the mode M as well as several additional modes of very high circumferential order. The propagation of these high circumferential order modes is restricted by their high cut-off frequencies.

When $\phi_n \neq 0$, additional circumferential modes, other than those specified by Equation A.4, are generated but at a reduced level. These spurious modes include circumferential modes in both the clockwise and counterclockwise directions. If these modes can propagate above their cut-off frequencies, their presence further complicates radial mode shapes.

For an array containing eight elements with individual phase variations, the relative amplitudes of spurious modes, together with the desired mode, are indicated in Table A.1. The speakers chosen for the array designed in this study, were within approximately ± 12° in phase. However, the relative levels of spurious modes for the examples in Table A.1 indicate the significance of these phase variations.

TABLE A.1

THE GENERATION OF SPURIOUS MODES DUE TO PHASE VARIATIONS BETWEEN ELEMENTS OF THE SOURCE ARRAY

ϕ_n for 8 elements: -14, -10, -8, 9, 10, 13, 7, -15

Generated Mode	Amplitude of Circumferential Mode in dB						
M	m=0	m=1	m=2	m=3	m=-1	m=-2	m=-3
0	0	-18	-35	-28	-18	-32	-27
1	-18	0	-18	-35	-32	-27	-45
2	-32	-18	0	-18	-27	-35	-28

ϕ_n for 8 elements: 12, -11, 13, 2, 5, -15, -5, 8

Generated Mode	Amplitude of Circumferential Mode in dB						
M	m=0	m=1	m=2	m=3	m=-1	m=-2	m=-3
0	0	-27	-22	-27	-26	-22	-28
1	-26	0	-27	-22	-22	-28	-21
2	-22	-26	0	-27	-28	-21	-27

VITA

Barry Robert Wyerman was born [redacted] in [redacted] [redacted]. He graduated from Mount Lebanon High School in Pittsburgh, Pennsylvania in June 1967. In March 1971 he received a B.S., cum laude in Physics from Ohio University, Athens, Ohio and in June 1974 an M.S. in Engineering Acoustics from The Pennsylvania State University, University Park, Pennsylvania.

Mr. Wyerman currently holds the position of Graduate Assistant in the Engineering Acoustics Program of The Pennsylvania State University.

Mr. Wyerman is a member of Phi Beta Kappa, Sigma Pi Sigma and the Society of Sigma Xi.